CONVERGENCE OF MILLIMETER-WAVE AND PHOTONIC INTERCONNECT SYSTEMS FOR VERY-HIGH-THROUGHPUT DIGITAL COMMUNICATION APPLICATIONS

A Dissertation
Presented to
The Academic Faculty

by

Shu-Hao Fan

In Partial Fulfillment
of the Requirements for the Degree
Doctor of Philosophy in the
School of Electrical and Computer Engineering

Georgia Institute of Technology
December 2011

CONVERGENCE OF MILLIMETER-WAVE AND PHOTONIC INTERCONNECT SYSTEMS FOR VERY-HIGH-THROUGHPUT DIGITAL COMMUNICATION APPLICATIONS

Approved by:

Dr. Gee-Kung Chang, Advisor
School of Electrical and Computer
Engineering
Georgia Institute of Technology

Dr. Thomas K. Gaylord
School of Electrical and Computer
Engineering
Georgia Institute of Technology

Dr. Bernard Kippelen
School of Electrical and Computer
Engineering
Georgia Institute of Technology

Dr. Shyh-Chiang Shen
School of Electrical and Computer
Engineering
Georgia Institute of Technology

Dr. Umakishore Ramachandran
College of Computing
Georgia Institute of Technology

Date Approved: November 8, 2011

To my parents,
Pau-Lo Fan and Sung-Ling Jung

ACKNOWLEDGEMENTS

TABLE OF CONTENTS

LIST OF TABLES

LIST OF FIGURES

LIST OF ABBREVIATIONS

ADC	Analog-to-Digital Converter
ADSL	Asymmetric Digital Subscriper Loop
ASE	Amplified Spontaneous Emission
AWG	Arbitrary Waveform Generator
AWGN	Additive White-Gaussian Noise
BER	Bit Error Rate
BJT	Bipolar Junction Transistor
BPSK	Binary Phase Shift Keying
CMOS	Complementary Metal Oxide Semiconductor
CO	Coherent-Optical
CP	Cyclic Prefix
DAC	Digital-to-Analog Converter
DCF	Dispersion Compensation Fiber
DDO	Direct-Detection-Optical
DSP	Digital Signal Processing
DVB	Digital Video Broadcasting
DWDM	Dense Wavelength Division Multiplexing
ECL	External Cavity Laser
EDFA	Erbium-Doped Fiber Amplifier
EHF	Extremely High Frequency
EVM	Error Vector Magnitude
FDE	Frequency Domain Equalization
FEC	Forward Error Correction
FFT	Fast Fourier Transform

FIR	Finite Impulse Response
FOC	Frequency Offset Correction
FSR	Free Spectral Range
GPGPU	General-Purpose Graphics Processing Unit
I	In-Phase
ICI	Inter-Channel Interference
IIR	Infinite Impulse Response
IR	Infrared Ray
LD	Laser Diode
LEAF	Large Effective-Area Fiber
IL	Optical Interleaver
LO	Local Oscillator
LoS	Line-of-Sight
LPF	Low-pass Filter
MF	Match Filter
MIMO	Multiple-Input-Multiple-Output
MMSE	Minimal Mean Square Error
MZ-DI	Mach-Zehnder Delay Interferometer
MZM	Mach-Zehnder Modulator
mmWave	Millimeter Wave
NLO	Nonlinear Optics
NRZ	Non-Return-to-Zero
OBPF	Optical Band-Pass Filter
OFDM	Orthogonal Frequency Division Multiplexing
OOK	On-Off Keying

OSNR	Optical Signal-to-Noise Ratio
PAPR	Peak-to-Average Power Ratio
PBS/PBC	Polarization Beam Splitter/Combiner
PD	Photodetector
PM	Phase Modulator
PolMux	Polarization Division Multiplexing
PON	Passive Optical Network
Q	Quadrature
QAM	Quadrature-Amplitude Modulation
QPSK	Quadrature Phase-Shift Keying
OWDM	Orthogonal Wavelength Division Multiplexing
RF	Radio Frequency
rms	Root Mean Square
RoF	Radio-over-Fiber
RZ	Return-to-Zero
SER	Symbol Error Rate
SHF	Super High Frequency
SLFL	Slow-Light Fiber Laser
SNR	Signal-to-Noise Ratio
SSMF	Standard Single-Mode Fiber
TSV	Through Silicon Via
VCSEL	Vertical-Cavity Surface-Emitting Laser
VOA	Variable Optical Attenuator
WDM	Wavelength Division Multiplexing
ZF	Zero-Forcing

SUMMARY

In the past, radio-frequency signals were commonly used for low-speed wireless electronic systems, and optical signals were used for high-speed wired communication systems. However, as the emergence of new millimeter-wave technology, which is capable of providing multi-gigabit transmission over a wireless radio-frequency channel, the borderline between radio-frequency and optical transport systems becomes blurred. As a result, there are ample opportunities to design and develop next-generation broadband systems by combining the advantages of these two technologies to overcome inherent limitations of various broadband end-to-end interconnects, such as signal generation, transportation, data recovery, and synchronization. For the transmission distances of a few centimeters to thousands of kilometers, the integration of radio-frequency electronics and photonics to build radio-over-fiber systems ushers in a new era of research opportunity for the upcoming very-high-throughput broadband services.

Recent developments in radio-over-fiber systems have garnered momentum to be recognized as the most promising solution for the backhaul transmission of multi-gigabit wireless access networks, especially for the license-free, very-high-throughput 60-GHz band. Adopting radio-over-fiber systems in local-access or in-building networks can greatly extend 60-GHz signal reach by using ultra-low loss optical fibers. However, systems operating at such high frequency are difficult to generate in an old fashion way. In this dissertation, several novel techniques of homodyne and heterodyne optical-carrier suppressions for radio-over-fiber systems are investigated and various system architectures are designed to overcome these limitations of 60-GHz wireless access

networks, bringing the dream of delivering multi-gigabit wireless services of any content, at anytime and anywhere closer to the reality.

In addition to the advantages for the access networks, extremely high spectral efficiency, which is the most important parameter for long-haul networks, can be achieved by radio-over-fiber signal generation. As a result, the transmission performance of spectrally efficient radio-over-fiber signaling technique, including orthogonal frequency division multiplexing and orthogonal wavelength division multiplexing, is broadly and deeply investigated in this research as well. On the other hand, radio-over-fiber is also used for the frequency synchronization that can resolve the performance limitation of wireless interconnect systems for off-chip high-performance-computing transmission. A novel wireless interconnect system assisted by a new carrier-over-fiber technique is proposed and analyzed in this dissertation.

In conclusion, multiple advantageous facets of radio-over-fiber systems can be found in various levels of networking systems. The rapid development of new applications using radio-over-fiber technology developed in this research will revolutionize the conventional wisdom of broadband optical and wireless digital communications.

CHAPTER 1

INTRODUCTION

1.1 Radio-over-Fiber System

Electromagnetic waves and photons are two sides of the same thing. They interpret the oscillation of electric fields and the propagation of energy in different ways. When the oscillating frequency of the electric field is low, its behavior is more similar to a wave. At very high frequency, its behavior is more like a particle especially when its frequency is close to the resonant frequency of common molecules. Because electromagnetic waves (or photons) have two different behaviors according to their frequency, they have very different detection mechanisms in modern digital communication systems. When the frequency of electromagnetic waves is low, the electric field activates the resonance of a metal piece of the certain length (approximately a quarter wavelength of the electric field) that can be easily fabricated by current manufacturing technology (from a few millimeters to meters). Therefore, the resonant activities can be easily detected by metal electronic devices to deliver digital information. When the frequency is too high, for example, in the infrared-ray (IR) domain, the resonant length is close to roughly one micrometer and not feasible for the fabrication of an artificial metal structure. However, the frequency is so high that the energy of the photon is high enough to break through the electron bandgap of some semiconductor materials. This photon can stimulate the photoelectric effect and generate an electron-hole pair in the semiconductor, and this pair can be collected by semiconductor devices in the form of electric currents.

Because of their difference in detection mechanisms and frequencies, the electromagnetic waves are categorized into two different applications in modern digital communication systems: wireless and wired transmissions. Considering the number of photons, both high-frequency and low-frequency electromagnetic-wave detectors require thousands to tens of thousands of photons

to achieve effective information transmission. However, the receiver sensitivity of a low-frequency radio detector is much lower than that of a high-frequency photodetector. For example, Wi-Fi receivers, such as Orinocco cards or CISCO cards Aironet 350 series, need only 2×10^{-19} Watt/bit to achieve a bit error rate (BER) of 10^{-5}, because the energy per photon of low-frequency electromagnetic waves is low. The low receiver-sensitivity requirement of a radio detector makes it suitable for the lossy free-space (wireless) transmission. These kinds of frequency bands are referred to as radio-frequency (RF) bands. On the contrary, the typical receiver sensitivity of a direct-detection optical (DDO) photodetector is approximately 1×10^{-14} Watt/bit. The high level of the DDO receiver sensitivity makes the high-frequency photons can only be applied for the low-loss wave-guided (wired) transmission.

According to the U. S. National Telecommunications and Information Administration [1], the frequencies from 3 KHz to 300 GHz are defined as RF bands and used for wireless communications. The frequencies above 300 GHz are defined as optical-frequency bands, starting from the IR domain (as shown in Figure 1.1). A rule of thumb in digital communications states that the channel bandwidth of an electromagnetic carrier is no more than one-tenth of its carrier frequency. Therefore, the low frequency of an RF carrier restricts the transmission data rate of the RF band, which can only handle the low-speed (lower than 1Gb/s) wireless links. Conversely, the IR band has almost unlimited bandwidth; for example, there is approximately 40-THz bandwidth available in an optical standard single-mode fiber (SSMF) near the wavelengths of 1310 nm and 1550 nm.
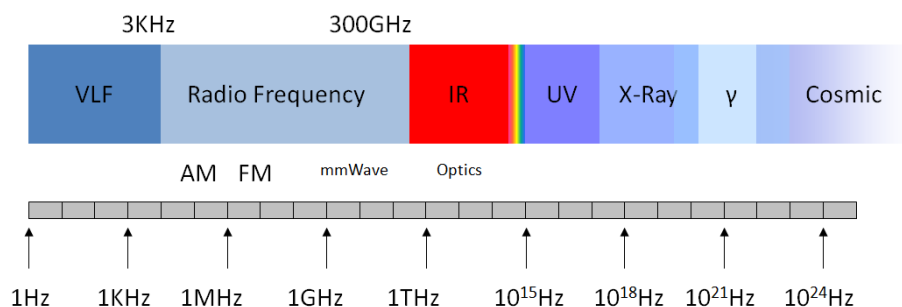
Fig. 1.1. Spectrum definition of electromagnetic waves.

As a result, optical communications usually deal with high-speed long-distance transmission. The high cost and high power of optical systems limit its development in short-range communications. In conventional digital communication, RF and IR bands have their unique advantages and specialties in their respective applications without concerning each other. However, as technology evolves, when the speed of semiconductor electronics catches up with optical systems, the borderline between RF and IR bands becomes ambiguous. Low-cost semiconductor materials, such as silicon or silicon germanium, now can support electronics of nearly 100-GHz frequency. Since the wavelength of this frequency band is approximate few millimeters, this is known as millimeter-wave (mmWave) technology. This technology enables the RF transmission over the super-high frequency (SHF: from 3 GHz to 30 GHz) or extremely high frequency (EHF: from 30 GHz to 300 GHz) bands, which can offer transmission data rates of tens of gigabits per second wirelessly. Therefore, in terms of data rates, optical systems and RF systems do not exhibit significant difference in transmission speed. In the aspect of the energy requirement in signal propagation, because the poor air penetrability and high Friis path loss of signals carried by electromagnetic waves at 60GHz, typical mmWave receivers require more received power and almost a line-of-sight (LoS) connection, similar to the characteristics of photodetectors. Because of the non-traditional characteristics of mmWave signals, a conventional infrastructure of wireless systems may not be suitable for mmWave wireless transport systems. New system architectures are in demand for mmWave technology. The development of new mmWave systems can learn from and even take advantages of the unique properties of optical communication systems.

On the other hand, optical communication systems can also learn a lot from conventional wireless transmission. Wireless communications often encounter a very tough transmission condition with lots of signal distortions, multi-path reflections, and frequency-selective fading. In the mean time, spectral efficiency is also critical for RF systems because of the limited inadequate bandwidth in RF spectrum. Therefore, a complete digital system of advanced algorithms and modulations has been derived for decades to deal with all of these impairments

and spectral efficiency. It was not useful for optical communication systems before because the data rate of optical transmission was too high and there is no digital electronics capable of deploying these modulation schemes and algorithms in a real-time manner. Currently, because the speed of mmWave electronics catches up with the data rate of optical systems, an optical receiver can afford adapting the complexity of these advanced algorithms and, and it can use digital signal processing (DSP) to improve the signal quality, to lower the cost of optical recovery modules, and to increase the spectral efficiency. DSP is especially important for long-haul optical networks or unrepeatered submarine fiber optic systems, where the transmission distance ranges from 100 km to 10,000 km [2, 3]. Distortion recovery and spectral efficiency are two of the most critical criteria in the long-distance optical transmission. While all-optical methods are usually unstable and costly, DSP methods usher in a new area of long-haul optical transmission systems.

As the characteristics of optical lightwaves and mmWaves are becoming more and more alike, the convergence of mmWaves and photons in digital communication systems can be achieved by radio-over-fiber (RoF) systems. Instead of transmitting baseband data directly by optical photons, in RoF systems, RF signals are carried by photons in optical fibers. For different applications and transmission distances, these RF/optics hybrid systems can offer various advantages to fulfill a variety of system demands. In RoF systems, the photons are not just a group of energy directly detected by a photodetector in the baseband anymore; the RF signals no longer propagate unrestrainedly in the free space, either.

So far, RoF is mostly referred to the applications of wireless-coverage extension by utilizing the ultra low loss of optical fibers. However, the transmission of guided RF signals in optical fibers can not only decrease the propagation attenuation of RF waves but can also be used for frequency synchronization or spectral-efficiency enhancement. These RF/optics hybrid systems can be a promising solution to various digital communication systems. As a result, the meaning of RoF can be generalized to three major categories of applications: the long-haul

networks, the medium-range wireless-over-fiber systems, and the short-reach links for high-performance computing (HPC).

For the long-haul systems, extremely high spectral efficiency can be achieved by multi-orthogonal-carrier systems, whose generation methods are based on the RF oscillation. Meanwhile, using fast DSP to recover the impairments from the optical channel in the optical receiver can save expensive optical recovery modules. The DSP algorithms can also utilize various advanced modulation/demodulation schemes originating from RF wireless systems [4-6] to improve the performance and power efficiency of optical transmission systems. For medium-range transmission systems, it is in great demand to use mmWave technology to establish wireless links of multi-gigabit per second for mobile end-users. The wireless signal coverage of mmWave technology can be extended by optical fibers dramatically in RoF systems [7]. For HPC applications, the reliability, size, and power consumption are the most critical factors that matter in terabit-interconnects among chips and boards. The performance of these ultra-short-range interconnects dominates the overall throughput of HPC under the prevailing von Neumann architecture [8-10]. RF/optics hybrid systems have great potential to overcome the bottleneck of the conventional optical and copper-wire interconnects by establishing a synchronized wireless-link condition. With more and more inspiring interplays between RF signals and optical systems coming out, RoF systems can provide versatile potential in modern digital communication systems

1.2 Research Objective

RoF systems have been applied for various applications for years, such as cable TV (CATV) transmission lines or fiber-to-the-antenna (FTTA) transmission for dead-zone cellular-coverage extension. However, not until recently are RoF systems considered for high-speed wired and wireless applications. The maturity of mmWave technology and the explosive growth

of multi-media demands quickly drive the revolution of conventional digital communication systems. It is still a new exploration era for RoF systems to take place in high-data-rate applications. The debate of the best choice in various applications between digital baseband communications and RoF communications has not settled down, neither.

The research objective of this thesis is to identify the problems of RoF systems composed of contemporary components and devices and to investigate the aptitude, limitation, and versatility of RoF technology. Not limited to the conventional meaning of RoF, which is applied for the wireless-signal extension exclusively, adapted or original designs of RoF systems are proposed and evaluated to overcome the limitation of modern digital communication systems in various applications.

The impact of radio-over-fiber systems is upon various levels of digital communication systems. One of the most important applications is in the wireless access network. Combining 60-GHz technology, one can make multi-gigabit transmission over a wireless local area network (WLAN) a reality. In this research, novel optical-carrier-suppression techniques are proposed to overcome the bandwidth restriction of current optical millimeter-wave signal generation in radio-over-fiber systems. High conversion efficiency, simple and straightforward 60-GHz signals can now be generated using homodyne optical-carrier suppression systems. Robust and more spectrum-efficient vector signals can be feasibly transported by the original heterodyne optical-carrier suppression systems. I believed that implementing these two techniques flexibly can accelerate the development of very-high-throughput wireless local-access or in-building networks in the near future.

Radio-over-fiber signals are also found to be advantageous in the long-haul transmission systems and high-performance computing systems because of the unique features of optical millimeter-waves. The main contributions of this research in different distances for communications are listed below:

For long-haul transmission, the performance of orthogonal radio channels inside a fiber is investigated and current transmission techniques are improved with our modified radio-over-fiber systems:

1. A review of current technology for coherent optical (CO) transmission developed for long-haul optical digital communications is given.

2. A review of optical transmission systems of multiple orthogonal carriers for long-haul optical communications is given, including orthogonal frequency-division multiplexing (OFDM) and orthogonal wavelength-division multiplexing (OWDM).

3. The performance and limitation of DDO-OFDM and CO-OFDM systems, including high peak-to-average-power ratios and sensitivity to phase noise, are experimentally and theoretically investigated. Modified DDO-OFDM and CO-OFDM systems are proposed to overcome these fundamental limitations

4. The performance and fundamental limitation of CO-ODWM and DDO-OWDM systems using optical or digital demultiplexing schemes are first theoretically and experimentally investigated and discussed in detail.

For access networks, the limitation of current radio-over-fiber signal generation at 60-GHz is investigated and discussed. Novel optical millimeter-wave generation techniques, such as homodyne and heterodyne optical-carrier-suppression schemes, are introduced.

1. A review of wireless-over-fiber systems is discussed in detail. The problems caused by optical mmWaves, including vector-signaling, multi-band beating interference, and uplink bottleneck, are discussed.

2. Conventional and new optical mmWave generation methods are presented and theoretically and experimentally evaluated.

3. Integration and testing of modified optical-carrier suppression systems for wireless-signal extension are achieved. A novel system architecture adapting conventional optical-carrier suppression for dispersion-resistant wired and wireless coexisting signals is introduced.

4. A novel access-networking system, which combines optical polarization multiplexing and multiple-antenna systems, is demonstrated based on the conventional optical-carrier suppression scheme.

5. A heterodyne optical-carrier suppression technique is invented to carry bidirectional radio-over-fiber signals using low-cost transmitter components. Two experimental demonstrations with theoretical analysis are presented.

For the first time, a wireless interconnect system for high-performance computing using a carrier-over-fiber technique, is implemented with a novel wireless interconnect multiplexing scheme.

1. A review of the von Neumann bottleneck of current HPC architectures.

2. A new architecture of short-range wireless interconnects is proposed for the memory access applications of the HPC implementation. In the new architecture, RoF systems are integrated with RF transceivers to achieve local-oscillation synchronization.

3. Wireless multiple-input-multiple-output (MIMO) subsystems with RoF synchronization for parallel signal transmission have been proposed and evaluated theoretically and experimentally.

1.3 Thesis Overview

After the introduction of RoF systems in various applications and infrastructures in Chapter 1, research results are presented in the order of long-haul RoF systems, medium-range wireless-over-fiber systems, and short-range RoF-synchronized wireless interconnects.

Chapter 2 reviews the development of current CO digital communication systems, which are designed mainly for long-haul applications. Adapted OFDM and OWDM RoF systems are introduced for high-capacity transmission applications. The performances of OFDM and OWDM systems are theoretically and experimentally evaluated both for DDO and CO receivers. The

fundamental limitations of OWDM systems caused by optical and digital demultiplexing schemes are derived and discussed in the end.

Chapter 3 reviews the current development of wireless-over-fiber systems, especially the uprising mmWave-over-fiber networks. Various optical mmWave generation methods are proposed and evaluated for the transportation of mmWaves over optical fibers. Based on the proposed optical mmWave generation methods, a variety of RoF system architectures are proposed and experimentally examined to fulfill practical requirements and to overcome limitations of RoF mmWave systems.

Chapter 4 reviews the von Neumann bottleneck of current HPC architectures. The current developing trends of optical, copper, and wireless interconnects are discussed respectively. A new approach of RoF-synchronized MIMO wireless interconnects is proposed. The pros and cons of the conventional and proposed interconnects are compared and evaluated.

Chapter 5 summarizes the research development of each chapter. Potential applications and future works are presented and discussed for continuing development.

CHAPTER 2

HIGH-CAPACITY RADIO-OVER-FIBER SYSTEM

2.1 Review of Long-Haul Optical Transmission

Long-haul optical transmission plays an important role in internet backbone networks. Aggregating all the data transmitted from access networks and end-users, 40-Gb/s or 100-Gb/s per optical fiber over 100 km is now under the field installation in today's internet backbone networks. To fulfill the exponential growth of global internet usage, much faster transmission systems are under competitive development. For example, the newest lab experiment has demonstrated 101.7-Tb/s transmission over a single 165-km optical fiber in 2011 [11]. To achieve such a long distance and a high data rate, only optical fibers are capable of affording this level of bandwidth-distance product. Glass optical fibers, such as SSMFs or large-effective-area fibers (LEAFs), are low-loss, wide-bandwidth, lightweight optical waveguides to transport guided photons in the IR band, making them suitable for optical-signal transmission over a very long distance. However, lots of signal impairments inside these fibers accumulate along with distances, such as chromatic dispersion, polarization-mode dispersion, filtering effects and nonlinearity optics (NLO). The dominating factors of the signal impairments are various kinds of linear dispersion effects. Therefore, the dispersion effects can be restored by using the fiber that is called an optical dispersion compensation fiber (DCF), which has the opposed dispersion effects to reverse the dispersion process. As a result, the most common fiber deployment of long-haul transmission to mitigate dispersion effects is through cascading multiple SSMF-DCF spans. As shown in Fig. 2.1, in each span, an erbium-doped fiber amplifier (EDFA), which is followed by a long SSMF and a short DCF, is used to increase the power of the optical signal to compensate the propagation loss in the fiber. Using DCF modules can reduce the complexity of the far-end optical receivers. However, the cost of DCF modules is high, and the maintenance

and scalability of DCF modules are not cost-effective, especially when these fibers are often fixed deeply underground or undersea. In addition, for wavelength-division multiplexing (WDM) systems, the dispersion slope (a higher-order dispersion coefficient) and NLO of fibers dominates the signal impairments. The DCF effectiveness is decreased after a very long distance [12]. DCFs also have higher NLO properties than ordinary fibers, and they limit the bandwidth-distance product of optical fibers by inducing higher NLO distortions in the long-haul transmission [13].
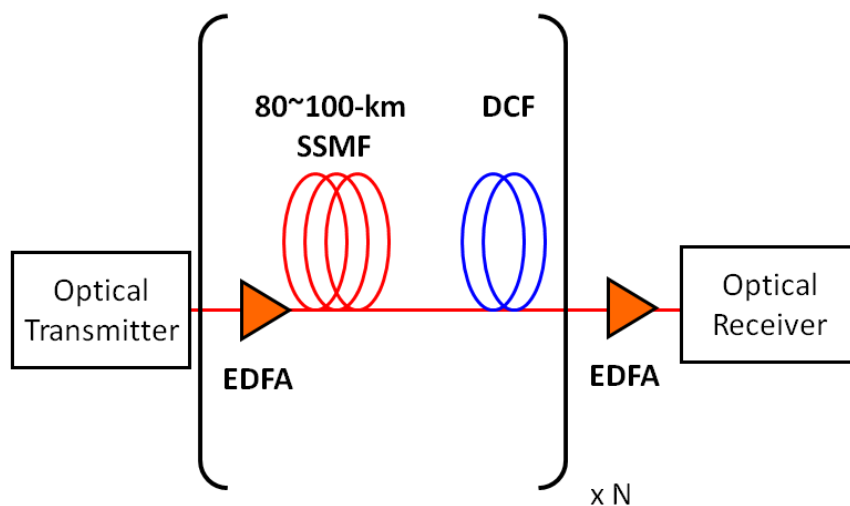
Fig. 2.1. Conventional fiber transmission system composed of SSMF, DCF, and EDFA.

To improve the bandwidth-distance product of optical fibers and to lower the system cost, using DSP in the far-end receiver to restore the fiber impairments without DCF modules provides an alternative solution. Using DSP-based dispersion compensation in the far-end receiver can eliminate the need of in-line DCF modules and increase the bandwidth-distance product of optical fibers dramatically. It stimulates a worldwide interest since the first demonstration of the digital CO receiver in 2005 [14 – 16]. In addition to saving cost of DCF modules, DSP can not only compensate chromatic dispersion but can also restore polarization-mode dispersion, filtering effects, phase noise, and nonlinear effects at the same time [17, 18].

11

As a result, the emergence of DSP compensators accelerates the development of digital CO receivers in the last few years.

Research studies of CO communications were active in the early 1980s. It was mainly used to increase the optical receiver sensitivity after long-distance transmission then. However, there was a hiatus in CO research activities when the EDFA was widely deployed in high-capacity WDM systems. The optical power amplification by EDFAs greatly weakens the necessity of optical-receiver sensitivity. However, because the computational speed of electronics started to catch up with the data rate of optical systems recently, the DSP-based CO receiver catches people's attention again. CO receivers detect the phase and the amplitude of incoming photons, unlike the mere energy detection of conventional DDO receivers. Because most of the fiber impairments are phase-dependent, detecting the phase information of incoming photons by a CO receiver realizes the possibility of DSP compensation. With the help of high-speed electronics, the DSP receiver not only makes all the digital dispersion compensation possible, but also enables the deployment of higher-order modulation formats (such as QPSK, 16-QAM, 64-QAM) in a CO system.

A typical DSP-based CO receiver is shown in Fig. 2.2(a). The input optical signal is coupled into an optical hybrid. After beating with another laser used as a local oscillator (LO), two balanced receivers detect the two signals, in-phase (I) and quadrature (Q) signals, respectively. And the two analog-to-digital converters (ADCs) are used to transfer these signals into digital domain for DSP-based compensation. Neglecting any noise for simplicity, the recorded signals can be represented by

$$i_{o1} = -2\text{Im}\left\{E_{LO}{}^*E_s e^{j(\omega_s - \omega_{LO})t}\right\},$$

$$i_{o2} = +2\text{Re}\left\{E_{LO}{}^*E_s e^{j(\omega_s - \omega_{LO})t}\right\},$$

(Eq. 2.1)

where i_{o1} and i_{o2} are the output currents of the two balanced receivers; E_{LO} and E_s are the complex phasors of the electric fields of the LO and the input signal respectively; ω_{LO} and ω_s are the optical angular frequencies of the LO and the input signal respectively. When the wavelengths of the input signal and the LO are the same, the received signals are equivalent to

12

the received signals from an RF homodyne receiver. When the wavelength of the LO laser is set to be far apart from the input signal, the setup is equivalent to an RF super-heterodyne detection with the intermediate frequency (IF) equal to the difference of their two wavelengths, as depicted in Fig. 2.2(b).

$$\begin{bmatrix} \dfrac{1}{\sqrt{2}} & \dfrac{-j}{\sqrt{2}} \\ \dfrac{-j}{\sqrt{2}} & \dfrac{1}{\sqrt{2}} \end{bmatrix}$$

$E_{LO} = |E_{LO}|e^{j\phi}$

$E_s(t)e^{j\omega_s t}$
Input signal

LO
$E_{LO}e^{j\omega_{LO}t}$

$i_{o1} = -2\operatorname{Im}\left\{E_{LO}^{*}E_s e^{j(\omega_s - \omega_{LO})t}\right\}$

$E_s(t)e^{j\omega_s t}$
Input signal

LO
$jE_{LO}e^{j\omega_{LO}t}$

$i_{o2} = 2\operatorname{Re}\left\{E_{LO}^{*}E_s e^{j(\omega_s - \omega_{LO})t}\right\}$
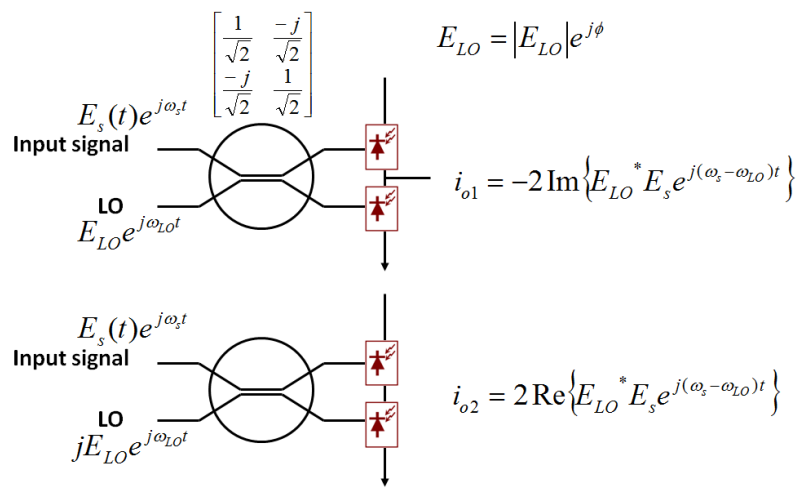
(a) CO Receiver and Optical Hybrid

$\operatorname{Re}\left\{E_{LO}^{*}E_s(t)e^{j(\omega_s - \omega_{LO})t}\right\}$

$\operatorname{Re}\{E_s(t)\}\cos(\omega_s t)$
$- \operatorname{Im}\{E_s(t)\}\sin(\omega_s t)$

$|E_{LO}|\cos(\omega_{LO}t - \phi)$

$90°$

$\operatorname{Im}\left\{E_{LO}^{*}E_s(t)e^{j(\omega_s - \omega_{LO})t}\right\}$
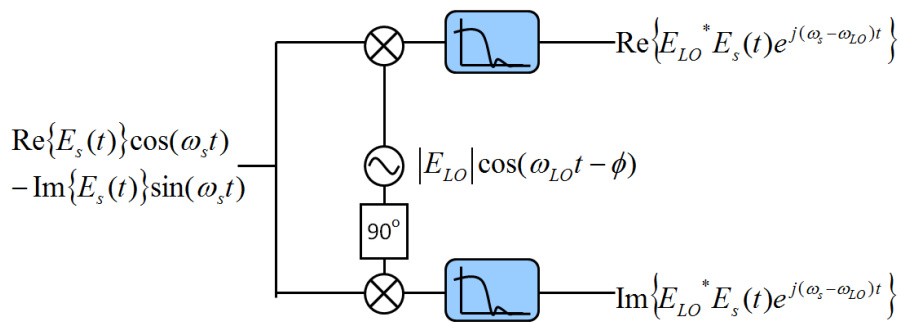
(b) RF Receiver

Fig. 2.2. CO and RF receiver.

13

Dispersion and frequency-selective fading in optical systems can be modeled as a linear system, and a CO receiver can use a finite-impulse-response (FIR) or an infinite-impulse-response (IIR) digital filter to compensate these linear impairments in the digital domain. However, this digital filter requires a large amount of memory and computational complexity, which will increase with the transmission distance. For example, even with the time-domain truncation, more than 250 $T_s/2$-spaced filter taps are required for a 28GBaud 1000-km transmission system, where T_s is the symbol period [14]. An alternative way is to use Fast Fourier Transform (FFT) to equalize the signals in the frequency domain. While the complexity of FIR digital filters scales with the square law of the symbol rate, the computational complexity of frequency-domain equalization (FDE) only increases with the symbol rate on a logarithmic scale.

The feasibility of FDE drives the development of multi-orthogonal-carrier signals. Instead of transmitting data in series in the time domain, multi-orthogonal-carrier signals divide the data into many slow orthogonal RF carriers and transmit them in parallel in the frequency domain. This concept, also known as orthogonal frequency-division multiplexing (OFDM), was already proposed for wireless systems since 1966 [19]. However, not until late 1980s was OFDM deployed globally in wireless and cable networks because the processing speed of electronics became fast enough to modulate and demodulate OFDM in practical applications. Today, OFDM is applied to almost everywhere, from Digital Video Broadcasting (DVB), Asymmetric Digital Subscriber Loop (ADSL), and home networks (such as ITU-T G.hn) to Wi-Fi (802.11n) and 4G cellular networks (WiMAX and LTE). OFDM is becoming ubiquitous in such a time mainly because it has better flexibility, robustness and spectral efficiency than conventional single-carrier modulation formats.

Currently, the processing speed of electronics begins to catch up with the data rate in optical systems. Therefore, the implementation of OFDM optical transceivers begins to draw more and more attention. The core of modulating and demodulating OFDM signals is the FFT digital processing. The vantage of OFDM mainly comes from the ease of FFT implementation

and the orthogonality of OFDM subcarriers. In one OFDM symbol period T, multiple subcarriers with frequencies spaced 1/T apart are orthogonal to each other. That is, if you integrate the summation of any two subcarriers in T, the integral is always zero. This orthogonality enables the parallel transmission of data without any interference.

Assuming that we have 2K+1 data symbols $\{X_{-K}\ X_{-K+1}...X_0...X_K\}$ to be modulated in one OFDM symbol with a subcarrier frequency spacing f_{sc} (f_{sc} =1/T), the transmitted signal can be expressed by a continuous-time function in one symbol period:

$$s(t) = \sum_{k=-K}^{K} X_k e^{j2\pi k f_{sc} t}. \qquad\qquad 0 < t < \frac{1}{f_{sc}} \qquad \text{(Eq. 2.2)}$$

This modulation process can be achieved easily by an inverse FFT (IFFT) process of the sampling rate at $N_T f_{sc}$, where N_T is the OFDM FFT size. At the receiver side, the signal is distorted by a channel impulse response $h(t)$ and the carrier frequency offset $\Delta\omega$. Adding the time-variant phase variation $\phi(t)$ and additive complex noise $w(t)$ from the channel and the LO laser, we can obtain the incoming signal:

$$r(t) = \big(s(t)\otimes h(t)\big)e^{j\Delta\omega t + j\phi(t)} + w(t), \qquad\qquad \text{(Eq. 2.3)}$$

where $\otimes$ represents the operator of convolution. Assuming that we have perfect synchronization and the sampling rate is precisely at $N_T f_{sc}$, the OFDM receiver samples the incoming OFDM signal at the discrete time $t_n = \{0, \frac{1}{N_T f_{sc}}, \frac{2}{N_T f_{sc}} ... \frac{n}{N_T f_{sc}} ... \frac{N_T-1}{N_T f_{sc}}\}$ as

$$r_n = \left(\sum_{m=1}^{\infty} s_m h_{n-m}\right) e^{j\frac{2\pi n \epsilon}{N_T} + j\phi_n} + w_n, \qquad n = 1,2,... N_T \qquad \text{(Eq. 2.4)}$$

where s_n, h_n, ϕ_n, and w_n represent the discrete-time samples of $s(t_n)$, $h(t_n)$, $\phi(t_n)$, $w(t_n)$ respectively. Using the channel frequency response, we can also express the received signals by

$$r_n = \left(\sum_{k=-k}^{K} H_k X_k e^{j\frac{2\pi n k}{N_T}}\right) e^{j\frac{2\pi n \epsilon}{N_T} + j\phi_n} + w_n, \qquad n = 1,2,... N_T \qquad \text{(Eq. 2.5)}$$

where H_k represents the channel frequency response to the k-th subcarrier. Since each subcarrier occupies very small bandwidth, we can assume that the channel frequency response to the k-th

subcarrier is a flat-fading constant. We depict the frequency offset in terms of the normalized frequency offset ϵ, which is related to the continuous-time frequency offset by

$$\triangle \omega = 2\pi f_{sc}(\epsilon + N_T\Lambda). \qquad \text{(Eq. 2.6)}$$

The normalized frequency offset ϵ is defined so that its value is limited to $-N_T/2 \leq \epsilon < N_T/2$. When $\triangle \omega$ is out of the range $\pm\pi N_T f_{sc}/2$, the integer Λ is added to Eq. 2.6 to make up for the additional frequency offset. Nevertheless after the sampling process, as implied in Eq. 2.4, the effect of the additional frequency offset $2\pi f_{sc}N_T\Lambda$ will be totally eliminated. The residual frequency offset can induce the amplitude reduction of each subcarrier, generate inter-channel interference (ICI), and reduce the signal-to-noise ratio (SNR) [20].

The frequency offset can be corrected by a frequency offset correction (FOC) algorithm [21-30]. If the frequency offset is compensated accurately, the received signal is demodulated by the FFT process. Neglecting the phase noise, the demodulated signal is

$$R_k = H_k X_k + W_k, \qquad k = -K, -K+1, \dots K \qquad \text{(Eq. 2.7)}$$

Using a repetitive signal, named a cyclic prefix (CP), attached to the front of each OFDM symbol as a guard interval, the effect of the fiber dispersion can be neglected. There is still a phase rotation of the original signal X_k. Once the phase rotation and frequency response is estimated by the OFDM receiver as $\hat{H}_k$, the original signal can be estimated from $\{R_k\}$ by the zero-forcing equalization:

$$\hat{X}_k = \hat{H}_k^{-1} R_k, \qquad k = -K, -K+1, \dots K \qquad \text{(Eq. 2.8)}$$

Therefore, a typical OFDM digital CO receiver includes the function of synchronization, phase-noise compensation, FOC, and equalization, as shown in Fig. 2.3. Compared with traditional single-carrier modulation schemes, the CP of OFDM saves the complexity of dispersion compensation, and the flat-fading FDE simplifies the channel equalization. In the meanwhile, because it divides information into multiple low-speed subcarriers, it occupied much smaller bandwidth than single-carrier modulation formats because of the sharp-edged spectrum of each slow-speed subcarrier. In Fig. 2.4, the spectra of different modulation formats of a 10-

Gb/s data rate are depicted, including non-return-to-zero (NRZ) on-off keying (OOK), return-to-zero (RZ) OOK, quadrature phase-shift keying (QPSK), duobinary, and quadrature-amplitude modulation (QAM) OFDM.
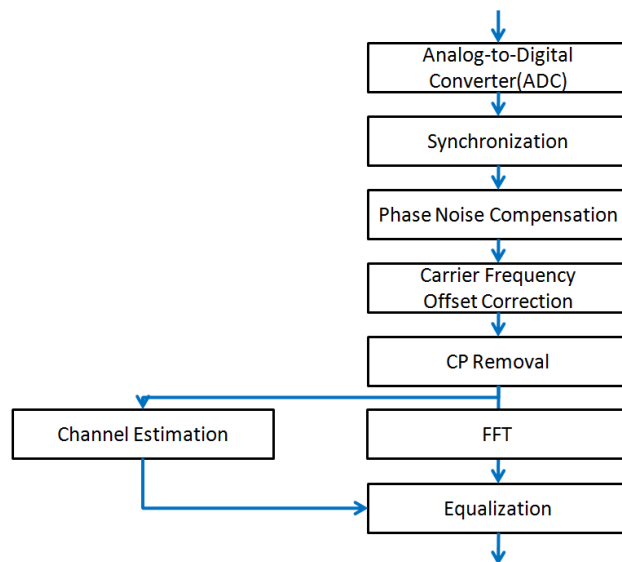
Fig. 2.3. DSP process of a CO-OFDM receiver.

However, OFDM waveforms are similar to analog waveforms rather than digitalized waveforms. This means that the OFDM amplitude is almost randomly distributed and requires a high-resolution ADC and a digital-to-analog converter (DAC) in the receiver and the transmitter respectively. The summation of multiple sinusoidal subcarriers makes the OFDM waveforms have a very high peak-to-average power ratio (PAPR). The high PAPR of a signal makes it vulnerable to the nonlinearity of a transmission channel, especially to the nonlinearity of the amplifiers. The perfect linearity requirement of EDFA becomes one of the most critical issues for OFDM transmission. Nevertheless, it is almost impossible to achieve perfect linearity in the long-haul system with so many cascaded EDFAs. Furthermore, OFDM waveforms are sensitive to the received optical SNR (OSNR) and the I/Q imbalance of a CO receiver. These

17

vulnerabilities bring different kinds of difficulties in the system implementation from the single-carrier modulation formats.
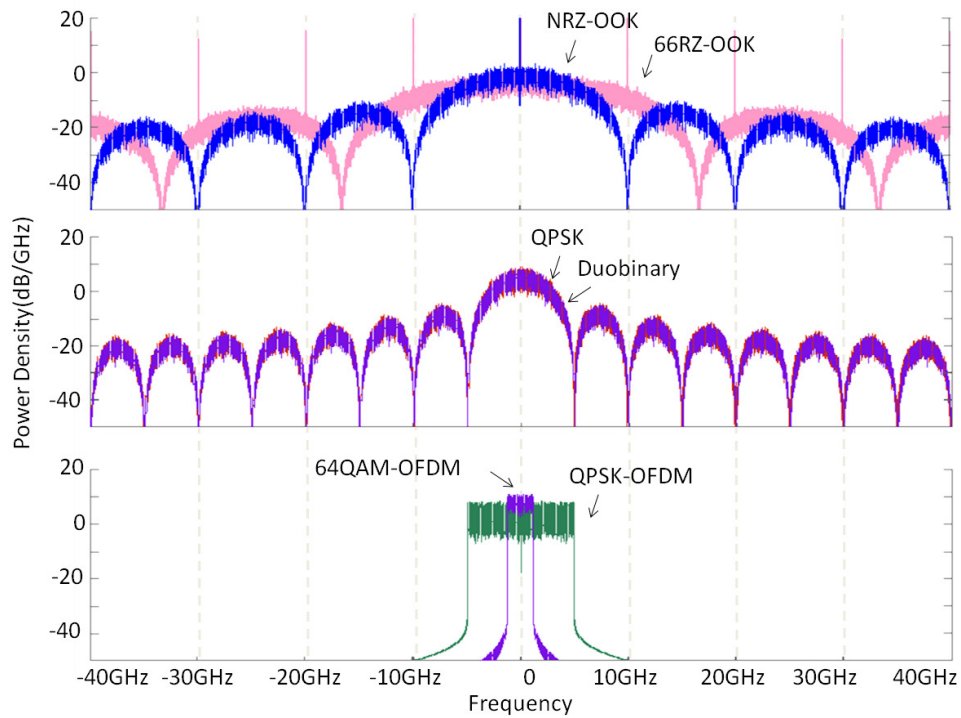
Fig. 2.4. Spectra of single-carrier modulation formats (NRZ-OOK, 66RZ-OOK, QPSK, Duobinary) and multi-orthogonal-carrier modulation formats (OFDM).

2.2 Optical OFDM

2.2.1 Baseband and RF Optical OFDM

Optical OFDM can be used either directly in the baseband or carried by an RF carrier. Optical baseband-OFDM signals have to be detected by a CO receiver in order to extract the I/Q information of the optical phases. Optical RF-OFDM signals first up-convert baseband OFDM signals to the RF band, the I/Q detection of which can be realized by mmWave electronics,

which is usually more stable than a CO receiver, because an mmWave LO has better frequency stability and less phase noise than an LO laser. However, both CO and DDO receivers can be used for the detection of optical RF-OFDM signals. In summary, optical RF-OFDM signals require less complicated optical components in an optical system, but the higher complexity and bandwidth requirement of the electronics are the major drawbacks [31, 32].

Considering the CO detection, if the electric field of an LO laser is normalized to the unity, and the electric field of the incoming optical signals is equal to the baseband OFDM signal $s(t) = r(t)+jx(t)$ at the optical frequency of ω_s, the outputs of a CO receiver can be normalized and rewritten as

$$\tilde{I} = i_{o1} = -x(t)\cos((\omega_s - \omega_{LO})t + \theta) - r(t)\sin((\omega_s - \omega_{LO})t + \theta),$$

$$\tilde{Q} = i_{o2} = r(t)\cos((\omega_s - \omega_{LO})t + \theta) - x(t)\sin((\omega_s - \omega_{LO})t + \theta).$$

(Eq. 2.9)

Here θ represents the phase difference between the LO laser and the signal laser. Note that either of the I/Q components is informative enough to obtain the full OFDM signals if the frequency difference between the signal laser and the LO laser $((\omega_s - \omega_{LO})/2\pi)$ is much higher than the OFDM signal bandwidth. And, the received signals are equivalent to the RF-OFDM signals with an RF carrier at $(\omega_s - \omega_{LO}))/2\pi$. The mmWave down-conversion is then deployed to retrieve the baseband OFDM signal electrically. The difference between CO-RF-OFDM and DDO-RF-OFDM signals is that CO-RF-OFDM signals can use the optical balanced detectors to eliminate the square-law distortion of the photodetectors (PD), while DDO-RF-OFDM signals cannot avoid the distortion from the single-ended PD. When the $(\omega_s - \omega_{LO})/2\pi$ is designed to be zero, the original baseband OFDM signal can be obtained from

$$\tilde{s} = \tilde{I} + j\tilde{Q} = [r(t) + jx(t)]je^{j((\omega_s - \omega_{LO})t + \theta)} = [s(t)]je^{j\theta}. \qquad \text{(Eq. 2.10)}$$

2.2.2 I/Q Imbalance

The OFDM receiver demodulates I and Q components of the incoming signals into two paths either electrically or optically. However, because the o/e efficiency and phase/wavelength of optical components are more sensitive to the environment and the manufacturing process than electrical components, it is very difficult for a CO receiver to have two perfectly identical paths. Any imperfection of the receiver results into the I/Q imbalance [33]. The I/Q detection of a CO receiver can be modeled as the RF down-conversion, as shown in Fig. 2.5. The two paths of the LO have the phase shift of $\Delta\theta$ from orthogonality, and the amplitudes of the I/Q are α and $1-\alpha$ respectively, where $0 < \alpha < 1$. For the CO-baseband-OFDM detection, considering only the OFDM n-th subcarriers, whose subcarrier angular frequency is ω_n, the electric field of the signal laser can be expressed by

$$S(t) = Re[s_n(t)e^{j\omega_s t}] = r\cos((\omega_s + \omega_n)t) - x\sin((\omega_s + \omega_n)t), \quad \text{(Eq. 2.11)}$$

where the n-th OFDM-subcarrier signal $s_n(t) = X_n e^{j\omega_n t} = (r_n + jx_n)e^{j\omega_n t}$. Assuming that after calibration, the LO and signal lasers have an small angular frequency difference $\Delta\omega = \omega_s - \omega_{LO}$, which is smaller than the OFDM subcarrier spacing, then the demodulated complex signal can be derived as

$$\widetilde{s_n} = \tilde{I} + j\tilde{Q}$$

$$= \frac{[\alpha + (1-\alpha)e^{-j\Delta\theta}]}{4} e^{j\Delta\omega t - j\theta}(r_n + jx_n)e^{j\omega_n t} + \frac{[\alpha - (1-\alpha)e^{j\Delta\theta}]}{4} e^{-j\Delta\omega t + j\theta}(r_n - jx_n)e^{-j\omega_n t}. \text{ (Eq. 2.12)}$$
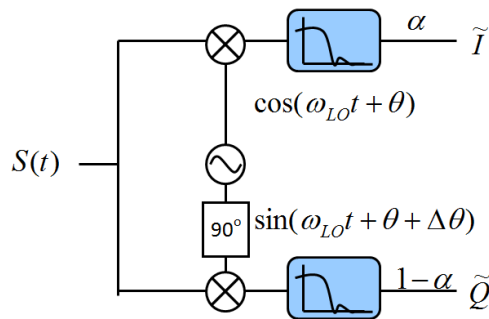
Fig. 2.5.Schematic of an I/Q Imbalanced RF receiver.

20

For simplicity, we first assume that the LO and signal lasers have exactly the same wavelength. The effect of the I/Q imbalance brings an interference to the (-n)-th OFDM subcarrier, as depicted in Fig. 2.6(a). If the data symbol on the n-th and (-n)-th subcarriers are X_n and X_{-n} respectively, the interference from the I/Q imbalance can be expressed as a simple coupling matrix:

$$\begin{bmatrix} \widetilde{X_n} \\ \widetilde{X_{-n}}^* \end{bmatrix} = \begin{bmatrix} A_1 & A_2 \\ A_2{}^* & A_1{}^* \end{bmatrix} \begin{bmatrix} X_n \\ X_{-n}{}^* \end{bmatrix}. \tag{Eq. 2.13}$$

Here we assume that $A_1 = \frac{[\alpha+(1-\alpha)e^{-j\Delta\theta}]}{4}e^{-j\theta}$ and $A_2 = \frac{[\alpha-(1-\alpha)e^{j\Delta\theta}]}{4}e^{j\theta}$. As a result, the original OFDM data can be recovered if this coupling matrix is estimated by the training symbols correctly. However, if the LO and signal lasers have a small wavelength difference, the IQ-imbalanced-induced interference falls into the non-orthogonal frequency, as depicted in Fig. 2.6(b). Instead of inducing ICI on one orthogonal subcarrier, the non-orthogonal-frequency components induce interferences on all the nearby orthogonal subcarriers. This complicates the recovery scheme dramatically. However, the wavelength difference between the LO and signal lasers is ineluctable in a practical CO receiver.

An alternative approach of the CO-OFDM detection is to use an LO laser, whose wavelength is far away from the signal laser, at least away from the highest frequency of the OFDM subcarriers. The frequency difference between the two lasers is the RF in the electrical down-conversion after the CO receiver. As shown in Fig. 2.6(c), the I/Q-imbalance-induced interference falls into the negative frequency, which can be filtered out completely in the digital domain. This approach, also known as CO-RF-OFDM, moves the down-conversion from the optical components to the electrical components. Although the electrical down-conversion also has the I/Q imbalance effect, the frequency tracking in the electrical and digital domain can be much more precise and stable than the laser wavelength drifting.

To wrap up the optical-OFDM detection, the comparisons among CO-baseband-OFDM, CO-RF-OFDM and DDO-RF-OFDM are summarized in Table 2.1. In conclusions, baseband-OFDM signals have the greatest spectral efficiency and simplest receiver design. However,

baseband-OFDM signals require the most complicated DSP to compensate the imperfection of the receiver. On the other hand, RF-OFDM signals require high-frequency mmWave electronics to detect the OFDM signals, but the mmWave electronics are more controllable than the optical components.
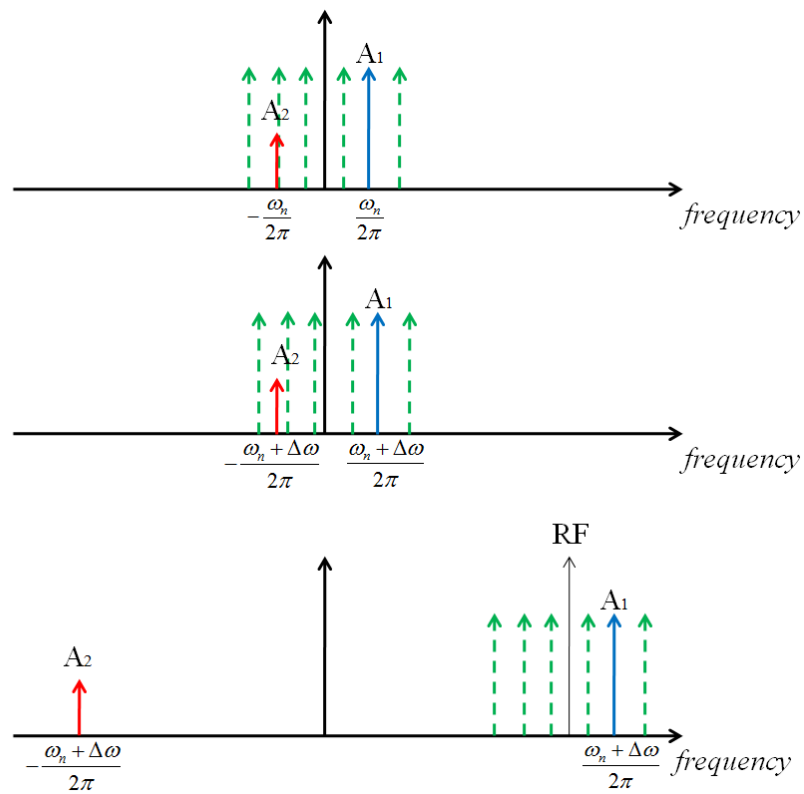
Fig. 2.6. Schematic Spectra of I/Q Imbalanced CO-OFDM signals.

Table 2.1. Comparison of optical OFDM detection.

	CO-baseband-OFDM	*CO-RF-OFDM*	*DDO-RF-OFDM*
Optical Component Bandwidth	Low	High	High
Electrical Component Bandwidth	Low	High	High
Optical Component Complexity	High	Medium	Low
Electrical Component Complexity	Low	High	High
Signal Distortions	Low	Low	High
Optical Spectral Efficiency	High	High	Low
I/Q Imbalance Recovery	Hard	Easy	Easy
Central Frequency Phase Noise	High	High	Low
Central Frequency Offset	High, Unstable	High, Unstable	Low, Stable

2.3 Amplitude-Modulated CO-RF-OFDM

High spectral efficiency, defined by b/s/Hz, is the most important requirement for high-capacity long-haul transmission systems. It allows high-speed data to occupy narrow optical bandwidth. In the past, the 40-THz bandwidth of optical-fiber systems was considered more than enough for data transmission. However, as the Internet grows exponentially in the last decade, the demand for a higher data rate in the backbone network soon occupies the whole bandwidth that SSMFs and EDFAs can offer. For example, the transmission of more than 60-Tb/s in a single fiber was demonstrated by NEC Labs America [11, 34] and NTT Corporation [35]. Hundreds of wavelengths have been deployed to occupy the whole effective bandwidth of SSMF-EDFA spans in these dense WDM (DWDM) systems. It is believed that the only way to

23

increase the data rate further within the limited bandwidth to another extent is to increase spectral efficiency of signals.

Therefore, research interests of long-haul communication systems are now focused on the discovery of different degrees of freedom to increase the spectral efficiency other than the wavelength. For example, a CO receiver enables the detection of optical phases and amplitudes to map data into a 2-dimensional constellation (I/Q). The electric-field orthogonal polarizations of optical wave in the fast axis and the slow axis of optical fibers respectively offer another degree of freedom to carry information without using extra optical bandwidth [36]. The diversity of spatial locations is another dimension to carry information. Various kinds of researches have shown some preliminary results to use spatial multiplexing in the fiber systems [37, 38]. In additional to wavelengths, time, I/Q, and space, OFDM deploys the degree of freedom in frequency.

The main advantage of OFDM in spectral efficiency is that it divides the serial high-speed data symbols into multiple slow parallel data symbols, which are separately carried by closely spaced RF subcarriers. Therefore, unlike the conventional single-carrier modulation, slow data symbols of OFDM signals occupy very narrow bandwidth, and therefore they make OFDM signals have a very compact main lobe in the optical spectrum without spectral sidelobe leakage.

Therefore, to demonstrate the performance and spectral efficiency of a CO-OFDM system, we take full advantage of three technologies to maximize the spectral efficiency: first, the CO detection (the degree of freedom in I/Q); second, the 64QAM-OFDM signal (the degree of freedom in RF); third, the polarization multiplexing (PolMux) technique to double the data rate without additional bandwidth (the degree of freedom in polarizations). The CO-baseband-OFDM transmission is used to maximize the frequency efficiency. In the CO receiver, the CO-RF-OFDM system can be realized by generating the RF carrier in the receiver with a wavelength-shift frequency to improve the transmission performance.

We set up a 70.5-Gb/s PolMux 64QAM CO-RF-OFDM system over a 80-km non-compensated SSMF with the spectral efficiency of 12 bit/s/Hz per subcarrier. The PolMux CO-RF-OFDM experimental setup is shown in Fig. 2.7. In the transmitter, the OFDM signal is modulated to the output of a laser diode (LD) by an IQ Mach-Zehnder Modulator (IQ-MZM). Then, the optical signal is separated into two polarizations (x-pol and y-pol) by a polarization beam splitter (PBS). An optical delay line of two OFDM symbol periods is added to the y-pol path to make the signals of the two polarizations uncorrelated, representing two independent OFDM signals in the two polarizations respectively. Then a polarization beam combiner (PBC) combines the two polarizations and an EDFA amplifies its power before the 80-km SSMF. At the receiver side, an EDFA used as a pre-amplifier first amplifies the received signal power, and an optical band-pass filter (OBPF) is used to remove out-of-band EDFA amplified-spontaneous-emission (ASE) noise. The optical PolMux hybrid can demodulate the PolMux signals by the LO laser into four photodetectors (PDs). In the end, a digital real-time scope captures the instant input and sends the recorded data to a personal computer for the offline process by the LabView interface.
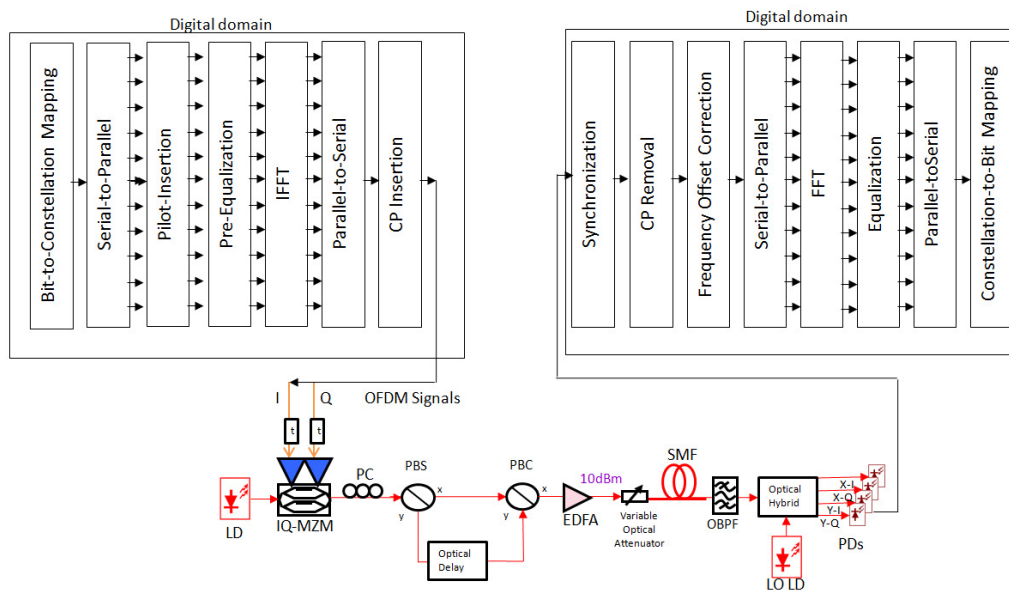
Fig. 2.7. Experimental setup of 70.5-Gb/s PolMux 64QAM CO-RF-OFDM.

The choice of the laser is important because the transmission performance of 64QAM-OFDM signal is very vulnerable to any noise and signal impairment. The phase noise of the laser is one of the most dominant intrinsic noises in CO-OFDM systems. The phase noise comes from the random phase variations between the signal laser and the LO laser. As depicted in Eq. 2.5, the phase noise ϕ_n not only adds phase uncertainty to each subcarrier but also mitigates the subcarrier orthogonality. In general, the laser phase noise can be modeled as the Wiener process, which assumes the differentiation of the phase variation as the probability of the normal distribution [39]. Since the standard variation of the normal distribution determines the laser linewidth, the phase noise of the laser can be estimated from the continuous-wave operation of the laser. Assuming the phase noise is the Wiener process, the full-width-half-maximum laser linewidth ($\triangle v$) is

$$\triangle v = \frac{E\left[|\phi(t+\Delta t) - \phi(t)|^2\right]}{2\pi t}. \qquad \text{(Eq. 2.14)}$$

To estimate the influence of the laser phase noise in the 64QAM CO-RF-OFDM system, we simulated its transmission with various linewidths of both the signal and LO lasers. Table 2.2 shows the OFDM parameters used for the simulation and for the experiments latter. The simulation results of the back-to-back transmission of the 40-dB OSNR are shown in Fig. 2.8. Here the root-mean-square (rms) error-vector magnitudes (EVMs) and the BERs are used as the performance criteria. From the simulation, the linewidth of the laser requires at least 100 KHz to minimize the influence of the laser phase noise. When the laser linewidth is smaller than 100 KHz, the system performance is dominated by the ASE noise in the simulation.

Table 2.2. 64QAM CO-RF-OFDM system parameters.

Transmitter Sample Rate	8GSample/s
Receiver Sample Rate	50GSample/s
FFT Size	128
Number of Cyclic Prefix Samples	4
Number of Data Subcarriers	94
Number of Pilot subcarriers	6
Modulation Format	64-QAM
Number of Training Symbols	4 OFDM Symbols
OFDM Frame Size	104 OFDM Symbols
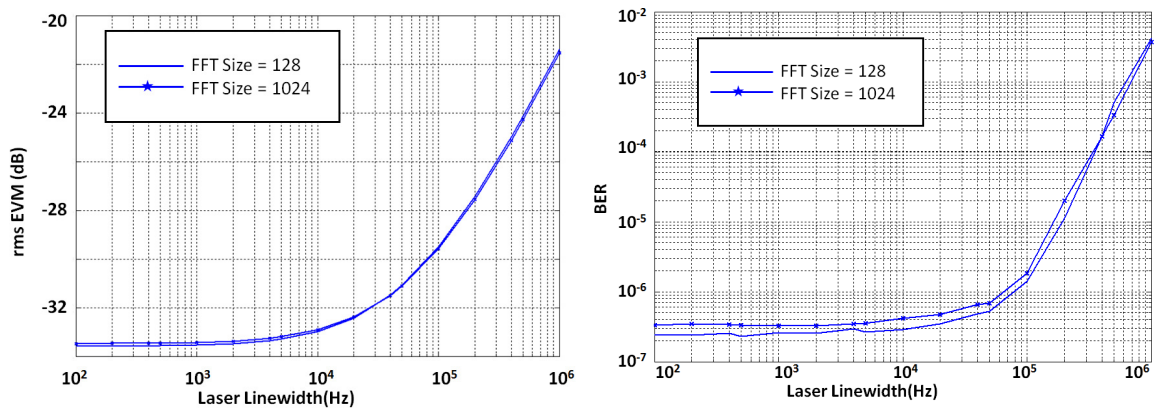
Fig. 2.8. Simulation results of BER versus laser linewidth for 64QAM CO-OFDM systems.

The back-to-back transmission experiment has been done by two types of lasers. One is the slow-light fiber laser (SLFL) of linewidth smaller than 400 Hz, whereas the other is the external cavity laser diode (ECL) of linewidth smaller than 100 KHz. In this experiment, the wavelengths of both lasers are set to be the very close (the CO-baseband-OFDM receiver). No pre-amplifier is used in the receiver, and two single-ended PDs are used with the optical hybrid. The BER measurements are shown in Fig. 2.9. Since there is no pre-amplifier, the OSNR is measured as a constant of 42 dB in the receiver. The best BER measurement is obtained when a single SLFL is used as the signal and LO lasers at the same time. Since the coherent length (>240 km) of the SLFL is much longer than the experimental setup, we can assume that this measurement is phase-noise free and the BER is affected mainly by the ASE noise. The BER of two ECLs is about ten times higher than the phase-noise-free measurement, which agrees with the simulation results.
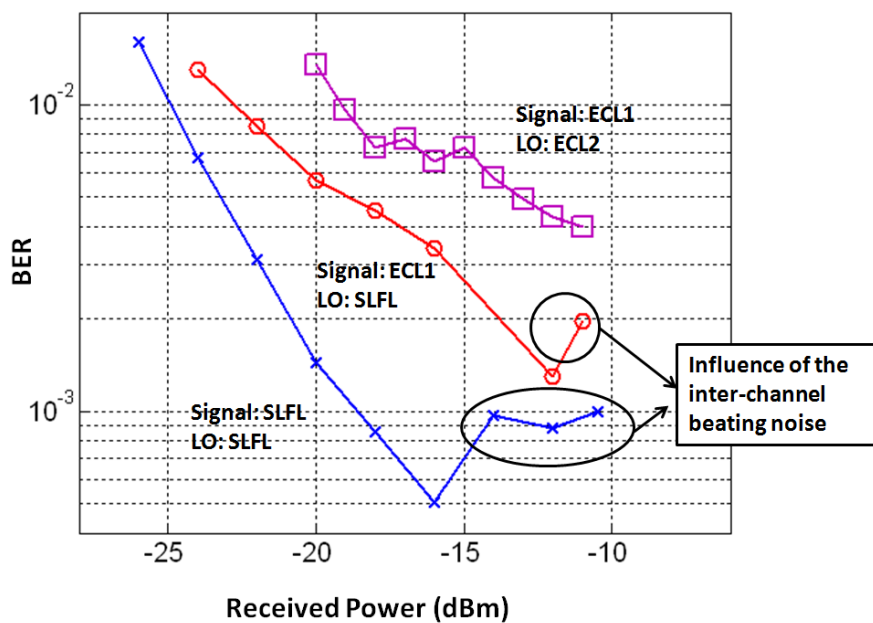
Fig. 2.9. Experimental results of BER measurements in the back-to-back single-polarization 64QAM CO-baseband-OFDM system.

It is worth noticing the inter-channel beating noise caused by the single-ended PD. In this experiment, the BER increases when the received power is too high, as shown in Fig. 2.9. This is due to the inter-channel beating noise of the single-ended PDs in the baseband CO-OFDM. The single-ended PD is a simple, reliable PD commonly used for a DDO system, but it cannot cancel the signal beating from the square law of the semiconductor PD. In the CO system, the influence of the signal beating can be reduced by the ratio of the LO power to the received signal power. For example, if the electric field of the LO is *L* and the electric field of the signal is *S(t)*, the outputs of the two single-ended PDs after the optical hybrid is

$$I_1 = |L|^2 + |S(t)|^2 + 2Re\{L^*S(t)\},$$
$$I_2 = |L|^2 + |S(t)|^2 - 2Im\{L^*S(t)\}. \qquad \text{(Eq. 2.15)}$$

When *L* >> *S(t)*, the second term, $|S(t)|^2$, which is the source of inter-channel beating, can be negligible. However, when the received power is too high, the BER performance of CO systems is affected by the beating noise. For CO-baseband-OFDM systems, since the beating noise results from the beating between adjacent channels, the subcarriers of lower frequencies suffer from more beating interferences than the subcarriers of higher frequencies. As shown in Fig. 2.10, if we divide the first 50 data subcarriers, including the pilots, into different groups and observe their symbol error rate (SER) separately, the high-frequency subcarriers have more errors because the channel frequency response is low at high frequency and therefore their OSNR is low. However, the low-frequency subcarriers also have more errors even their OSNR is very high because of the inter-channel beating noise. Optical balanced receivers can be used to cancel this beating noise. However, if the system cost is of major concern, a CO-RF-OFDM system can be deployed to mitigate the inter-channel beating noise because all the subcarriers are up-converted to the RF band that is away from the low-frequency band.

To further increase the SNR of high-frequency OFDM subcarriers, the pre-equalization can be used in the OFDM transmitter. For wideband OFDM signals, it is very difficult to have a flat channel. High-frequency subcarriers suffer from higher channel attenuation and have lower SNR. Although optical fiber has a very wide and flat frequency response, the electronics

29
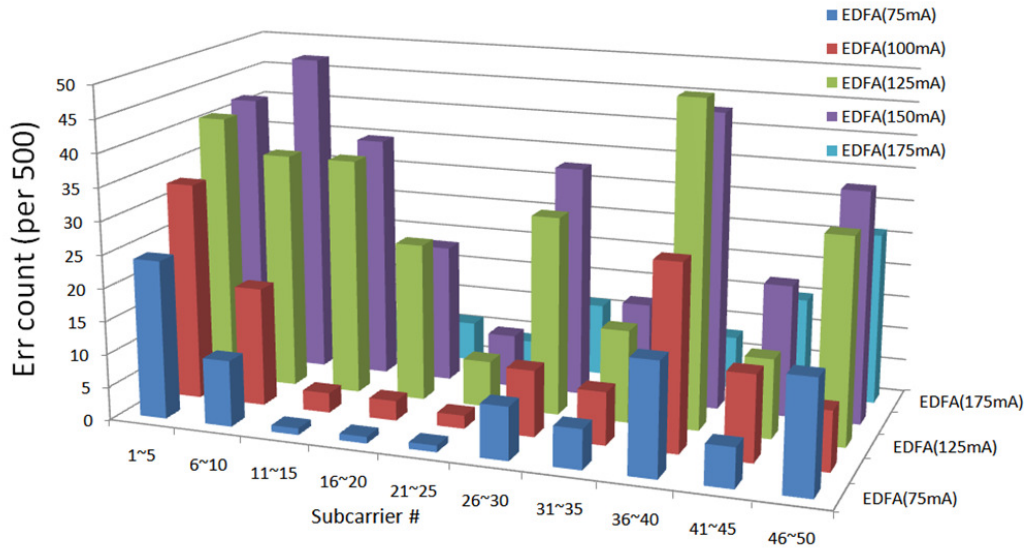
Fig. 2.10. Experimental results of the errors for different OFDM subcarriers by using single-ended PDs.

components, the WDM filters, and the o/e interfaces are all band-limited. For CO-OFDM systems, the subcarriers with higher frequencies usually have lower power at the output of the optical transmitter. Using the zero-forcing equalization in the OFDM receiver can recover the frequency-dependent attenuation:

$$\hat{X}_k = \hat{H}_k^{-1} H_k X_k + \hat{H}_k^{-1} W_k. \qquad k = -K, -K+1, \dots K \qquad \text{(Eq. 2.16)}$$

However, in the ASE-noise-dominant condition, this post equalization also increases the noise. Even when the overall OSNR is kept high in the optical system, the subcarriers of low-frequency responses have much worse BER performance than the subcarriers of high-frequency responses because of the zero-forcing equalization.

To amend the damage from the frequency-dependent attenuation, the digital pre-equalization can be added in the transmitter. Assuming that the frequency response of the overall CO-OFDM system is known, more power can be added to the low-frequency-response

30

subcarriers in the digital domain to compensate the attenuation in the system. As a result, the output power of each OFDM subcarrier can be designed to be equal at the output of the transmitter (Fig. 2.11). Once the ASE noise is added in the EDFA, all subcarriers will have equal OSNR levels without losing any high-frequency subcarrier in the noise floor.
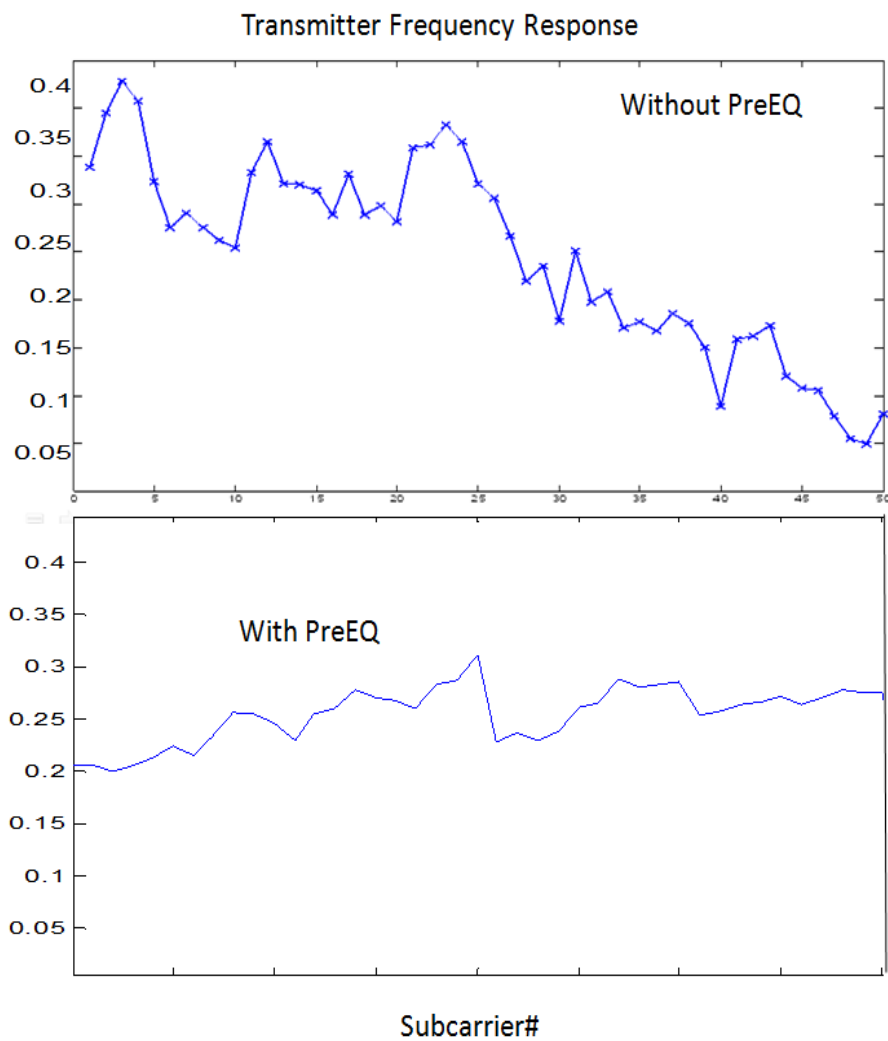
Fig. 2.11. Measurements of the frequency responses of the OFDM transmitter with or without pre-equalizations.

Applying the pre-equalization technique, the experimental results of the PolMux 64QAM CO-RF-OFDM transmission are shown in Fig. 2.12. The launched power is controlled by the variable optical attenuator (VOA). The wavelengths of the LO and signal ECLs are separate from 7.5 GHz. The RF down-conversion is done in the digital domain. A PolMux optical hybrid with four optical balanced receivers is used to demodulate the duo-polarization signals. Figure 2.13 shows the side-by-side comparison of the measured BERs of the back-to-back and the 80-km-SSMF transmission. The lowest BER after 80 km is well below the 7%-overhead forward error correction (FEC) limit (4.5×10^{-3}). There is almost no OSNR penalty after 80 km, because the OFDM signal is intrinsically resistive to the fiber dispersion effect. However, after the 80-km SSMF, the nonlinear effect dominates the system impairments when the launch power is higher than 0.0 dBm. Although the OSNR increases with the launch power, the BER performance degrades when the launch power is too high. The achieved raw data rate is 70.5 Gb/s. Taking into account the 7% FEC overhead, 4/132 cyclic prefix, and 4/104 OFDM training overhead, the net transmission data rate is 62.43 Gb/s within 6.25 GHz optical bandwidth. Therefore, the net spectral efficiency of the PolMux 64QAM CO-RF-OFDM system is 9.99 bit/s/Hz.

This preliminary experiment proves the possibility of extremely high spectral efficiency of CO-OFDM signals, but there is still plenty of space for improvement. For example, the overhead can be dramatically decreased by adopting better frequency-offset-correction algorithms [30] without compromising the transmission performance. The BER is limited mainly by the laser phase noise and can be improved by phase-noise-compensation algorithms [11]. As the optical OFDM modulation and demodulation becomes more and more mature, the main trend of future research will also start to focus on the practical implementation of the real-time CO-OFDM receiver.
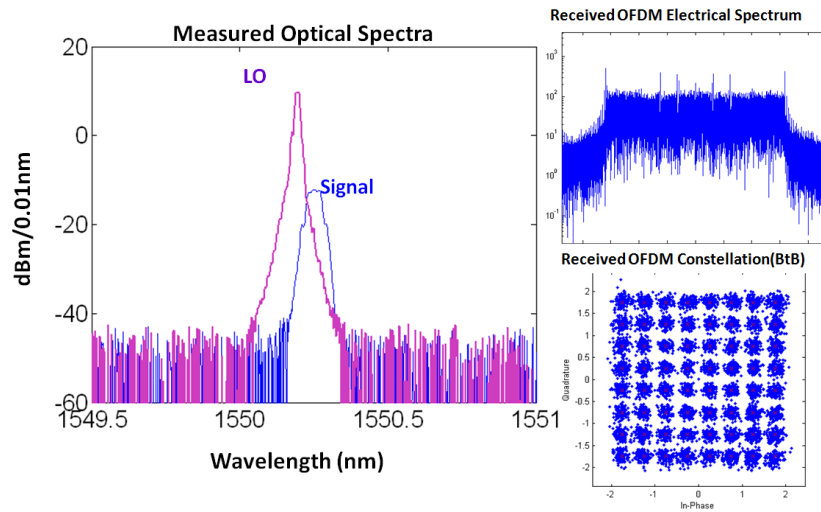
Fig. 2.12. Experimental results of the PolMux 64QAM CO-RF-OFDM system.
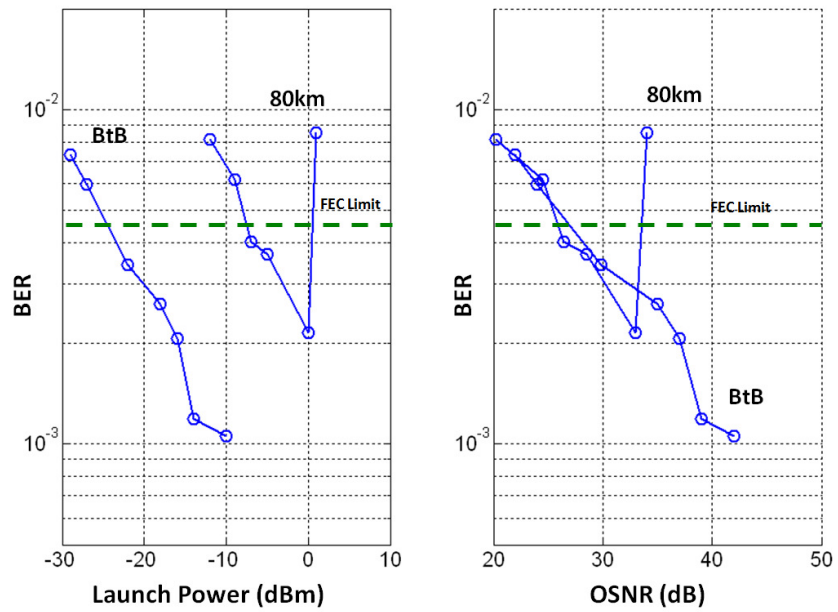
Fig. 2.13. BER measurements of the PolMux 64QAM CO-RF-OFDM system.

33

2.4 Phase-Modulated DDO-RF-OFDM

In additional to facing lower inter-channel beating noise when being detected by single-ended PDs and having better I/Q-imbalance management, RF-OFDM has another unique feature, which baseband-OFDM is unable to compete. That is, RF-OFDM can be directly detected by DDO receivers, which are much more inexpensive and more resistant to the laser phase noise than CO receivers. However, DDO-RF-OFDM does not have as high spectral efficiency as baseband-OFDM, but DDO-RF-OFDM still carries on the advantages of OFDM signals in the flexibility of a dynamic time-frequency allocation, FDE feasibility, and dispersion resistance. Therefore, DDO-RF-OFDM is still a powerful modulation schemes in the systems that spectral efficiency is not extremely demanding, such as passive-optical-network (PON) access systems [40, 41] or low-cost long-distance transmission systems [42].

Although OFDM gains great advantages for its effortless dispersion compensation, OFDM signals suffer from its high PAPR, which results into the inevitable nonlinear distortion in the optical communication systems. The waveform of an OFDM signal is similar to an analog waveform rather than a digital waveform, which has a discrete power level. Therefore, it requires much higher amplifier linearity than other single-carrier digital signals. However, after propagating through tens of SSMF-EDFA spans, the accumulated nonlinear effects inside the SSMF make the linearity requirement very difficult to satisfy.

There are two major nonlinear mechanisms that can cause the signal distortions in the SSMF-EDFA span: NLO and the gain saturation. The NLO effect mainly originates from the long SSMF. It takes place when the optical power inside the SSMF is too high and the transmission distance is too long. Its behavior can be modeled by the nonlinear Schrodinger equation. The gain saturation is induced in the EDFA. The amplification of an EDFA relies on the doped Er^{3+} atoms, which are pumped to the upper-energy level by the pump light. The coherent photons are then generated from these upper-energy-level atoms by the stimulated emission of the input photons. When the number of the input photons is low, the amplifying gain is constant and the population of the upper-energy-level atoms is high. A majority of these idling

34

upper-energy-level atoms hence spontaneously decay to the lower-energy level and radiate photons with random phases. Then, these photons start to multiply by the stimulated emission, generating the unwanted ASE noise. Therefore, the average input power of the EDFA is required to be high enough to saturate the EDFA. In the saturation region, the population of the upper-energy level atoms is depleted so fast that the ASE noise has little chance to be generated. However, when the pump light is incapable of replenishing the upper-energy-level atoms in time, the EDFA gain starts to saturate.

In this situation, if the PAPR of the input signal is high, peak-power signals may not retrieve enough EDFA gains in the saturation region, while medium- or low-power signals can still have the same gain. When the EDFA gain decreases with the increase of the input power, it will cause the clipping effect of high-PAPR signals. Reducing the average input power can prevent the clipping effect of the peak-power signals, but the OSNR of the low-power signals is reduced accordingly because of the ASE noise. The EDFA amplification process can be modeled by the rate equation of a two-level energy system [43]. As shown in Fig. 2.14, the simulation of this rate equation shows the relation between the EDFA gain and the input power. Increasing the pump power can increase the replenishing rate of the upper-energy-level atoms and the EDFA linearity. However, if the PAPR of the input signal is too high, the output signal may still be clipped to cause nonlinearity.
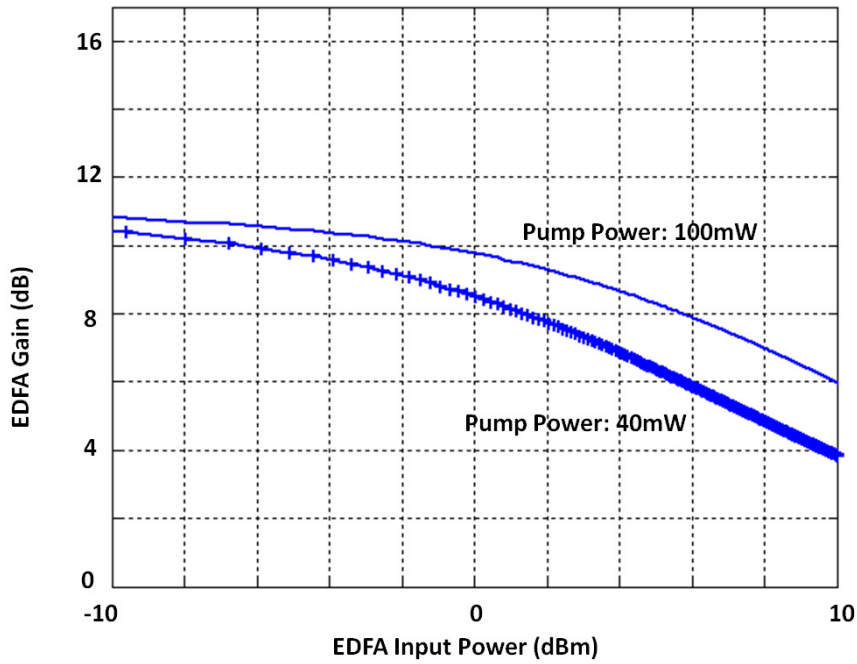
Fig. 2.14. The VPI simulation results of the EDFA gain versus the input power based on the rate equation. The simulation parameters: fiber length: 6m; Lifetime: 0.01s; Er^{3+} concentration: 2.5×10^{24} m^{-3}; fiber core radius 1.5×10^{-6}m; background loss: 0.03 dB/m; backward pumping wavelength: 980 nm.

Many research groups suggest remedying the nonlinear effect by maintaining the relative low power of each OFDM subcarrier in the long-distance transmission system [44 – 47]. However, the operation of the EDFA with low input power results into the increment of its noise figure and the degradation of the lower-power-subcarrier OSNR. Some groups suggest using DSP to reduce the OFDM PAPR in the digital domain [48, 49], while others suggest to use redundant lasers to saturate the EDFA and to reduce the clipping effect of the specific optical channels [50]. Although the DSP-based PAPR reduction scheme can lower the PAPR of OFDM signals in the beginning, the PAPR will increase back soon after the OFDM subcarriers walk off because of the fiber chromatic dispersion. Using redundant lasers may increase the cost and power consumption of the optical OFDM system.

36

To alleviate the nonlinear effects in a cost-effective way, phase-modulated OFDM (PM-OFDM) signals can be utilized with an RF carrier. The phase modulation of the optical signals results into the uniform-power transmission, paying the drawback of occupying broader bandwidth. Without the variation of optical power, all the EDFAs can be operated in the saturation region without worrying about the clipping effect. In [51], it is mentioned that the PM-OFDM can also have better tolerance of the 2nd- and the 3rd-order NLO effects in the SSMF. That is, the tolerance of the input power of PM-OFDM signals is higher than intensity-modulated OFDM (IM-OFDM) signals in the SSMF-EDFA spans. To look into the NLO effects, we simulate the optical OFDM transmission with the fixed power of the transmitter, but we change the output power of the EDFA in each 80-km SSMF-EDFA span. The system performance is evaluated by the received signal EVM of the 10-Gb/s QPSK-OFDM constellation. Figure 2.15 shows the simulation results of the PM-OFDM and the IM-OFDM signals after fifteen 80-km SSMF-EDFA spans. Each EDFA has the same noise figure of 4.0 dB and is assumed to have the perfect linearity. In this simulation, the PM-OFDM system tolerates higher input power in the SSMF than the IM-OFDM system. The NLO effects start to dominate and distort the signal after 2.0-dBm EDFA output power in the IM-OFDM system. The PM-OFDM system can tolerate the EDFA output power up to 5.0 dBm.

The experimental setup of the PM-OFDM transmission system is shown in Fig. 2.16. The baseband OFDM signal is first up-converted to the RF band and then modulated onto the output of the ECL by a lithium-niobate optical phase modulator (PM). According to the Jacobi-Anger expansion, the normalized electric field of the output signal can be expressed by the summation of multiple optical carriers spaced with RF:

$$e^{jx(t)\cos(\omega_{RF}t)} = \sum_{n=-\infty}^{\infty} j^n J_n\big(x(t)\big)e^{in\omega_{RF}t}, \qquad \text{(Eq. 2.17)}$$

where x(t) represents the original complex OFDM signal; ω_{RF} is the angular frequency of the RF; and $J_n(.)$ is the n-th order Bessel function of the first kind. If we intentionally lower the modulation index of the PM, $J_n(.)$ can be approximated by
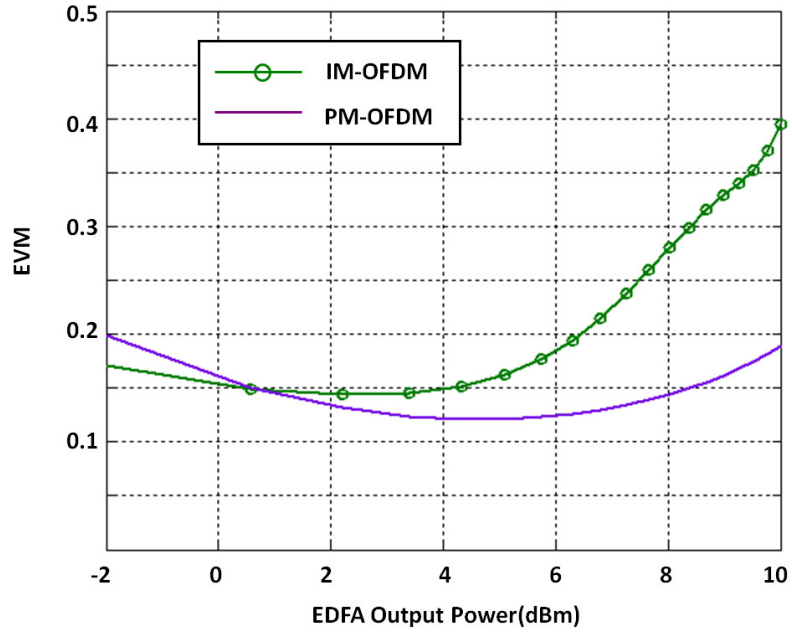
Fig. 2.15. The VPI simulation results of the EVM versus the EDFA output power in 15 80-km SSMF-EDFA spans. The 10-Gb/s OFDM signal is composed of 256 subcarriers of QPSK symbols.
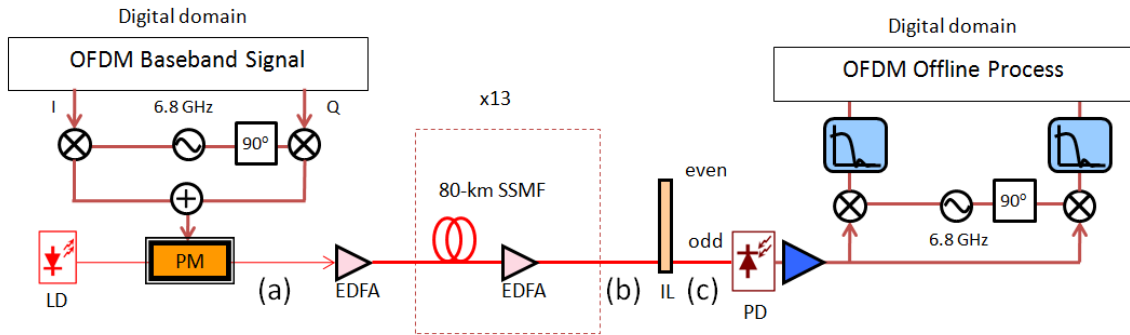
Fig. 2.16. Experimental setup of the 1040km transmission of 10-Gb/s optical PM-OFDM signal.

$$J_n\big(x(t)\big) = \frac{1}{2^n n!}\, x(t)^n \qquad\qquad \text{(Eq. 2.18)}$$

38

As implied by Eq. 2.17, the power of the PM-OFDM signal is constant through the fiber transmission system. The PM-OFDM signal can be demodulated either by a CO or a DDO receiver. To simplify the OFDM receiver, the DDO-RF-OFDM demodulation is demonstrated in the experiment with an additional OBPF. In the experimental setup, the optical interleaver (IL) is used as the OBPF to select the zeroth- and the first-order optical carriers, which are then detected directly by the single-ended PD. The output current of the PD can be expressed by

$$\left| 1 + \frac{j}{2} x(t) e^{j\omega_{RF}t} \right|^2 =$$

$$\left(1 + \frac{|x(t)|^2}{4} \right) - (Re\{x(t)\} \sin(\omega_{RF}t) + Im\{x(t)\} \cos(\omega_{RF}t)). \qquad \text{(Eq. 2.19)}$$

Considering the signals in the RF band, the output current of the PD is proportional to the transmitted RF-OFDM signal. The inter-channel beating noise caused by the first term can be avoided by increasing the frequency of the RF carrier.

In the experiment, the RF band is centered at 6.8 GHz, and the baseband OFDM signal occupies the total bandwidth of 6.25 GHz, delivering the effective data rate of 10.58 Gb/s. The measured spectra of the generated multiple optical carriers after the PM are shown in Fig. 2.17(a). In the transmission system, each 80-km SSMF has an average loss of -17dB. All the EDFAs are operated in the saturation region of the output power of 10 dBm. After 13 SSMF-EDFA spans, the ASE noise submerges all the low-power, high-order optical carriers (Fig. 2.17(b)). The DDO receiver uses the 25-GHz/50-GHz IL to extract the zeroth- and the first-order optical carriers. Although the unwanted second-order optical carrier also passes through the optical interleaver (as shown in Fig. 2.17(c)) because the passband of the interleaver is too wide, the effect of the second-order optical carrier is negligible as long as it is much smaller than the central carrier (the zeroth-order optical carrier). The output signal of the interleaver is detected by the single-ended PD and then down-converted by the RF electronics. The baseband OFDM signal is recorded and demodulated by the Tektronix 40-GSample/s real-time digital oscilloscope. The measured BERs versus OSNRs are depicted in Fig. 2.18. After the 1040-km-SSMF transmission, the measured

OSNR is 12.8 dB, and the measured BER is 1.1×10^{-3}, which is below the 7%-overhead FEC requirement of 4.5×10^{-3}.
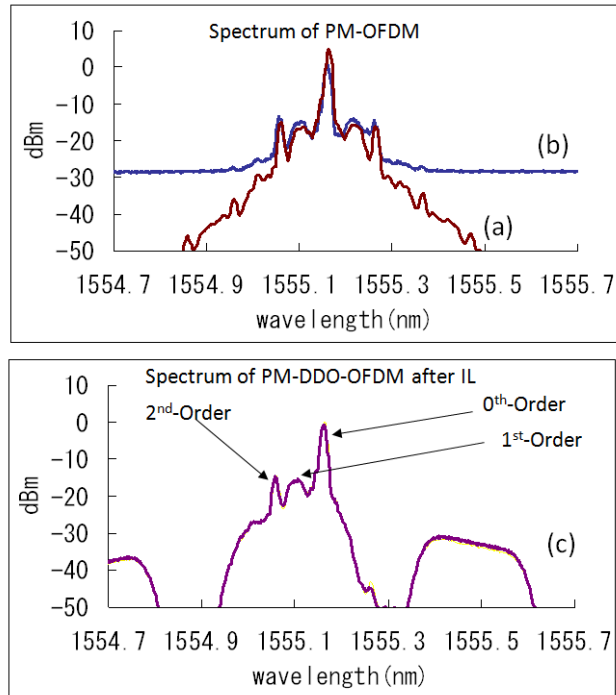
Fig. 2.17. Measured spectra of the experimental PM-OFDM system (a) at the output of the PM-OFDM transmitter; (b) after the 1040-km SSMF; (c) after the IL.
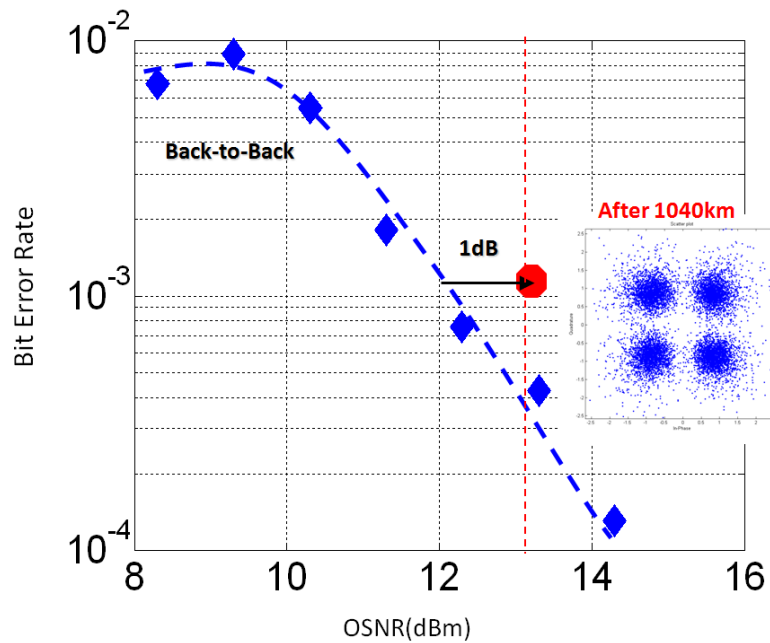
Fig. 2.18. The plot of the BER measurements versus the received OSNR of the PM-OFDM system. The inset shows the QPSK constellation after 1040-km with the OSNR of 12.8 dB.

In comparison against the bandwidth of other optical OFDM signals using the same RF and the same modulation formats, single-sideband (SSB) IM-DDO-RF-OFDM signals occupy the optical bandwidth of around 10 GHz, while the proposed PM-DDO-RF-OFDM signals occupy the total optical bandwidth of 27.2 GHz. When the same data rate is transmitted by CO-baseband-OFDM signals, the occupied bandwidth is 6.25 GHz. Therefore, the PM-OFDM transmission is not considered suitable for a bandwidth-limited optical system. In addition, the PM-OFDM signals use redundant optical carriers to keep the optical power constant. However, the extra optical power does not contribute to the received OFDM power of the PD and therefore it lowers the DDO receiver sensitivity.

Although the PM-OFDM signals occupy more bandwidth than the other OFDM modulation schemes, it exhibits better NLO tolerance in the optical fibers. Compared with the CO-OFDM system, the PM-DDO-RF-OFDM system only requires simpler optical transmitters and receivers. In conclusion, for an optical system of adequate bandwidth, such as ITU-grid DWDM or PON systems, PM-OFDM provides a costless transmission scheme of high flexibility, reliability and fine performance.

2.5 Orthogonal-Wavelength-Division Multiplexing

OFDM is at a great advantage in spectral efficiency and dispersion resistant in the long-distance transmission over other single-carrier modulation formats. However, OFDM also has its disadvantage in a high PAPR and complexity. In a WDM system, because of the random wavelength drifting of each laser, the closest wavelength spacing of any two lasers is restricted. That is, the spectral efficiency of WDM systems is limited even when using the compact spectrum of OFDM signals. In addition, the complexity and the latency of OFDM modulation and demodulation are fairly high. Although the data transmission of a single FFT modulator has been experimentally demonstrated up to 294 Gb/s in the offline process [11], the FFT processing capability of a real-time CO-OFDM receiver has achieved no more than 4 Gb/s [52]. The latency and high complexity of FFT is durable in ultra-long-haul systems since their power budget is sufficient and the latency is dominated by the fiber transmission delay. However, the applications of OFDM are hence restricted from access networks and some cost-effective transmission systems for its high latency and high cost.

An alternative way to generate multiple-orthogonal-carrier signals is to use the optical frequency comb generation. Using an optical circulating loop or a phase modulator, multiple orthogonal optical carriers can be generated from one laser by an electrical LO [53, 54]. The wavelength spacing between each optical carrier is strictly fixed by the LO frequency. This is essential to preserve the orthogonality of the optical carriers. Instead of using IFFT to multiplex these carriers, the orthogonal optical carriers can be individually modulated at the symbol rate up

to the LO frequency without ICI. Because the modulation method is similar to WDM, it is sometimes named as orthogonal wavelength-division multiplexing (OWDM) [55, 56], or coherent WDM [57, 58]. On the other hand, because its spectral usage is equivalent to OFDM but is generated by all-optical modulation methods, it is sometimes called all-optical OFDM [54, 59-61].

The multiplexing of an OWDM super-channel is straightforward. For example, as shown in Fig. 2.19, a five-orthogonal-carrier OWDM super-channel can be generated by a PM, an LO, and an optical arrayed-waveguide-grating (AWG) filter. Then each orthogonal optical carrier is individually modulated to form spectrum-overlapped sub-channels. On the other hand, demultiplexing the OWDM sub-channels is challenging. A narrow Nyquist filter can be used to demultiplex each OWDM sub-channel, but the interference from adjacent sub-channels limits the signal BER performance [58]. Using digital FFT demultiplexing to eliminate this interference can be realized in a CO receiver. However, a 1x2 FFT demultiplexer requires the sampling speed twice as fast as the sub-carrier spacing and a 1x4 FFT demultiplexer requires four times. As a result, a digital OWDM demultiplexer requires super-high speed ADCs in the CO receiver, which increases the OWDM system cost and complexity dramatically, because the orthogonal-carrier spacing cannot be too small for the coarse AWG resolution.
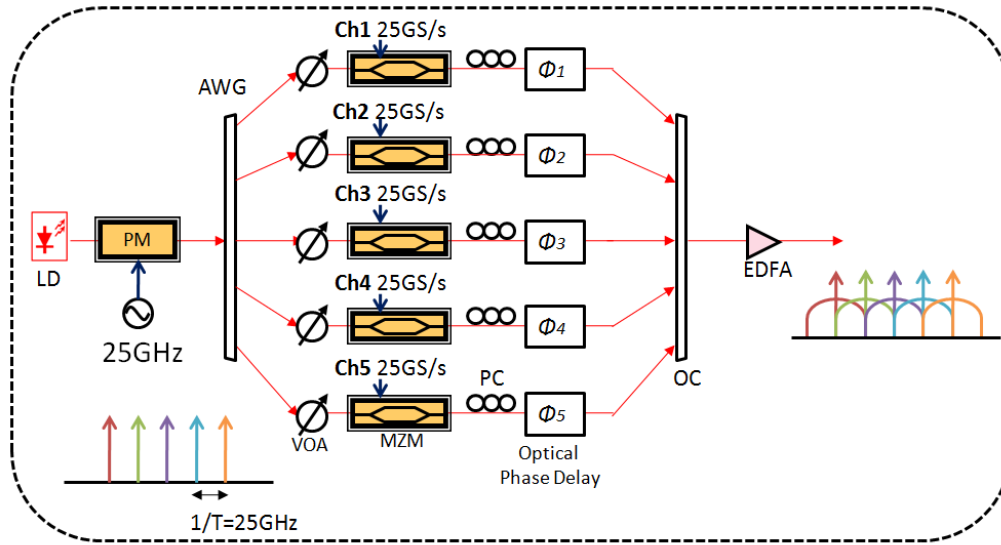
Fig. 2.19. Schematic of a 5-sub-channel 25-GHz-spaced OWDM multiplexer.

Another approach is to utilize an optical demultiplexer composed of delays and couplers. As shown in Fig. 2.20, a Mach-Zehnder delay interferometer (MZ-DI) is composed of two optical paths with a delay T. The output of the MZ-DI is actually equivalent to having the 1x2 FFT process on the input optical electric field. In other words, the OWDM sub-channels can be separated into the even output and the odd output by the MZ-DI when the OWDM orthogonal-carrier spacing is half of the MZ-DI free spectral range (FSR). Afterwards, the receiver can use an OBPF to filter out other unwanted sub-channels to detect the specific sub-channel. Similarly, the optical demultiplexer can be extended to 1x4, 1x8, and so on by adding more delay lines and couplers to perform the optical FFT processing [59, 62]. However, there is a tradeoff between the FFT size and the post-OBPF bandwidth, which can limit the performance of the OWDM signals. In the following sections, we would like to investigate the mechanisms and fundamental limitations of the OWDM optical demultiplexing.
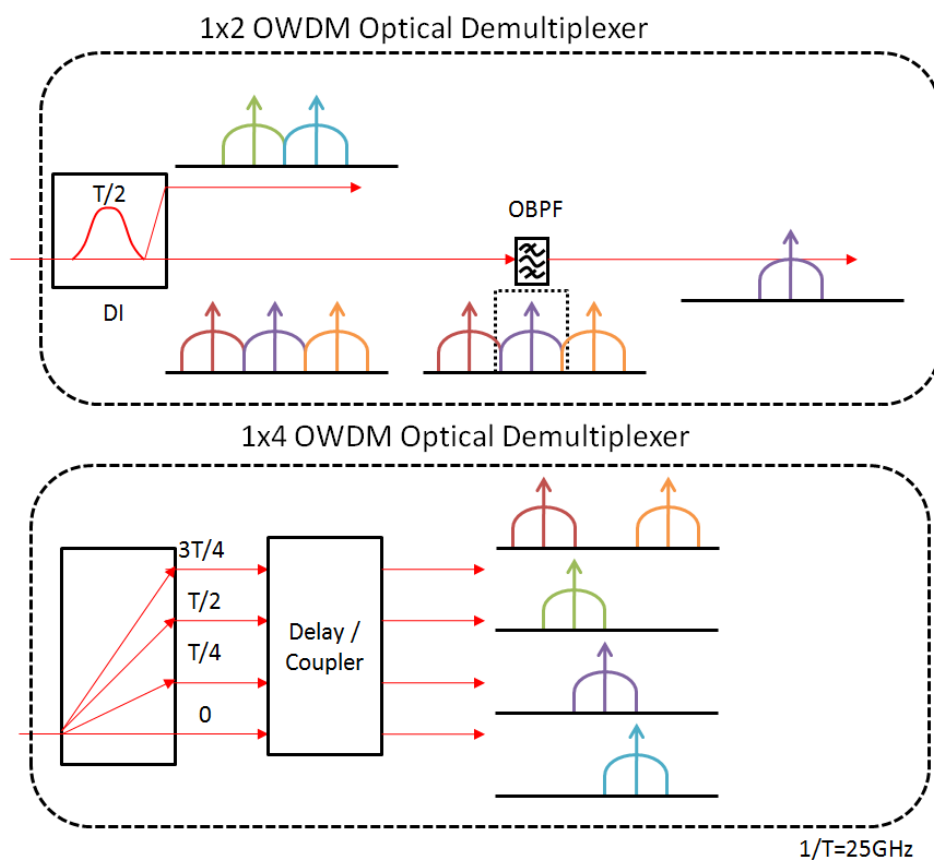
Fig. 2.20. Schematic of OWDM optical demultiplexer.

2.5.1 Coherent Detection and Synchronization

The negative effect of an OWDM optical demultiplexer mainly arises from the time delay required for the optical FFT process. Take a 1x2 OWDM optical demultiplexer, a MZ-DI, for example, as shown in Fig. 2.21. First of all, assuming there are only two incoming sub-channels (even and odd) at frequencies ω_0 and $\omega_0 + 2\pi/T$ going to the optical demultiplexer, carrying the complex data sequence $\{x_0, x_1\}$ and $\{y_0, y_1\}$ respectively. The half-a-bit delay causes the overlap of the current signal with the previous signal, forming a transition signal of one half of the symbol length.
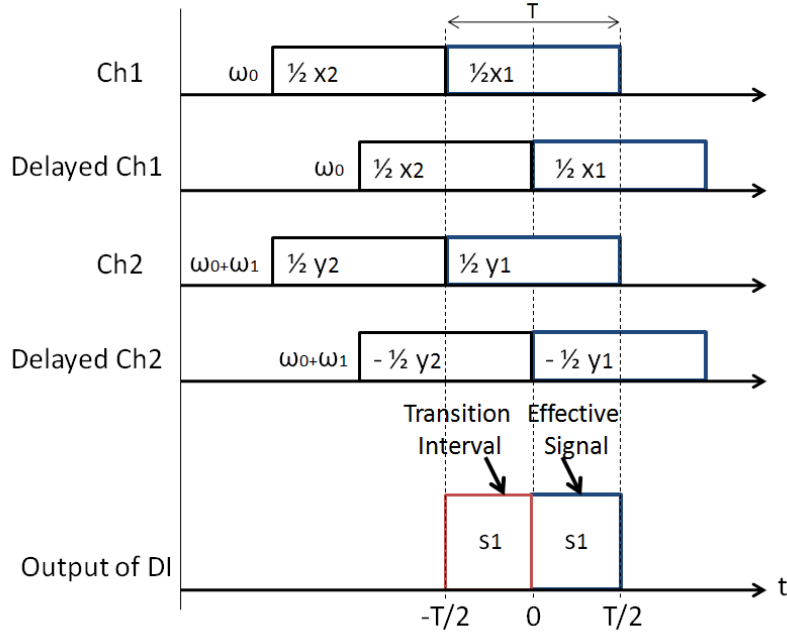
Fig. 2.21. Plot of the signal behavior in a 1x2 OWDM optical demultiplexer of two OWDM sub-channels.

One output of the optical demultiplexer can be divided into two parts: the effective signal of the half-a-bit length as

$$s_1(t) = x_0, \qquad\qquad 0 < t < T/2 \qquad\qquad \text{(Eq. 2.20)}$$

and the transition signal of the superposition of the current signal $\{x_0, y_0\}$ and the previous signal $\{x_1, y_1\}$ as

$$s_1(t) = \frac{1}{2}(x_0 + x_1) + \frac{1}{2}(y_0 - y_1)e^{j\frac{2\pi}{T}t + j\phi}, \qquad -T/2 < t < 0 \qquad \text{(Eq. 2.21)}$$

where ϕ is the phase difference of the two channels. Here we assume that the coherent receiver can distinguish their polarizations ideally, so only the electric fields of the same polarization are taken into account. For simplicity, the receiver frequency response is treated as infinite flatness. Even with such an ideal condition, the demultiplexed signals still suffer from severe jitters, which narrow the effective signal eye width. This eye narrowing effect increases in accordance

46

with the FFT size of the OWDM optical demultiplexer. Figure 2.22 shows the calculated eye diagrams of a 2-channel and a 4-channel binary phase-shift keying (BPSK) OWDM signals. The transition-signal region contains the slow signal transition of the desired channel and the interference of the adjacent channels. The increase of the demultiplexer FFT size narrows the temporal length of the effective signal proportionally.
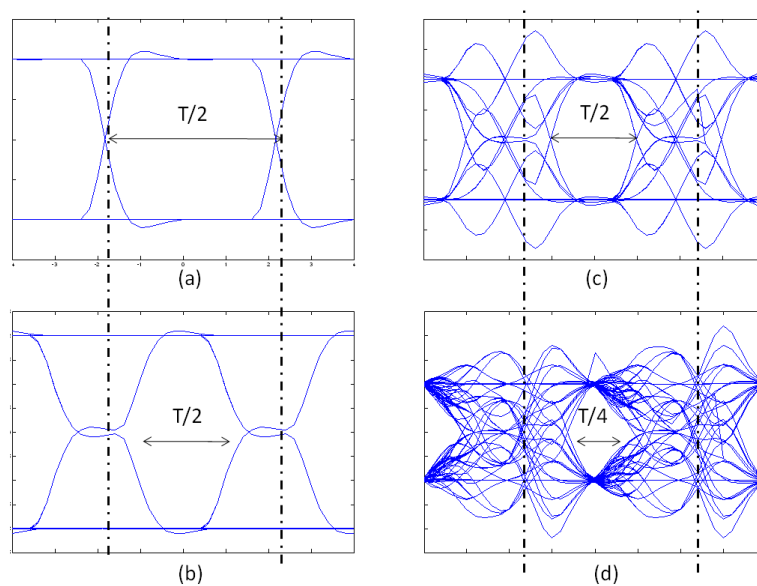
Fig. 2.22. Calculated eye diagrams of the input and output signals of OWDM optical demultiplexer: (a) the transmitted BPSK signal on each sub-channel individually; (b) the 1x2 demultiplexed signal when there is only one sub-channel transmitted; (c) the 1x2 demultiplexed signal when there are two sub-channels transmitted; (d) the 1x4 demultiplexed signal when there are four sub-channels transmitted.

As a result, increasing the FFT size of an OWDM optical demultiplexer makes the signals more vulnerable to fiber chromatic dispersion and filter bandwidth. Halving an eye width also indicates that the required receiver bandwidth becomes twice. Moreover, it makes both the optical transmitter and the optical receiver require more rigorous synchronization/sampling clock

precision. When there is an offset between the adjacent channels, the transition signal of each channel is no longer perfectly aligned. It further shortens the effective symbol length. As shown in Fig. 2.23, the Q-factor reaches a minimum when the adjacent channel has a signal offset of 0.5 symbol length, and returns to a maximum when the offset is exactly one symbol length because the transition signals of the two sub-channels are aligned in time again.
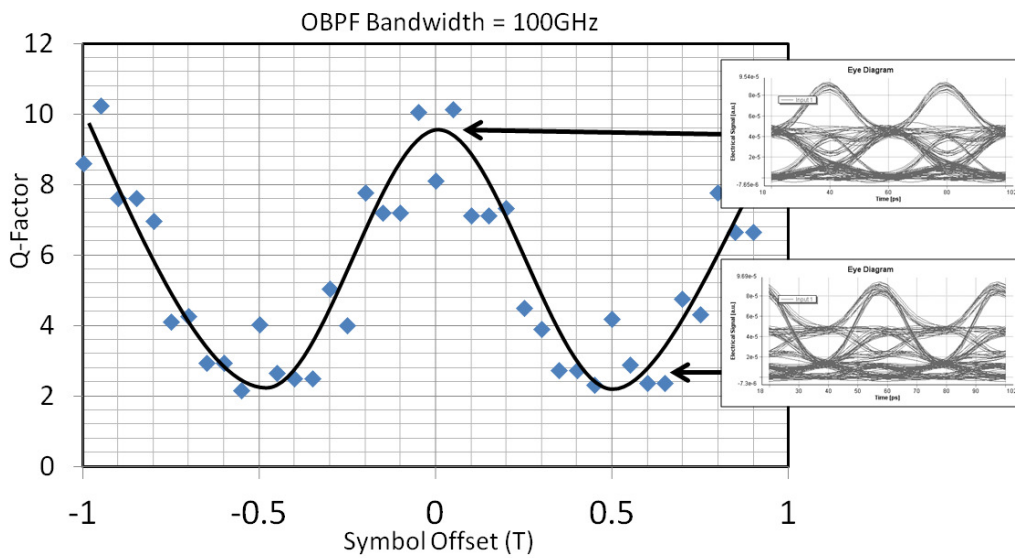
Fig. 2.23. Simulated Q-factors versus the symbol offset of two adjacent OWDM sub-channels.

Even for OWDM digital demultiplexers, the influence of synchronization/sampling offset is significant because FFT process has to be valid only if the sampling points of every sub-channel are within the same symbol. If synchronization offset causes the sampled points belonging to different symbols, then the FFT process will fail. CP can be used to improve the synchronization tolerance. However, increasing the FFT size in OWDM digital demultiplexers increases the synchronization requirement as well as OWDM optical demultiplexers. Even with an ideal coherent receiver, the FFT size of OWDM demultiplexers should be small. In addition, chromatic dispersion effects have to be taken care of before the OWDM demultiplexing.

48

Therefore, the OWDM optical demultiplexing is usually achieved only by a 1x2 OWDM demultiplexer followed by a digital lowpass filter (LPF) for OWDM digital demultiplexers or by an OBPF for OWDM optical demultiplexers.

2.5.2 Direct Detection and Filtering Effect

For a more general situation, consider there are three orthogonal sub-channels (Ch1, Ch2, and Ch3) carrying three independent complex data sequences ($\{y_n\}, \{x_n\}, \{z_n\}$) respectively. Assuming the central frequencies of Ch1, Ch2, and Ch3 are at $\omega_0 - 2\pi/T$, ω_0, and $\omega_0 + 2\pi/T$ respectively, a MZ-DI is used to separate Ch2 from the other two adjacent sub-channels. Similar to the coherent receiver, the output of the PD can be divided into two parts: the effective signal and the transition signal. For example, the effective signal of Ch2 at $n = 0$ of a DDO receiver contains

$$s_2(t) = |\vec{x_0}|^2. \qquad\qquad 0 < t < T/2 \qquad\qquad \text{(Eq. 2.22)}$$

The transition signal is composed of

$$s_2(t) = S_1 + S_2 + S_3, \qquad\qquad -T/2 < t < 0 \qquad\qquad \text{(Eq. 2.23)}$$

where

$$S_1 = \frac{1}{4}|\vec{x_0} + \vec{x_1}|^2, \qquad\qquad \text{(Eq. 2.24a)}$$

$$S_2 = \frac{1}{4}|\vec{y_0} - \vec{y_1}|^2 + \frac{1}{4}|\vec{z_0} - \vec{z_1}|^2, \qquad\qquad \text{(Eq. 2.24b)}$$

$$S_3 = \frac{1}{2}(\vec{x_0} + \vec{x_1}) \cdot (\vec{y_0} - \vec{y_1}) \cos(-\frac{2\pi}{T}t + (\phi_2 - \phi_1))$$

$$+\frac{1}{2}(\vec{x_0} + \vec{x_1}) \cdot (\vec{z_0} - \vec{z_1}) \cos(\frac{2\pi}{T}t + (\phi_2 - \phi_3))$$

$$+\frac{1}{2}(\vec{y_0} - \vec{y_1}) \cdot (\vec{z_0} - \vec{z_1}) \cos(\frac{4\pi}{T}t + (\phi_1 - \phi_3)). \qquad\qquad \text{(Eq. 2.24c)}$$

For the direct detection, we assume that the data are all real numbers, and ϕ_1, ϕ_2, and ϕ_3 are the relative phases of the three orthogonal carriers. In addition to the Ch2 signal transition (S_1) and the interference of the adjacent channels (S_2), there is a fast fluctuation term (S_3) in this

transition signal. Combining the influence of the filtering effects in the OBPF or the electrical LPF, the interference of this transition signal will migrates to the center of the effective-signal region at $t = T/4$, which can be approximated by

$$I = \int_{-\frac{T}{4}}^{\frac{3T}{4}} (s_2(t) - |x_0|^2) h_{LPF}\left(t - \frac{T}{4}\right) dt, \tag{Eq. 2.25}$$

where $h_{LPF}(t)$ is the impulse response of the filtering effect, which is equal to the convolution of the impulse responses of the OBPF and the LPF. Taking OOK-modulated signals for example, the Q-factor of the received signal can therefore be estimated as

$$Q_{OOK} = \frac{|\overrightarrow{x_0}|^2}{2E[|I|^2]}. \tag{Eq. 2.26}$$

The Q-factor upper bound of the OWDM sub-channels can be obtained by assuming that $h_{LPF}(t)$ is the impulse response of an ideal rectangular filter, which has the central angular frequency at ω_0 and the total bandwidth of $2/T$. As a result, the performance of the OWDM DDO receiver is influenced by the relative phases and polarizations of the adjacent sub-channels, even though the interference from the adjacent sub-channels is cancelled out completely in the effective-signal region. These phenomena have been observed from various experimental results [58, 59, and 63]. The simulated results (using VPI Photonics Simulator) and calculated results based on Eq. 2.26 of the received Q-factors versus the relative phases and the relative polarizations are shown in Fig. 2.24. The performance of the DDO-OWDM receiver can be optimized by adjusting the relative phases of the adjacent sub-channels in the OWDM transmitter. However, after the transmission in a piece of optical fiber, the relative phases will be adjusted rapidly by the fiber chromatic dispersion and thermal vibration. To achieve the best performance, a feedback signal from the receiver to the transmitter is necessary to dynamically adjust the relative phases of each channel.
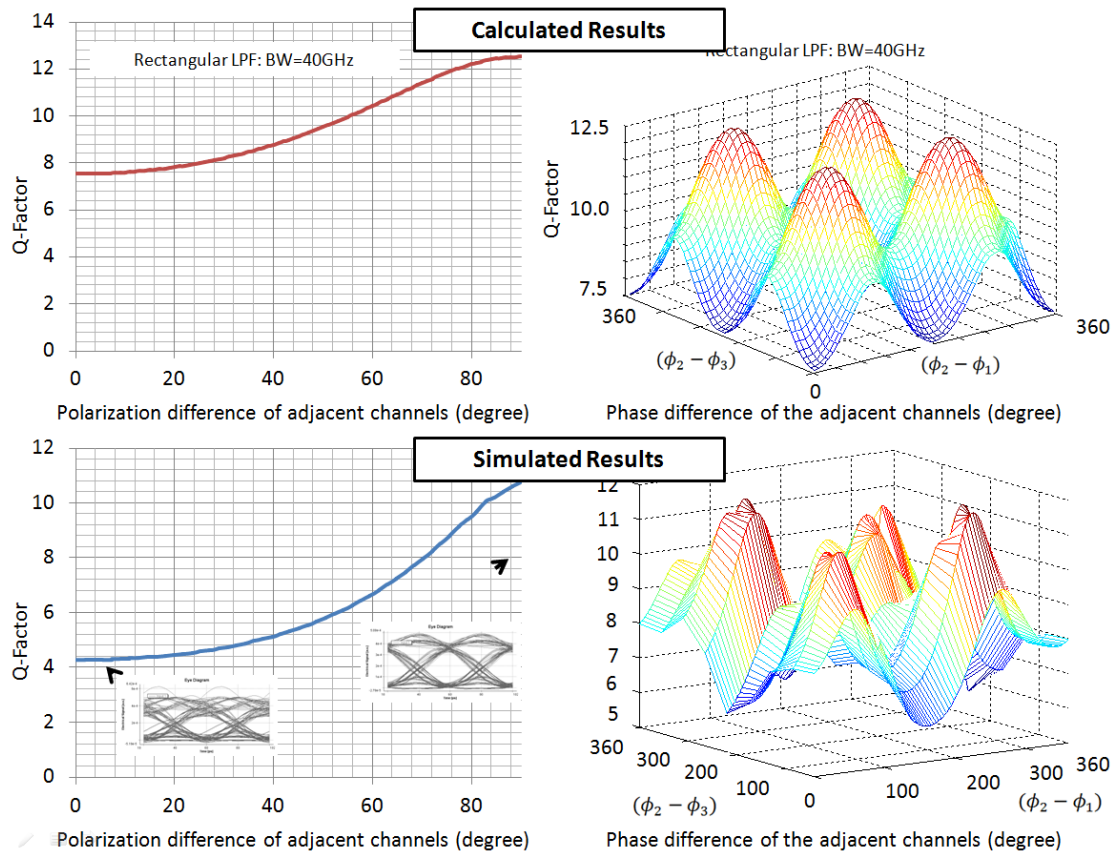
Fig. 2.24. Calculated and simulated results of Q-factors of the center sub-channel of a three-OOK-sub-channel OWDM system.

In addition to phases, the polarizations of the adjacent sub-channels can be set to be orthogonal in the DDO systems. As implied by Eq. 2.25, the amplitude of the fast fluctuation can be minimized when the adjacent channels have orthogonal polarizations. The fluctuation at $\cos(4\pi t/T)$ from the beating between Ch1 and Ch3 is negligible when the LPF takes effect. The experimental results of a three-sub-channel DDO-OWDM system are shown in Fig. 2.25. The two odd sub-channels carry the same 25-Gb/s OOK data to serve as interferers while the center even sub-channel carries the uncorrelated 25-Gb/s OOK data. The relative polarizations of the adjacent channels can be detected by the beating power at the sub-carrier spacing (25 GHz). As shown in the insets of Fig. 2.25, the most clear eye diagram is obtained when the beating power

51

is minimal, indicating that the polarizations of the adjacent sub-channels spaced at 25 GHz are orthogonal at that time. The measured Q-factors before and after the 15-km SSMF transmission are shown in Fig. 2.26. The received power penalty is mainly due to the dispersion inside the fibers.
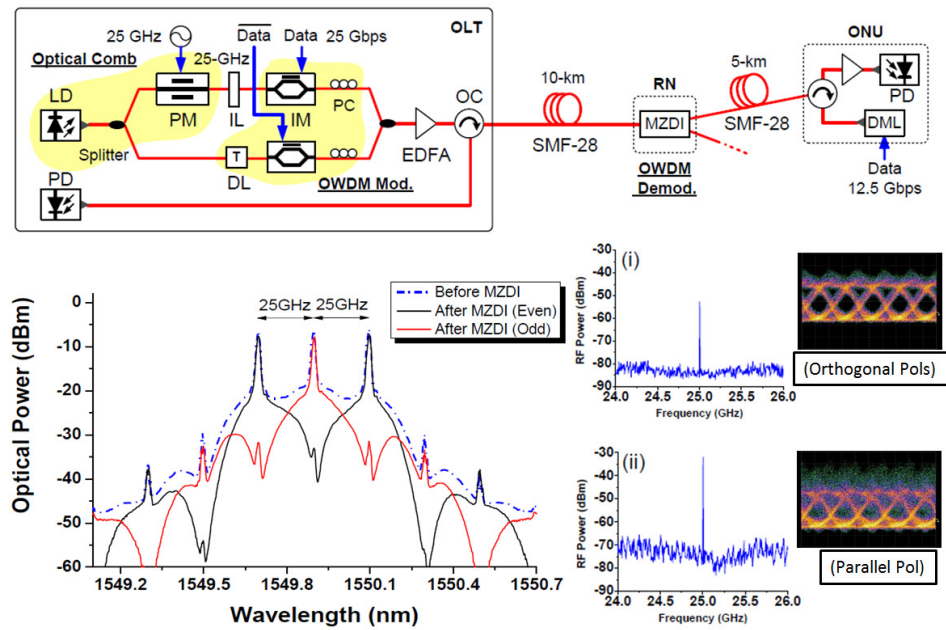
Fig. 2.25. Experimental results of a three-OOK-sub-channel OWDM DDO system of the subcarrier spacing at 25 GHz.
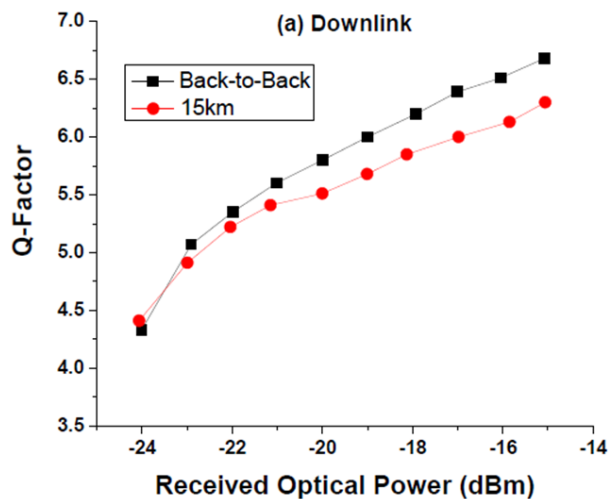
Fig. 2.26. Measured Q-factor versus the receiver optical power before and after the 15-km SSMF transmission.

52

2.5.3 Bandwidth Tradeoff

For a 1x2 OWDM optical demultiplexer, the halving of its effective signal width indicates that the optical receiver requires twice the bandwidth of its symbol rate. However, the maximal bandwidth is limited by the interference of the second-adjacent channels. For example, if there are five channels (Ch1, Ch2, Ch3, Ch4, Ch5), the signals of Ch2 and Ch4 can be eliminated in the effective-signal region by a 1x2 OWDM optical demultiplexer; afterwards, Ch1 and Ch5 are supposed to be filtered out by an OBPF or an electrical LPF. The selection of the bandwidth of these filters becomes a tradeoff between increasing the bandwidth for minimizing the transition-signal interference and decreasing the bandwidth for eliminating the interference from Ch1 and Ch5.

In DDO systems, the interference from Ch1/Ch5 is dominated by their baseband signals detected by the PD. Every optical signal, whatever its wavelength is, contributes to the detected power in the baseband. This interference can cause some misleading results in the even/odd sub-channel configuration, which are widely used to demonstrate OWDM systems for simplicity. In the even/odd sub-channel configuration, all the odd sub-channels carry the same data whereas all the even sub-channels carry the same data that are uncorrelated to odd sub-channels. However, using the eve/odd sub-channel configuration in DDO systems, the interference from the other odd sub-channels to the desired odd sub-channel will be neglected because their data are all the same. Figure 2.27 shows the simulated results of the Q-factor of the center odd sub-channel in a 5-sub-channel OWDM system. The Q-factor keeps rising with the increase of the OBPF bandwidth in the even/odd sub-channel configuration. On the other hand, when all five sub-channels have different data sequences and orthogonal polarizations, the optimal OBPF bandwidth is around 50 GHz, which is just substantial to filter out the interference from the other odd sub-channels. However, the optimal OBPF bandwidth of demultiplexing five parallel-polarization sub-channels falls between 100 GHz and 50 GHz in the 25-GHz OWDM system because the bandwidth tradeoff becomes more dominant when the beating power in the transition-signal region becomes higher.
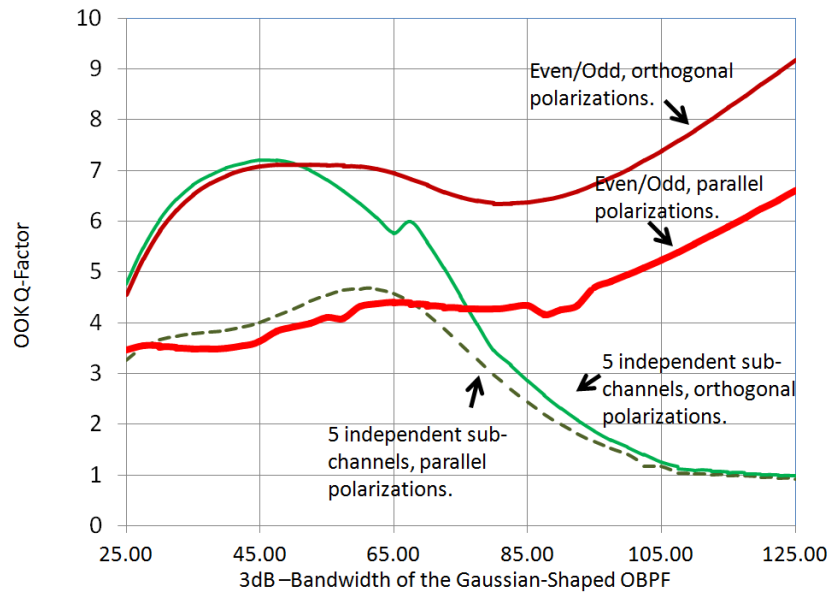
Fig. 2.27. Simulated Q-factors of a 5-sub-channel DDO-OWDM system with the even/odd sub-channel configuration and with 5 independent sub-channels.

In CO systems, the interference from the second-adjacent channels is dominated by the periodic fluctuations at higher frequencies, since the balanced PD in a coherent system can eliminate baseband-signal interferences from the other sub-channels. Therefore, the even/odd sub-channel configuration induces little difference to the demultiplexed signals from all independent sub-channels. The simulation results of the demultiplexed center sub-channel in a 5-QPSK-sub-channel CO-OWDM system are shown in Fig. 2.28. Using optical demultiplexing, the optimal QPSK-EVM is obtained when the LPF bandwidth is between 25 GHz and 50 GHz due to the bandwidth tradeoff between the transition-signal interference and the second-adjacent sub-channel interference. For the OWDM digital demultiplexing, because there is also a bandwidth tradeoff, which requires at least twice as wide sampling bandwidth as the symbol rate, the OWDM digital demultiplexing is lower-bounded as well as the OWDM optical demultiplexing. The simulation results show the bandwidth tradeoff sets a lower bound for the OWDM demultiplexing even when there are no noise and no dispersion. However, the digital

54

demultiplexing outperforms the optical demultiplexing because there is no transition signal generated in the digital demultiplexing. The simulation results of a CO receiver without any FFT-based OWDM demultiplexing are also shown in Fig. 2.28 for comparison. The optimal LPF bandwidth without using any OWDM demultiplexing is 12.5 GHz, which is the Nyquist frequency of a 25-GS/s signal.
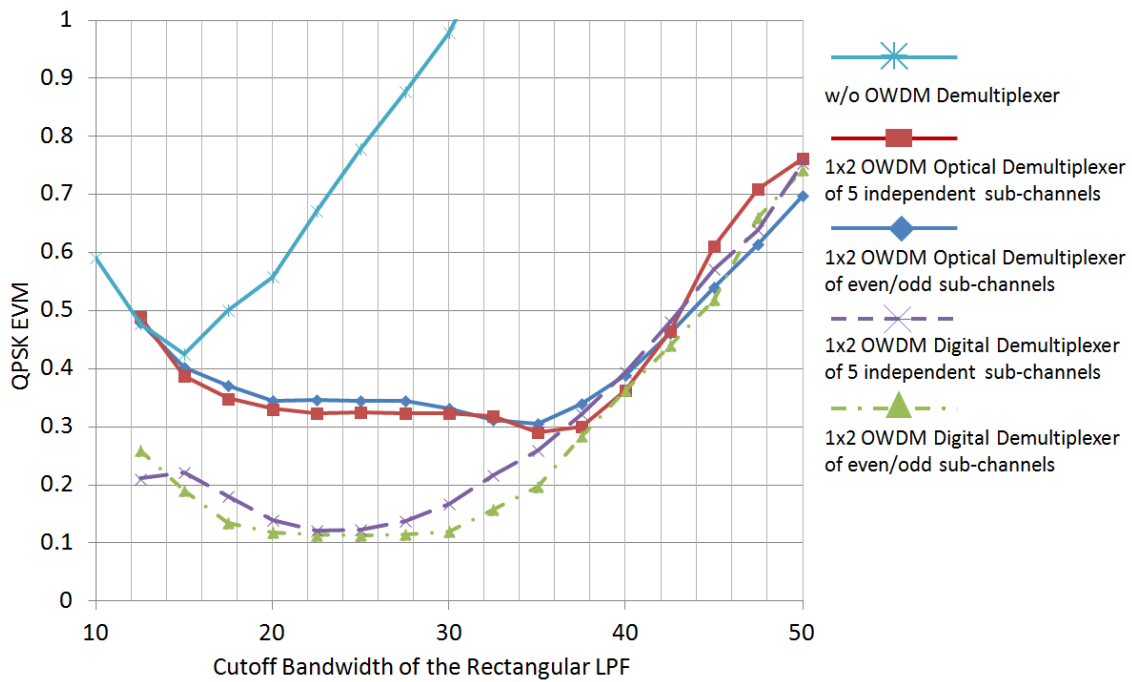
Fig. 2.28. Simulation EVM of a 5-sub-channel CO-OWDM system with the even/odd sub-channel configuration and with 5 independent sub-channels.

2.6 Conclusions

For the long-haul networks, while the power budget and complexity tolerance of the transmission system are sufficiently high, RoF systems can help mitigate channel distortions and improve spectral efficiency. Thanks to the advance of the semiconductor integrated-circuit (IC) capability, it is possible to use DSP to handle the impairments in the optical channel. As a result, multiple-orthogonal-carrier communication systems are not only proven to be reliable and

spectrally efficient in tough wireless channels but also show great potential in highly detrimental long-distance optical channels. Compared to conventional single-carrier communication systems, multiple-orthogonal-carrier communication systems viably achieve extremely high spectral efficiency and low post-equalization complexity in the receiver. However, the complexity in the multiple-orthogonal-carrier transmitter is increased, and the multiple-orthogonal-carrier signals are becoming more vulnerable to the LO frequency offset and the NLO of fibers. These drawbacks are still the main obstruction to prevent the multiple-orthogonal-carrier systems from implementing feasible real-time systems. OWDM with optical demultiplexing can be a promising alternative to establish a real-time system in the near future, but it may give in some system performance because of the bandwidth tradeoff. Therefore the transmission distance of OWDM optical demultiplexing systems achieved so far is still far behind other modulation schemes.

CHAPTER 3

COVERAGE-EXTENDED WIRELESS-OVER-FIBER SYSTEM

3.1 Millimeter-Wave-over-Fiber Femtocell

Multi-orthogonal-carrier RoF systems can improve optical spectral efficiency dramatically in backbone long-haul networks. However, the pursuit of a higher transmission speed is never privileged for backbone networks. For access networks, which are deployed within the last miles or the last meters near consumers, it is a popular trend to develop high-speed access networks integrated with wireless services. From old-fashioned 2.5G/3G "Global System for Mobile" (GSM) to modern technologies, such as Long-Term Evolution (LTE), WiMAX, or Wireless Fidelity (WiFi), the wireless transmission rate has been growing from a few kilobits per second (Kb/s) to nearly one gigabit per second (Gb/s, but the highest data rate of these microwave bands is restricted by their available bandwidth of a few MHz.

On the other hand, RF carriers in mmWave bands have much higher frequency. As a result, mmWaves can easily occupy much wider bandwidth for wireless transmission. Among all the mmWave frequencies, from 30 GHz to 300 GHz, the mmWave band that draws the most attention is the 60-GHz band. Because the RF carriers in the 60-GHz band are highly absorbed by the atmosphere, particularly by oxygen molecules, the 60-GHz band is free of license in most nations, as shown in Fig. 3.1. The atmosphere absorption restricts the applications of 60-GHz mmWaves for long-distance transmission. Nevertheless, 60-GHz bands still hold great potential for indoor and short-range transmission.

In 2009, multi-gigabit 60-GHz wireless transceivers were already off-the-shelf products. The first 60-GHz standard is available through the WirelessHD Consortium [64], which is promoted by many major electronics companies, such as Broadcom Corporation, Intel Corporation, LG Electronics Inc., NEC Corporation, Samsung Electronics, Co. Ltd, SiBEAM,

Inc., Sony Corporation, and Toshiba Corporation. The 60-GHz transceivers enable the point-to-point wireless gigabit transmission over tens of meters, intending to replace conventional wired links (such as USB and HDMI cables).
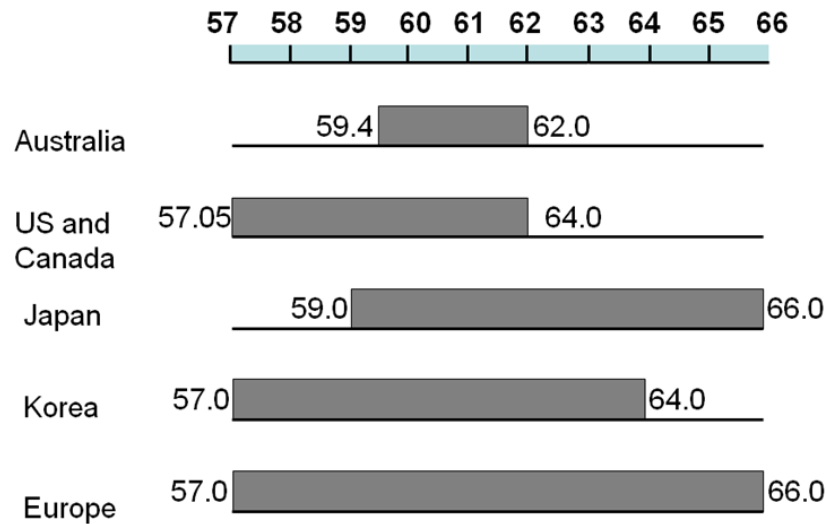
Fig. 3.1. License-free RF spectra around 60GHz regulated in the different regions.

Beyond point-to-point wireless links, the WirelessHD Consortium has announced its specification 1.1, providing up to 28-Gb/s transmission speed over its wireless video area network (WVAN) [64]. Not limited by only HD video transmission, the IEEE 802.11ad task group [65] and the WiGig Alliance [66] are searching for a solution to the convergence of Wi-Fi and 60-GHz for WLAN, while the IEEE 802.15.3c group specializes in development of 60-GHz wireless personal area networks (WPAN) [67].

To establish a wireless network, it is of great importance to extend mmWave signal coverage. In general, the valid transmission distance of an RF carrier is getting shorter and shorter as its frequency gets higher and higher. Regardless of the atmosphere absorption, the

negative effects of wireless channels, including the Friis free-space loss, multi-path interference, penetrability, and Rayleigh fading, all get worse as the frequency gets higher. These effects make the wireless signals in the mmWave band have small wireless coverage. Therefore, to establish a multi-gigabits-per-second very-high-throughput (VHT) WLAN in the mmWave band, it is necessary to partition the whole area into many small areas, each of which is covered by a wireless access point (WAP) individually. These small areas, which are known as femtocells ($\sim 10^2$ m^2) or picocells ($\sim 10^4$ m^2), confine the wireless distance between a mobile device and the WAP. As a result, it assures that the transmission distance is short enough for the 60-GHz VHT transmission. The femtocell infrastructure is particularly useful for the indoor environment, where the penetrability of mmWaves is extremely low for walls and furniture.

The challenge of the femtocell infrastructure then lies in the backhaul network architecture to support the data transmission among WAPs and from WAPs to the Internet. The network architecture of Ad Hoc meshes, such as the backhaul system used for the wireless-optical broadband access network (WOBAN) are not suitable here for their long routing delay and poor scalability when there are large numbers of WAPs [68, 69]. On the other hand, a typical wireless backhaul network, such as GSM networks or Fiber-Wireless (FiWi) access networks [70], is built upon a central-office-to-base-station architecture, as shown in Fig. 3.2. Because wireless transmission distances are mostly limited by high free-space attenuation, many base stations equipped with an RF front-end and a digital back-end to communicate with the central office by the packet-switching transmission are required to be deployed for the large coverage. The RF front-end has to handle the RF down-conversion, RF carrier/phase recovery, multi-path interference cancellation, and so on, while the digital back-end includes the multiple-access-control (MAC) protocol and network functions. The complexity of the base stations increases exponentially with the increase of the carrier frequency and the data rate. This system architecture is suitable for cellular systems because of its large wireless coverage and low data rate. However, for the 60-GHz technology, it is too expensive to have every base station in access networks (or every WAP in femtocell networks) equipped with RF/digital functions at

Gb/s operating speed. Because the number of WAPs in the femtocell infrastructure is so large, the system cost is greatly dominated by the cost of each WAP in the femtocell infrastructure.
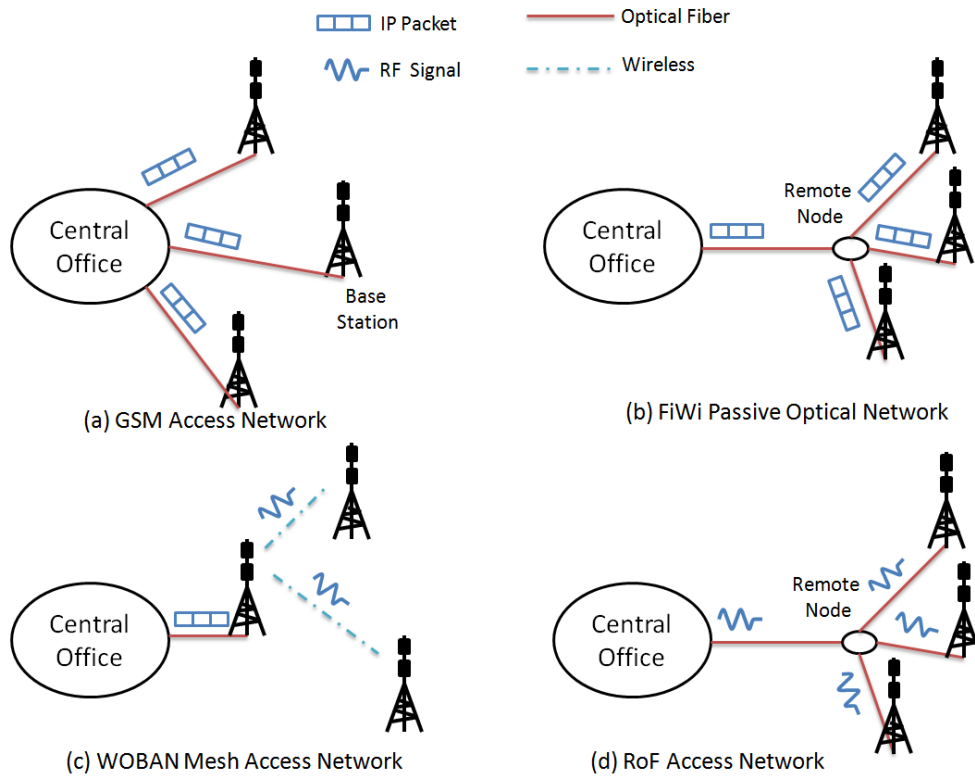
Fig. 3.2. Various kinds of wireless-optical hybrid access-network architecture.

To resolve the cost issue of the backhaul networks in the mmWave femtocell infrastructure, a novel scheme known as RoF has been undergoing development in recent years. Although the meaning of RoF is now generalized to a wide variety of applications, in the beginning, RoF is only referred to the application of wireless-coverage extension, which transmits wireless RF signals over low-attenuation optical fibers to remote WAPs. Instead of transmitting digital packets through optical fibers, an RoF system only transports RF signals back and forth between WAPs and an RoF gateway router. All the RF/digital functions are

centralized in the RoF gateway router, and all the RF signals in and out of a mobile device are directly received and transmitted by a WAP without the digital functions of an RF-front-end. All WAPs are simplified to only perform optical-electrical (o/e) conversion of RF signals through antennas. Therefore, an RoF system is equivalent to installing one single fully functional WAP, whose wireless signal coverage is extended by optical fibers. The optical fibers of an RoF system carry RF signals directly from the RoF gateway router to the WAP antennas, or vice versa, so the optical transmission is transparent between the RoF gateway router and any mobile device. Since each WAP is simplified to only have an o/e-conversion function, the cost and power consumption of the RoF femtocell infrastructure can be dramatically reduced.

3.2 Generation of Optical Millimeter Wave

The challenge of generating optical mmWaves mainly lies in the bandwidth limitation and nonlinearity of e/o interfaces, including optical amplitude modulators (AM), optical phase modulators (PM), directly modulated lasers (DML), and PDs. The bandwidth of a PD can be increased to almost 100 GHz by shrinking their sizes and increasing the input optical power [71]. However, the bandwidth of optical modulators and DMLs is much more difficult to enhance because it involves the tradeoff between electro-optical effects and electrical resistor-capacitor delays. So far, DMLs of slightly over 20-GHz bandwidth and optical modulators of 40-GHz bandwidth are not uncommon to obtain. However, for millimeter-wave applications, it is not easy to generate RF carriers over 40 GHz [72].

Linearity is also essential in RoF systems. The characteristics of RoF systems are similar to analog transmission systems. Unlike conventional digital baseband signals, the nonlinearity of e/o interfaces induces multiple RF harmonic carriers in RoF systems, which can cause various signal distortions and interferences. Conversely speaking, if this interface nonlinearity is

manipulated carefully, it can also be useful to multiply RF carriers that are difficult to be obtained directly.

There are various approaches to overcome the bandwidth limitation and nonlinearity of e/o interfaces. Various types of generation schemes and optical millimeter-waves are suitable for various RoF systems, ranging from microwaves to millimeters waves. In the next section, we summarize the mmWave generation schemes into two major types: the electrical up-conversion and the optical up-conversion, and four types of optical mmWaves are introduced in the following, including optical double-sideband (ODSB), optical single-sideband-plus-carrier (OSSB+C), homodyne optical-carrier-suppression (homoOCS), and heterodyne optical-carrier-suppression (heteroOCS) mmWaves. The RF carrier of interests is focused on 60-GHz mmWaves because of its high potential of multi-gigabit wireless transmission and high-frequency related constraints.

3.2.1 Electrical and Optical Up-Conversion

There are two major optical-mmWaves generation schemes: the electrical up-conversion and the optical up-conversion. In the electrical up-conversion, baseband signals are first up-converts to the mmWave band by a "pseudo-wireless" transmitter, which is composed of RF IQ mixers and LOs. Instead of feeding the RF signals to an antenna, the "pseudo-wireless" transmitter feeds the mmWave signals directly into an e/o interface to generate optical mmWaves, as shown in Fig. 3.3(a). When the frequency of mmWaves is much higher than the bandwidth of DMLs, an external amplitude modulator is used. The advantage of electrical up-conversion is its simplicity. Only one e/o interface is needed for one optical mmWave transmitter.

Usually there is no special optical modulation technique required in the electrical up-conversion. The simplicity of the o/e interface also allows any incoming RF signal to be transported through optical fibers directly. The RoF system, from the optical transmitter to the

62

optical receiver, is basically transparent to both the uplink and the downlink of the RF transceivers at all. However, it requires high-frequency electronics to mix signals with mmWaves. It is usually difficult to achieve high signal quality in the mmWave band directly. In addition, when there are lots of optical mmWave channels present, such as the WDM networks, it requires a large number of ultra-wide-bandwidth e/o interfaces.

(a) Electrical Up-Conversion

(b) Optical Up-Conversion
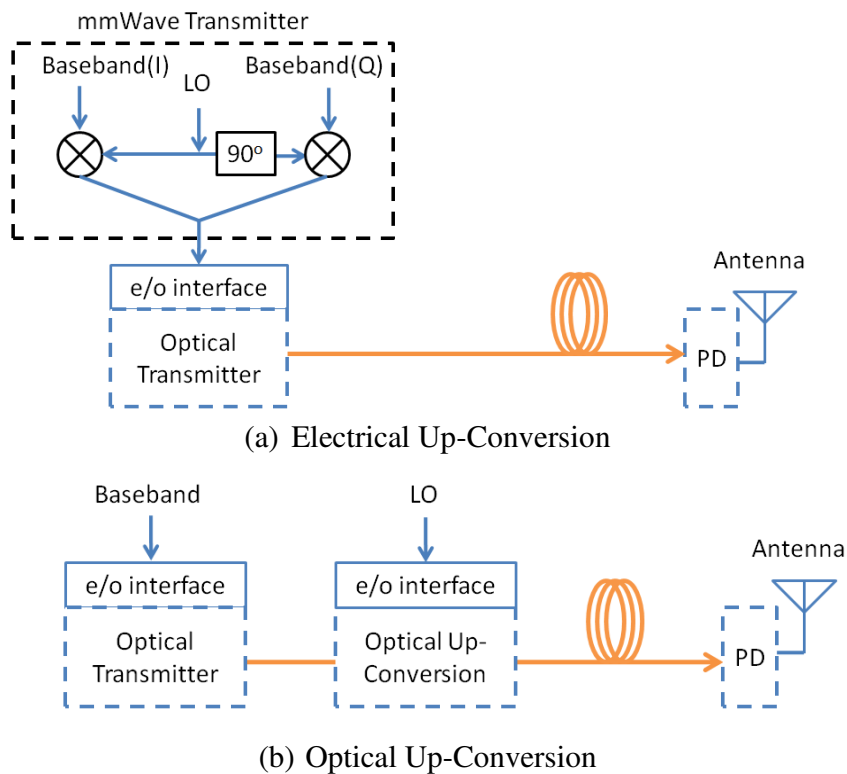
Fig. 3.3. Schematic of the electrical and optical up-conversion RoF link.

Optical up-conversion, as shown in Fig. 3.3(b), separates the baseband modulation and the up-conversion into two stages. Low-frequency baseband signals are first modulated onto a coherent lightwave by a low-frequency e/o interface (such as a DML or an external AM). Then, the optical signals are up-converted to the mmWave band by the second e/o interface with an RF

LO input. Since the baseband modulation is separated from the optical up-conversion, the optical up-conversion can be easily applied for optical frequency doubling or quadrupling schemes to overcome the e/o-interface bandwidth limitation [73, 74] without distorting the original baseband signals. When there are numerous optical channels in the RoF system, all these optical channels can share a single wide-bandwidth e/o interface for the optical up-conversion, which saves the need of numerous expensive components. However, because the RF signals are generated indirectly, the RoF system usually has to be designed for some specific RF carrier. Not any incoming RF carriers can directly fit into the same RoF system.

Furthermore, even though the optical up-conversion can overcome the bandwidth limitation by multiplying the LO frequency, transporting RF signals from mobile devices back to the RoF gateway router (the uplink) is still troublesome, especially when the RF is above the bandwidth limitation of the e/o interface and requires the indirect mmWave generation. In most RoF experimental demonstrations, the uplink still uses conventional digital baseband transmission, which is somehow contradictory the concept of RoF systems.

3.2.2 ODSB Millimeter Wave

An optical double-sideband (ODSB) mmWave is generated in the most straightforward way. Any RF carrier linearly modulated to the intensity of a coherent lightwave can be represented by an ODSB signal. As shown in Fig. 3.4, the optical spectrum of an ODSB mmWave signal is represented by an optical central carrier and two complex-conjugated data sidebands. ODSB signals can be generated straightly from an analog DML or an optical intensity modulator biased at the linear point with an RF-signal input. The electric field of an ODSB signal can be expressed by

$$E_{ODSB}(t)/E_0 = 1 + \alpha \text{Re}\{x(t)\exp{(j\omega_0 t)}\}, \qquad \text{(Eq. 3.1)}$$

where E_0 is the electric field for the purpose of normalization. Being detected by a PD, the beating between the optical central carrier and one of the data sideband generates the electrical signal at the RF band. Assuming the angular frequency of the RF is ω_1 and the complex data symbol is $x(t)$, the generated electrical signal is expressed by

$$s(t) \propto |1 + \alpha \text{Re}\{x(t)\exp(j\omega_0 t)\}|^2 \sim 1 + 2\alpha \text{Re}\{x(t)\exp(j\omega_0 t)\}, \qquad \text{(Eq. 3.2)}$$

where α represents the ratio of the sideband to the optical central carrier. And the beating frequency at $2\omega_0$ is neglected here. Therefore, the amplitude and phase information is preserved by the beating of the PD. However, when the ODSB signal travels along the optical fiber, the fiber chromatic dispersion will induce some phase difference between the two data sidebands, resulting in the interference of the two beating RF signals. When the phase difference is zero, the RF signals will have a constructive interference as Eq. 3.2. However, when the phase difference is 180 degree, the two RF signals will incur a destructive interference and RF power fading [75, 76]. The beating RF power varies periodically with the length of optical fibers, which have to be taken into account when designing the length of each RoF link. Nevertheless, the simplicity of ODSB generation makes it very suitable for short-distance fiber transmission.
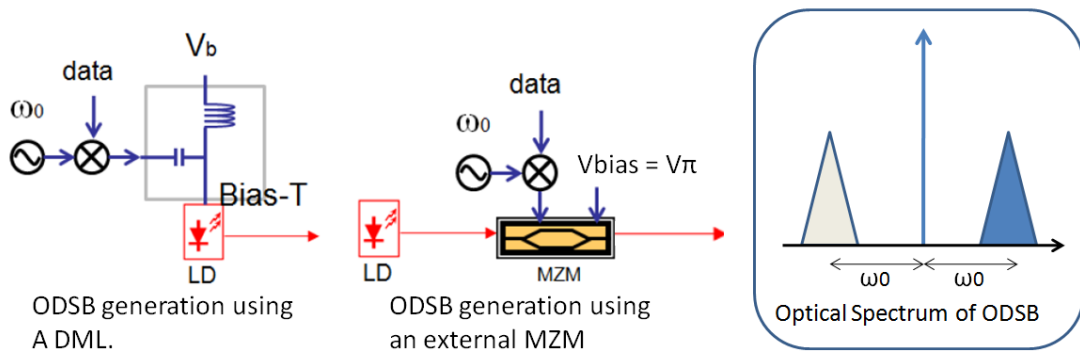
Fig. 3.4. Setup of ODSB generation and optical spectrum.

3.2.3 OSSB+C Millimeter Wave

The optical spectrum of OSSB+C mmWaves is shown in Fig. 3.5. It is similar to the ODSB optical spectrum except that one of the sideband is suppressed. OSSB+C mmWaves can be generated by a dual-arm MZM, whose two RF inputs have a 90-degree phase shift and two bias inputs have $V_\pi/2$ difference. Otherwise, the sideband can also be suppressed by an optical bandpass filter (OBPF). The electric field of an OSSB+C signal can be expressed by

$$E_{OSSB+C}(t)/E_0 = 1 + \alpha x(t)\exp(j\omega_0 t). \qquad \text{(Eq. 3.3)}$$

Neglecting out-of-band signals, the electrical signal detected by a PD can be approximated by

$$s(t) \propto |1 + \alpha x(t)\exp(j\omega_0 t)|^2 \sim 2\alpha\text{Re}\{x(t)\exp(j\omega_0 t)\}. \qquad \text{(Eq. 3.4)}$$

Therefore, the resulting electrical signal is proportional to the original RF electrical signal. Unlike ODSB signals, OSSB+C signals do not have RF power fading. Furthermore, because data are only carried by one sideband, the fiber chromatic dispersion between the sideband and the carrier has a minimal impact on OSSB+C mmWave signals. Therefore, despite the generation of OSSB+C signals is more complicated than ODSB signals, OSSB+C signals are more reliable when the optical-fiber length is long.

Both ODSB and OSSB+C mmWave signals are readily generated by electrical up-conversion, which assures the sensible convenience of downlinks and uplinks. However, the bandwidth of the required o/e conversion interface has to manage mmWave frequency. 60-GHz mmWaves, for example, cannot be modulated directly into 60-GHz ODSB or OSSB+C mmWave signals. Using indirect optical up-conversion to double or triple the carrier can be achieved [77]. However, it complicates the optical mmWave generation even more, and the problem of uplinks has still not been resolved.
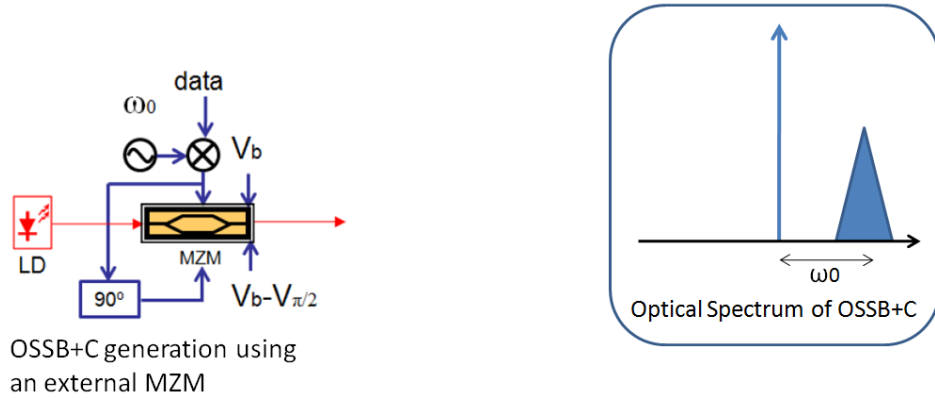
Fig. 3.5. Setup of OSSB+C generation and optical spectrum.

3.2.4 OCS Millimeter Wave

Instead of suppressing one of the sideband, OCS generates optical mmWaves by suppressing the optical central carrier of an ODSB mmWave. OCS can be realized by using a MZM biased at the null point or by using an optical stop-band filter to suppress the optical central carrier. When using an optical filter to suppress the optical central carrier, the two sidebands of OCS mmWave can be generated either by a MZM or by a PM. The OCS optical spectrum is shown in Fig. 3.6. Using electrical up-conversion, the electric field of the OCS mmWave carrying data symbol $x(t)$ can be expressed by

$$E_{OCS}(t)/E_0 = \text{Re}\{x(t)\exp(j\omega_0 t)\}. \tag{Eq. 3.5}$$

Being detected by a PD, the RF signal is given by

$$s(t) \propto |Re\{x(t)\exp(j\omega_0 t)\}|^2 \sim \text{Re}\{x^2(t)\exp(j2\omega_0 t)\}, \tag{Eq. 3.6}$$

where the low-frequency term is neglected. Notice that the RF frequency is doubled because of the OCS technique. Even if the bandwidth of the e/o interface in the transmitter is not enough to generate $2\omega_0$, the $2\omega_0$ mmWave can be still generated by the square law of a PD. Also, notice that the complex data symbol $x(t)$ is squared. This indicates that any modulation format except

67

OOK will be distorted by the OCS mmWave generation. It also means that the RF signals are generated indirectly. Therefore, the problem of uplinks is unsolved.

When using the optical up-conversion, the baseband signal $x(t)$ is modulated separately from the OCS mmWave generation. The electric field of the OCS generation then becomes

$$E_{OCS}(t)/E_0 = x(t)\text{Re}\{\exp{(j\omega_0 t)}\}. \qquad \text{(Eq. 3.7)}$$

The RF signal generated by the PD is

$$s(t) \propto |x(t)Re\{\exp(j\omega_0 t)\}|^2 \sim \frac{1}{2}|x(t)|^2 \cos(2\omega_0 t). \qquad \text{(Eq. 3.8)}$$

Therefore, the main difference between the electrical and optical up-conversion is that the phase information of the complex data symbol $x(t)$ is completely lost in the optical up-conversion. Because the data symbol is directly modulated onto the RF carrier ($2\omega_0$), this generation method is also known as homodyne OCS (homoOCS).

(a) Electrical Up-Conversion HomoOCS

(b) Optical Up-Conversion HomoOCS
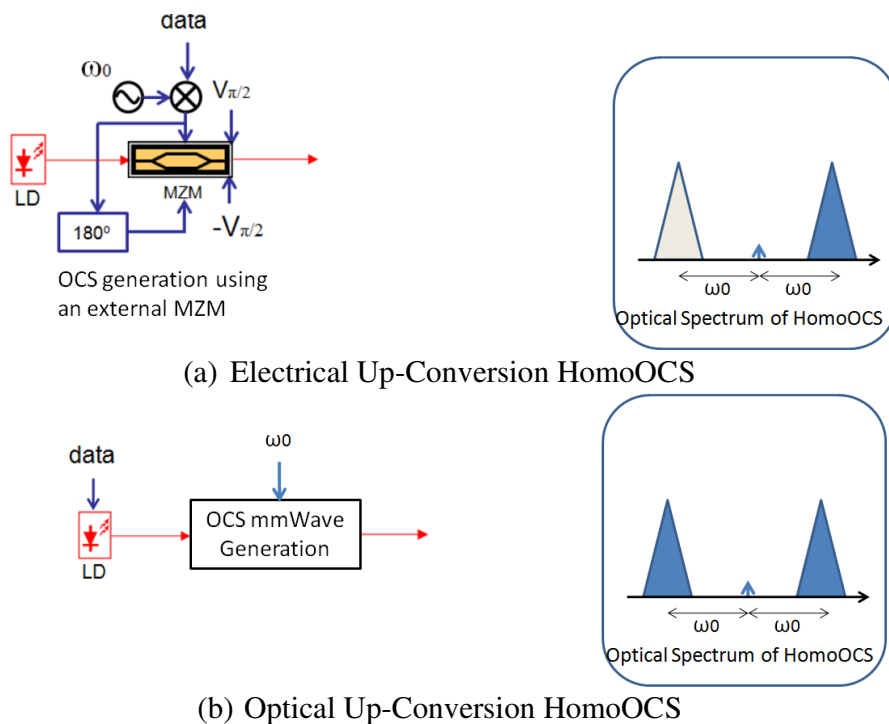
Fig. 3.6. Setup of HomoOCS generation with the electrical and optical up-conversion and optical spectrum.

To preserve the phase information in the optical up-conversion, we can use an intermediate frequency (IF) to carry the baseband data symbol by $\text{Re}\{x(t)\exp(j\omega_{IF}t)\}$ in electrical circuits, where the IF angular frequency ω_{IF} is usually much lower than RF angular frequency $2\omega_0$. Therefore, the IF signals can be directly modulated onto laser lightwaves (either ODSB or OSSB+C). Then OCS mmWave generation can be used as the optical up-conversion method to generate the optical mmWaves as

$$E_{OCS'}(t)/E_0 = (1 + \alpha \, \text{Re}\{x(t)\exp(j\omega_{IF}t)\}) \cos(\omega_0 t). \qquad \text{(Eq. 3.9)}$$

The RF signals of the PD becomes

$$s(t) \propto |E_{OCS'}(t)|^2 \sim \frac{1}{2}\cos(2\omega_0 t) + \frac{\alpha}{2}\text{Re}\{x(t)\exp(j(2\omega_0 + \omega_{IF})t)\}. \qquad \text{(Eq. 3.10)}$$

Here we neglect all the terms that are lower than $2\omega_0$ since low-frequency components are unable to pass through RF amplifiers. The RF carrier carries the complex data symbol at $(2\omega_0 + \omega_{IF})$ without any distortion. Another RF carrier at $2\omega_0$ is also generated without carrying any data, which should not cause any interference in the wireless channel. As a result of different IF generation methods, there are variants for the IF-carried OCS mmWave generation methods, as shown in Fig. 3.7.
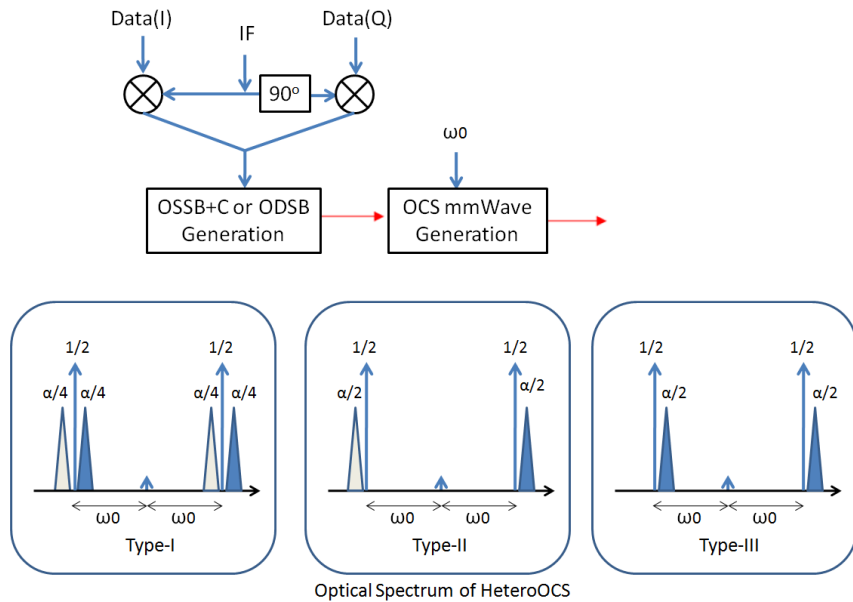
Fig. 3.7. Setup and optical spectra of various HeteroOCS optical up-conversion schemes.

When there are two sub-sidebands, which both beat at $(2\omega_0 + \omega_{IF})$ with the OCS sidebands, it will have a similar periodic fading effect with ODSB mmWaves because of the chromatic dispersion in fibers (Type-I and Type -II in Fig. 3.7). Otherwise, it is similar to OSSB+C and is more tolerant to the fiber chromatic dispersion (Type-III in Fig. 3.7). Because data symbols are first carried by a low-frequency IF and then up-converted to the mmWave band, this is referred to as heterodyne OCS (HeteroOCS).

To compare the optical mmWave generation, it would be interesting to know the optical-to-RF conversion efficiency of the various kinds of optical mmWaves. That is, when the optical power detected by a PD is the same, what is the RF power that the optical mmWave can produce? The optical power, in terms of Poynting Vectors, varies with time for RoF signals. However, we can calculate the average optical power by

$$P_{optical} = \frac{1}{T}\int_T \frac{|E(t)|^2}{2\eta}dt \times \text{Area}. \qquad \text{(Eq. 3.11)}$$

Here η represents the characteristic impedance of optical fibers and T is the period of mmWaves. Area is the effective area of the fiber. Assuming that the PD responsivity (Ampere/Watt) is one, the average RF power generated by a PD at the specific mmWave frequency is

$$P_{RF} = \frac{1}{T}\int_T \left|\frac{s(t)}{2\eta}\right|^2 Zdt, \qquad \text{(Eq. 3.12)}$$

where Z is the transimpedance of the PD electronics. Without considering data symbols, the optical-to-RF conversion efficiency can be approximated by $P_{RF}/P_{optical}$ as

(a) ODSB

$$\mu_{ODSB} = C_0 \frac{4\alpha^2}{1+\alpha^2/2}. \qquad \text{(Eq. 3.13a)}$$

(b) OSSB+C

$$\mu_{OSSB+C} = C_0 \frac{4\alpha^2}{1+\alpha^2}. \qquad \text{(Eq. 3.13b)}$$

(c) HomoOCS

$$\mu_{OCS} = C_0 \frac{1}{2}. \qquad \text{(Eq. 3.13c)}$$

(d) HeteroOCS Type-I

70

$$\mu_{OCS,}{}^{I} = C_0 \frac{\alpha^2}{2+\alpha^2}. \qquad \text{(Eq. 3.13d)}$$

(e) HeteroOCS Type-II

$$\mu_{OCS,}{}^{II} = C_0 \frac{\alpha^2}{2+2\alpha^2}. \qquad \text{(Eq. 3.13e)}$$

(f) HeteroOCS Type-III

$$\mu_{OCS,}{}^{III} = C_0 \frac{\alpha^2}{1+\alpha^2}. \qquad \text{(Eq. 3.13f)}$$

The parameter C_0 is represented by

$$C_0 = \frac{ZE_0{}^2}{2\eta Area}. \qquad \text{(Eq. 3.14)}$$

Notice that the parameter α can be individually adjusted for each kind of optical mmWaves by the modulation indices. To ensure the modulation linearity, α is usually much smaller than 0.5. Under this circumstance, HomoOCS is the most efficient optical-mmWave generation scheme. However, it is also the only optical mmWave that is unable to carry phase information (or called vector signals) without distortions by a PD (Eq. 3.7). In addition, part of the HeteroOCS power is dedicated to the RF carrier, so the RF conversion efficiency of HeteroOCS mmWaves is low. More importantly, even if not carrying any time-variant signal, the RF powers of ODSB, HeteroOCS Type-I, and HeteroOCS Type-II vary periodically with transmission distances when the fiber chromatic dispersion takes effect along the optical fiber.

3.3 Homodyne Optical-Carrier Suppression

Among all the optical-mmWave generation methods, HomoOCS with the optical up-conversion shows the highest advantages in the applications of short-distance fiber transmission. Although it is distorted by the fiber chromatic dispersion more severely than OSSB+C after long-distance fiber transmission, it requires only half of the o/e-interface bandwidth and has the highest o/e-conversion efficiency (Eq. 3.13). Because there is no non-data optical carrier required in HomoOCS mmWave signals, HomoOCS is perfectly suitable for optical up-

conversion and can fit into a DWDM system easily [78]. In DWDM systems, the separation of the data modulation and the mmWave up-conversion allows multiple optical channels to share only one high-frequency optical modulators.

Two practical experimental systems are demonstrated here to show the potential of HomoOCS mmWaves. The first one is a multi-service coexisting system, where it shows the seamless integration between high-frequency mmWave signals and low-frequency legacy signals in a simple setup. The second one is a PolMux RoF system embedded with a wireless MIMO subsystem, which demonstrates the integration of different degrees of freedom between optical-fiber and wireless transmission systems.

3.3.1 Multi-Service Coexisting System

Because of the high cost of the fiber installation, the prevalence of mmWave RoF systems depends on its feasibility to be compatible with existing optical-fiber networks. Therefore, it is important for mmWave RoF system to be downwardly compatible with legacy optical-fiber services at low frequency, such as 10Gb Ethernet or microwave (3G/4G) transmission.

Various multi-service coexisting schemes have been studied recently. They mostly use additional wavelengths or the central carrier generated in the OCS generation process to carry the low-frequency or wired data [79 - 82]. However, using additional wavelengths is spectrally inefficient, and separating the central carrier from the two OCS sidebands is usually difficult for the remote WAP or the wired remote access unit (RAU) when the wavelengths are too close. Sometimes, the wired and wireless data are designed to carry exactly the same data to fulfill the compatibility, but this scheme requires an upper-layer network control to distinguish the wired and wireless data. This can complicate the wireless transceivers [83].

A novel way to transmit independent low-frequency and mmWave signals simultaneously is to utilize the feature of the OSSB+C mmWave signal. The basic concept is simple: since one of the SSB carriers has the constant power, it is capable of carrying phase-modulated information without perturbing the mmWave beating. The schematic diagram of the concept is drawn in Fig. 3.8. Here the OCS mmWave generation is chosen instead of the direct OSSB+C generation since OCS requires only a 30-GHz o/e interface to generate 60-GHz mmWaves. The two OCS carriers are first separated into two paths, one of which is modulated with the OOK data.
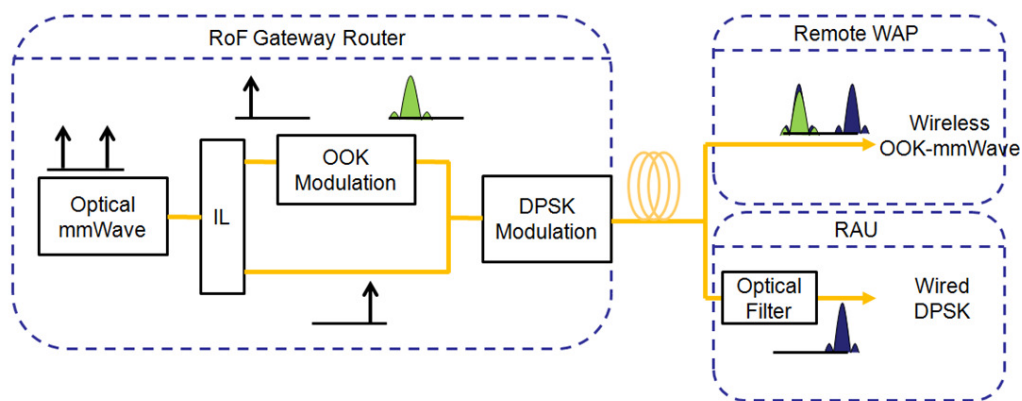
Fig. 3.8. Conceptual schematic of the multi-service coexisting RoF system.

After the recombination of the two carriers, low-frequency differential-phase-shift-keying (DPSK) data are phase-modulated on the two carriers simultaneously. Since the phases of the two carriers are still the same, the frequency beating is not influenced by the phase modulation. Being detected by the PD at the remote WAP, the two carriers beat to generate 60-GHz mmWave signals. Since the two carriers are separate from 60 GHz, a costless optical thin-film filter in the RAU can easily select the constant-amplitude carrier, which is then demodulated by a DPSK demodulator.

However, although the separation distance of the two optical carriers is much shorter than the LD coherent length, the intensity modulator, such as the MZM, can add some phase noise to one of the carrier and may degrade their coherency. The principle of the MZM replies on the phase difference controlled by the electrical data, so the noise of the electrical amplifier is transformed into the phase noise of the optical carrier, resulting into the phase noise of the mmWave beating frequency. Assuming that the electric fields of the two carriers are

$$E_1(t) = e^{j\omega_0 t + j\phi_{PM}(t)},$$
$$E_2(t) = e^{j\omega_0 t + j\delta + j\phi_{IM}(t) + j\phi_{PM}(t)},$$

(Eq. 3.15)

where δ is the constant phase difference due to the difference of the two optical paths, and $\phi_{IM}(t)$ and $\phi_{PM}(t)$ are the phase variations from the intensity modulator and the phase modulator respectively. Here we assume that the amplitudes of the two carriers are the same, and $\phi_{IM}(t)$ also contains other imbalanced phase noise generated from fiber dispersion [83], contributing to the normal-distributed noise in total. This phase noise results into the timing jitter and the amplitude variation of the mmWave beating frequency [84] and therefore can degrades the wireless transmission performance

The experimental setup of the new multi-service coexisting system is shown in Fig. 3.9. In the gateway router, the 60-GHz OCS mmWave is generated by a laser at 1550.36 nm, which is externally modulated by a LiNbO$_3$ PM driven by a 30-GHz sinusoidal wave, resulting in the multiple optical carriers with 30-GHz spacing, as shown in Fig. 3.10(a). A 25GHz/50GHz IL is used to select the 60-GHz-spaced first-order carriers and to suppress the central carrier. The two optical carriers are then separated by a 50GHz/100GHz IL into the even optical path and the odd optical path. The odd carrier is intensity-modulated at 2.5 Gb/s by a pseudorandom binary sequence (PRBS) with a word length of 2^{31}-1 as the wireless OOK signal. The even optical path is equipped with a passive polarization controller (PC). Both channels are then recombined with an optical coupler (OC), concurrently passing through another PM to modulate 10-Gb/s DPSK signals with 2^{31}-1 PRBS. After 25-km SSMF transmission, the optical mmWave signal is divided into the wireless (WAP) and the wired (RAU) receiver.
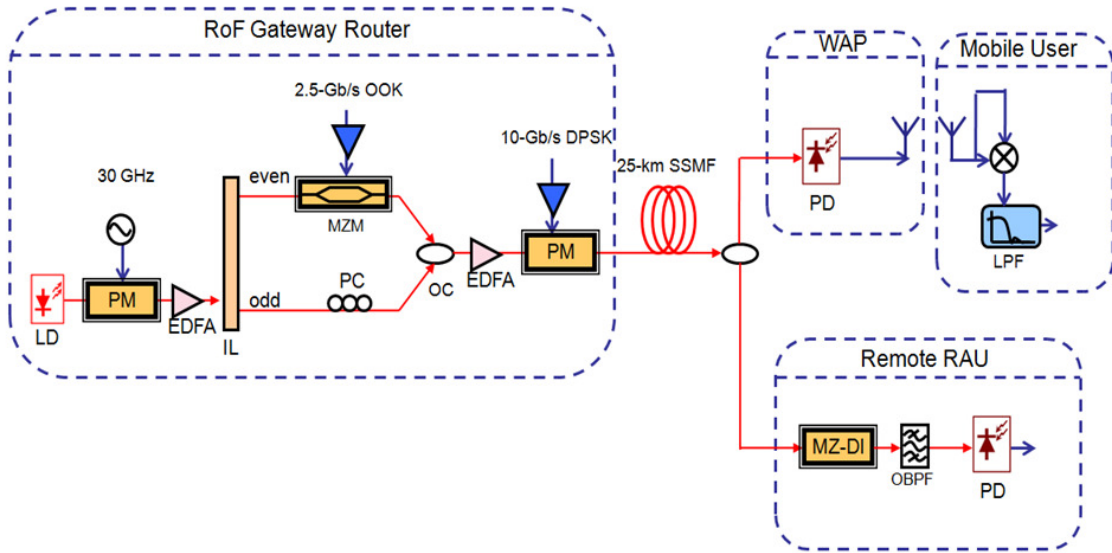
Fig. 3.9. Experimental setup of the multi-service coexisting RoF system.

(a)   (b)
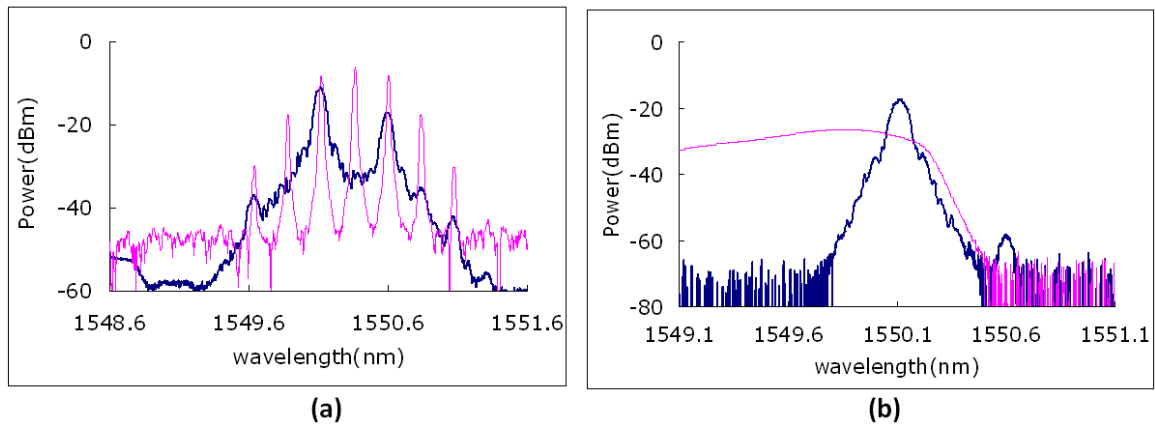
Fig. 3.10. Measured optical spectra of the multi-service coexisting RoF system. (a) Light line: output of the first PM; bold line: output of the second PM. (b) Light line: the passing spectrum of the OBPF; bold line: output of the OBPF.

For the wireless access, the signal is directly detected by a 60-GHz PD, amplified by a power amplifier, and transmitted through the 60-GHz horn antenna with 25-dBi gain. Another 60-GHz horn antenna placed at 4 meters away receives the signal, which is down-converted to the baseband by self-mixing in the RF receiver. On the other end, the 10-Gb/s DPSK signal is retrieved after a 10-GHz MZ-DI. Only the even optical carrier is selected by using the cutting edge of an optical thin-film filter for the wired data reception (Fig. 3.10(b)). Both signals are in the end sent to a bit-error-rate tester (BERT) to evaluate their performance.

The BER measurements are shown in Fig. 3.11. After 25-km SSMF transmission, the power penalties at 10^{-9} BER for the 2.5-Gb/s wireless and 10-Gb/s wired signals are 1-dB and 0.2-dB respectively. The insets in Fig. 3.11 show the measured eye diagrams for wired and wireless signals, with and without 25-km SSMF, respectively. The BER measurements of the DPSK signals also imply that the intrinsic phase noise of the $LiNbO_3$ PM is small, which therefore has minor influence on the degradation of the signal quality.

In this experiment, we successfully transmit both wired and 60-GHz wireless signals through a 25-km SSMF with the BER under 10^{-9}. To further improve the transmission performance, it is important to minimize the phase noise coming from the separate optical paths. For example, other OSSB+C signal generation schemes without the optical-carrier separation are also compatible with this scheme. Being capable of transmitting multi-services with the delicate spectrum usage, this wired/wireless hybrid RoF system can also facilitate its scalability to WDM-PON or other access network systems.
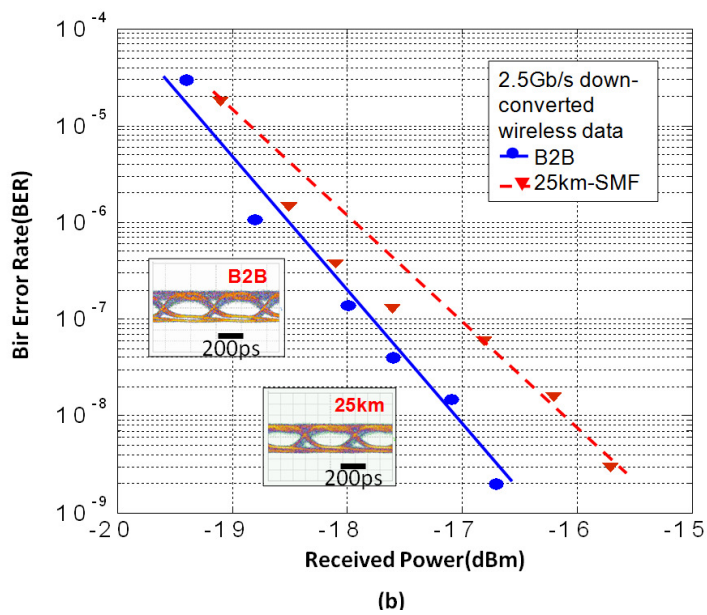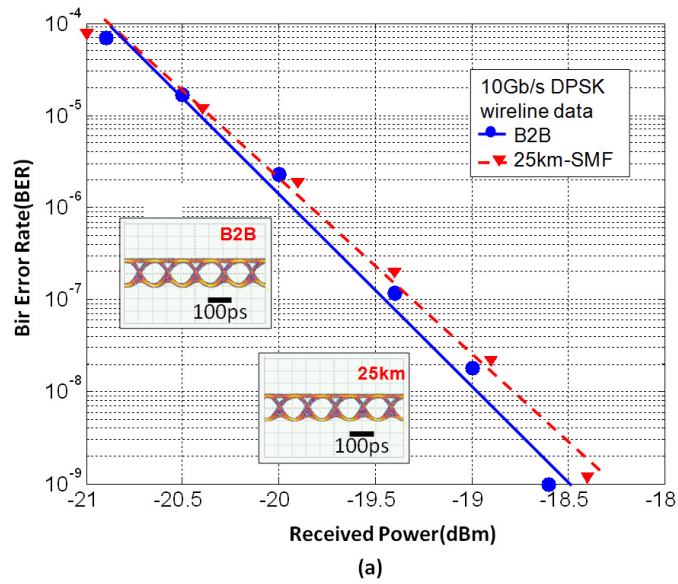
Fig. 3.11. Measured BER versus the received power of (a) the 2.5-Gb/s wireless OOK signal and (b) 10-Gb/s wired DPSK signal.

3.3.2 PolMux MIMO System

Wireless MIMO subsystems are excellent add-ons to improve the signal diversity, spectral efficiency, and power-transmission efficiency of wireless links. When the link is non-line-of-sight, the MIMO subsystem can increase the channel diversity to improve transmission reliability by the space-time coding [85]. When the link is established in a good condition, the MIMO subsystem can use the spatial multiplexing to improve the channel capacity. More discussions about the dilemma between the spatial diversity and multiplexing can be found in literatures [86, 87]. For a short-distance 60-GHz LoS wireless system, even a simple 2x2 MIMO system can help the transmission performance greatly. In the RoF system, there exists a phenomenon that is similar to the 2x2 MIMO signals propagating through the air. That is, the two orthogonal polarizations, including the fast axis (x-axis) and the slow axis (y-axis), of the optical fiber.

For a short distance, the optical fiber transmission can be viewed as a linear system for these two polarizations when the polarization-mode dispersion and the polarization nonlinear effect are negligible. If we transmit two signals $[t_x\ t_y]^{\mathrm{T}}$ by the two optical orthogonal polarizations respectively, after the random polarization rotation and polarization-dependent attenuation in SSMFs, the received signal can be expressed by

$$\begin{bmatrix} r_x \\ r_y \end{bmatrix} = R \begin{bmatrix} t_x \\ t_y \end{bmatrix}.$$

$$R = \begin{bmatrix} R_{xx} & R_{xy} \\ R_{yx} & R_{yy} \end{bmatrix}.$$

(Eq. 3.16)

This coupling matrix is usually well-conditioned. If the polarization-mode dispersion and polarization-dependent attenuation are small, this coupling channel matrix is simply a rotation matrix. The WAP can separate the two received optical polarizations $[r_x\ r_y]^{\mathrm{T}}$ by a PBS and send them to the mobile user with two antennas. For a 2x2 MIMO system, these signals go through another coupling channel matrix:

(Eq. 3.17)

$$\begin{bmatrix} r_{A1} \\ r_{A2} \end{bmatrix} = H_{MIMO} \begin{bmatrix} r_x \\ r_y \end{bmatrix}.$$

$$H_{MIMO} = \begin{bmatrix} M_{11} & M_{12} \\ M_{21} & M_{22} \end{bmatrix}.$$

The MIMO receiver of the mobile user then receives the two signals as

$$\begin{bmatrix} r_{A1} \\ r_{A2} \end{bmatrix} = H_{MIMO} R \begin{bmatrix} t_x \\ t_y \end{bmatrix}. \qquad \text{(Eq. 3.18)}$$

As a result, the MIMO receiver tells no difference whether the signals are transmitted from the RoF gateway router through a SSMF or just directly from the antennas. Without modifying the MIMO receiver, the MIMO signals can be directly demodulated in the mobile user. This RoF system, which embeds the 2x2 MIMO signals within the optical polarizations, is called a xy-MIMO RoF system here.

For example, if the wireless link is LoS and the wireless transmission distance is short, the MIMO coupling channel matrix is well-conditioned. We can estimate the total coupling channel matrix by sending two preset training signals $[t_x(1) \ t_y(1)]^T$ and $[t_x(2) \ t_y(2)]^T$, and the MIMO receiver receives two pairs of signals $[r_{A1}(1) \ r_{A2}(1)]^T$ and $[r_{A1}(2) \ r_{A2}(2)]^T$ accordingly. Assuming the total coupling matrix is

$$\begin{bmatrix} h_{11} & h_{12} \\ h_{21} & h_{22} \end{bmatrix} = H_{MIMO} R. \qquad \text{(Eq. 3.19)}$$

The total channel coupling matrix can be estimated by the solution of

$$\begin{bmatrix} r_{A1}(1) \\ r_{A2}(1) \\ r_{A1}(2) \\ r_{A2}(2) \end{bmatrix} = \begin{bmatrix} t_x(1) & t_y(1) & 0 & 0 \\ 0 & 0 & t_x(1) & t_y(1) \\ t_x(2) & t_y(2) & 0 & 0 \\ 0 & 0 & t_x(2) & t_y(2) \end{bmatrix} \begin{bmatrix} h_{11} \\ h_{12} \\ h_{21} \\ h_{22} \end{bmatrix}. \qquad \text{(Eq. 3.20)}$$

More training signals can be added to the transmitted signals to average out the influence of any channel noise. Once the estimated channel matrix is obtained, the MIMO receiver can demodulate the received signals by inverting the Eq. 3.18. Then two independent signals can be transmitted simultaneously in the xy-MIMO system without occupying additional time and bandwidth. The data rate can be easily doubled in this LoS condition by spatial multiplexing [88].

To demonstrate the xy-MIMO RoF transmission, we set up a 60-GHz RoF downlink system with the PolMux technique and a 2x2 MIMO subsystem. As shown in Fig. 3.12, the LoS transmission in our setup enables the spatial multiplexing to increase the channel capacity to 2 bit/s/Hz. In the gateway router, 1-Gb/s PRBS of a word length of 2^7-1 is modulated directly to the LD. The optical 60-GHz mmWaves are generated by the OCS technique with a LiNbO$_3$ PM. Then the mmWave signal is separated into two optical paths with different delays and polarizations, representing two independent data sequence. In the remote WAP, the PolMux mmWave signals are separated by the PBS, amplified by the RF power amplifiers, and sent to the air by two 15-dBi-directional-gain antennas. The input power of the transmitter antennas is measured as 1 mW. The received signals are down-converted to the baseband by the MIMO receiver. Then a 4-GSample/s real-time digital scope is used to record the baseband signals, which is offline-processed in Matlab.
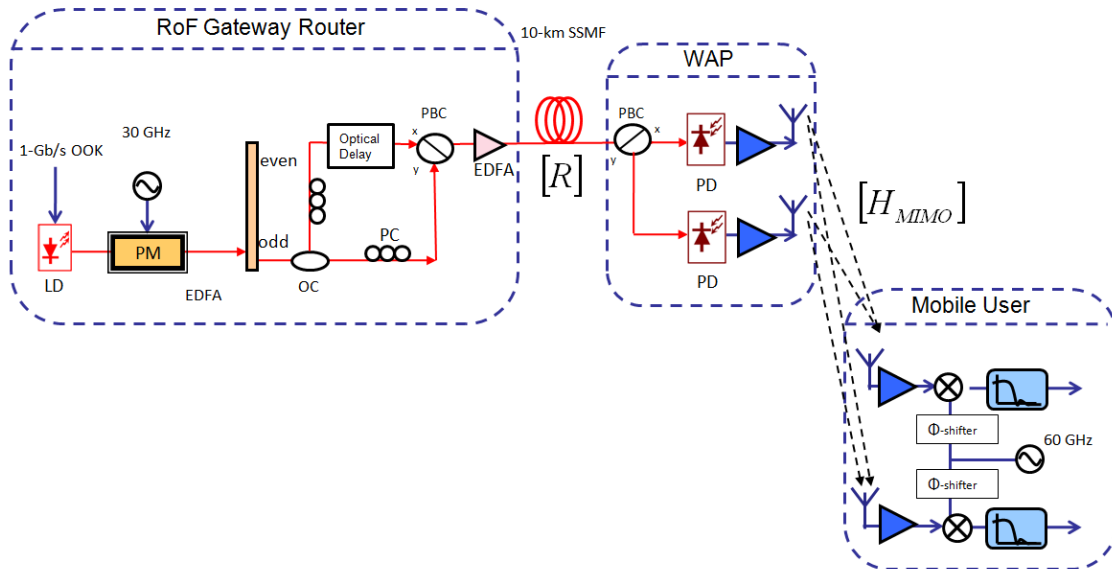
Fig. 3.12. xy-MIMO experimental setup.

In Fig. 3.13, the demodulated signals and the received signals are depicted along with the original signals. The BER measurements versus different OSNRs are shown in Fig. 3.14. The MIMO receiver is observed to require 8-dB more OSNR in the 10-ft wireless distance to compensate the Friis transmission loss. After 10-km-SSMF, the 10-ft wireless distance also gives more OSNR penalty than the one-ft wireless distance because of severe OCS chromatic dispersion in the SSMF. Nevertheless, the BER of 10^{-9} can still be achieved in all the measurements.

In the xy-MIMO RoF experiment, we have doubled the spectral efficiency of the OOK modulation by the MIMO spatial multiplexing with the optical PolMux transmitter. Higher spectral efficiency not only reduces the bandwidth requirement of the RF components, but also simplifies the DSP complexity in the mobile transceiver. This experiment shows an example of the convergence between different degrees of freedom in optics (polarizations) and in the air (spatial locations).
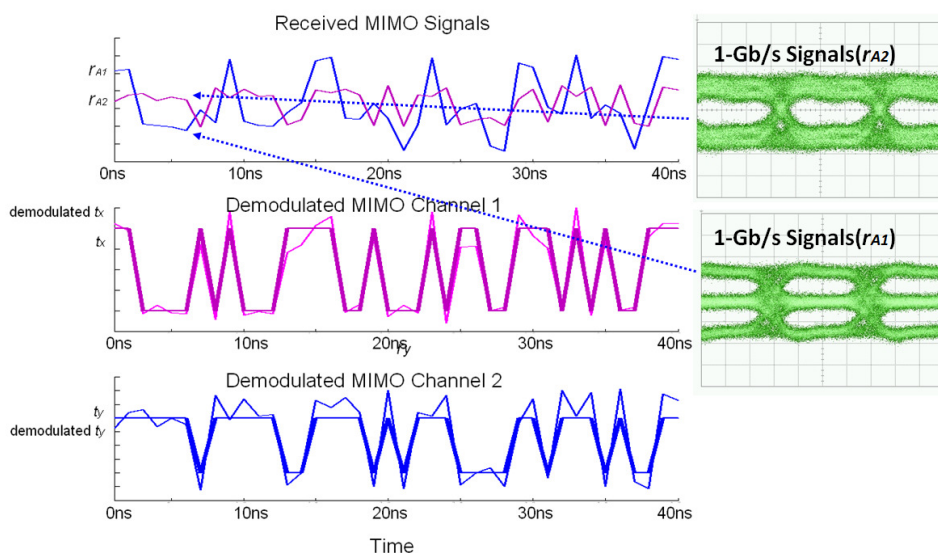
Fig. 3.13. Demodulated 2x2 MIMO OOK signals from the xy-MIMO RoF system.

81
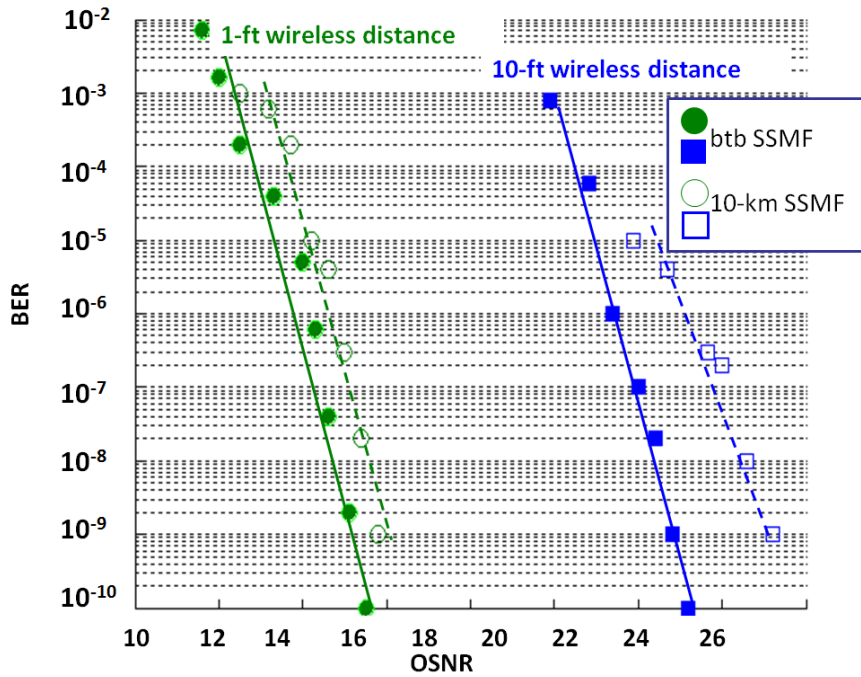
Fig. 3.14. Measured BERs versus OSNRs of the xy-MIMO RoF system.

3.4 Superheterodyne Optical-Carrier Suppression

The biggest advantage of HomoOCS mmWaves is its simplicity for frequency doubling and o/e-conversion efficiency. However, the square law of a PD distorts the phases of incoming electric fields and therefore scrambles any information in optical phases. As depicted in Eq. 3.6 and Eq. 3.8, HomoOCS mmWaves have difficulty in using the phase or frequency modulations of RF carriers. Moreover, like all indirect optical up-conversion methods, uplink 60-GHz signals from mobile devices are still unable to be delivered back to the RoF gateway router directly by a WAP, whose transmitter o/e-interface bandwidth is below 40 GHz.

In addition, when there are multiple RF bands transmitted simultaneously, HomoOCS mmWaves inevitably generate multiple-RF-bands interferences. The PD square law induces RF

82

beating among all optical carriers, generating interference in other RF bands. For example, if we want to transmit two RF carriers at ω_1 and ω_2 respectively, assuming the powers of the two RF optical carriers are the same, the electric field of the OCS mmWave signal is proportional to

$$E(t) = (\cos(\omega_1 t/2) + \cos(\omega_2 t/2))e^{j\omega_0 t}. \tag{Eq. 3.21}$$

The optical frequency of the electric field is assumed to be ω_0. Then, the output current of the PD can be obtained from the square law as

$$|E(t)|^2 = 1 + \frac{1}{2}\cos(\omega_1 t) + \frac{1}{2}\cos(\omega_2 t) + \frac{1}{2}\cos\left(\frac{\omega_1+\omega_2}{2}t\right) + \frac{1}{2}\cos\left(\frac{\omega_1-\omega_2}{2}t\right). \tag{Eq. 3.22}$$

In the mmWave band, there exists three RF bands $(\omega_1, \omega_2, \frac{\omega_1+\omega_2}{2})$ that are transmitted to the antennas. When the two desired frequencies (ω_1, ω_2) are close, the unwanted beating frequency $\frac{\omega_1+\omega_2}{2}$ will cause the optical beating interference to the desired RF bands. The 7-GHz bandwidth of the 60-GHz is often divided equally into four closely-spaced bands for the purpose of multiple access. When four RF bands are transmitted simultaneously, this OCS beating interference from any two of the RF bands may exactly fall into another RF band to cause the severe interference, whose power may be even larger than the desired signal [89].

HeteroOCS mmWaves, on the other hand, can eliminate the interference by adjusting the power ratio of the $\pm\omega_0$ optical carriers and the IF sidebands. As shown in Eq. 3.10, the amplitude, frequency, and phase information can be undistorted in the up-conversion transformation from the IF band (ω_{IF}) to the RF band $(2\omega_0 + \omega_{IF})$ without the induction of excess interferences, even when multiple RF bands are transmitted. In the RF band, a sinusoidal wave is generated at $2\omega_0$ by HeteroOCS mmWaves. This sinusoidal-wave RF carrier is phase- and frequency-locked with the LO of the RoF gateway router. Therefore, it can be used as a LO in the WAP to down-convert the incoming 60-GHz mmWave signals from mobile devices to the IF band at low frequency, which can be directly modulated by an o/e interface.

3.4.1 60-GHz OFDM RoF System

OFDM signals are a summation of multiple orthogonal low-frequency subcarriers, each of which can carry a complex data symbol. RF signals with complex data symbols, which use the amplitude and the phase of the RF carrier, are also known as vector signals. As a result, HomoOCS signals are unable to transmit OFDM signals directly for the strong beating interference between each OFDM subcarrier. HeteroOCS mmWaves, however, are suitable to up-convert these orthogonal low-frequency subcarriers to the 60-GHz band because of its resistance to the inter-channel beating interference and its capability to carry phase information.

As shown in Fig. 3.15, heteroOCS mmWaves can be generated by electrical up-conversion when there is a LO power leakage of the RF mixer. Assuming all the OFDM signals are at the IF band, when the isolation of the RF mixer is not perfect, there will be three RF bands generated by the mixing of the IF band and the LO frequency: $\omega_{LO} + \omega_{IF}, \omega_{LO}, \omega_{LO} - \omega_{IF}$. This is called an RF double-sideband signals. The three RF bands carry the original OFDM signals (U), a sinusoidal wave at LO frequency, and the complex conjugate of the original OFDM signals (L) correspondingly. If the power of the LO frequency is strong, heteroOCS mmWaves can be generated [91]. By taking advantage of the inherent power leakage of the RF mixer, the incremental LO power can generate HeteroOCS Type-I mmWaves. In the optical spectrum, two non-data optical carriers ($\pm\omega_{LO}$) and four data optical sidebands can be found.
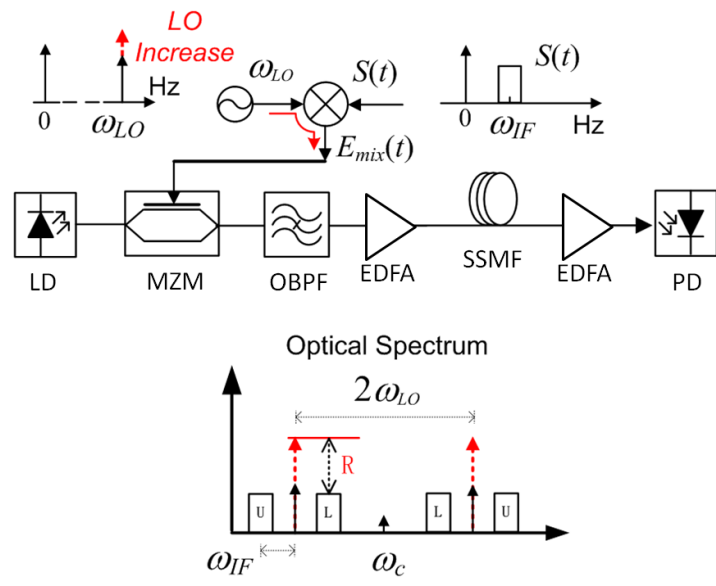
Fig. 3.15. Schematic of HeteroOCS mmWave generation using the LO power leakage through the RF mixer.

After detected by a PD, the HeteroOCS Type-I mmWaves generate three RF bands: $2\omega_{LO} + \omega_{IF}, 2\omega_{LO}$, and $2\omega_{LO} - \omega_{IF}$. However, only the RF band of $2\omega_{LO} + \omega_{IF}$ is used for the wireless transmission and the other two are just redundancy. The experimental results of a 60-GHz OFDM RoF system are shown in Fig. 3.16, while the LO frequency is 30 GHz and the OFDM signals are from 60 MHz to 180 MHz. As the LO power is increased at the RF mixer, the $\pm\omega_{LO}$ optical carriers are getting higher than the data optical sidebands. Therefore the beating interference between OFDM subcarriers is getting smaller and the received OFDM EVM is getting better. However, when the LO power gets too high, the RF mixer is saturated and the received OFDM EVM starts to increase after the LO power is higher than 0 dBm. After being transmitted through a 00-km SSMF and the 3-m wireless distance, the OFDM receiver requires higher RF power to obtain the same EVM because the loss in the fiber transmission degrades the received OSNR in the WAP.

The experimental results have proven the validity of HeteroOCS mmWave generation and transmission of phase/amplitude information with low beating interferences between the OFDM subcarriers. The ratio of the optical RF carriers ($\pm\omega_{LO}$) to the optical IF sidebands ($\pm\omega_{LO}\pm\omega_{IF}$), which is controlled by the LO power in the experiment, is significant in determining the tradeoff between o/e-conversion efficiency and the beating interference.
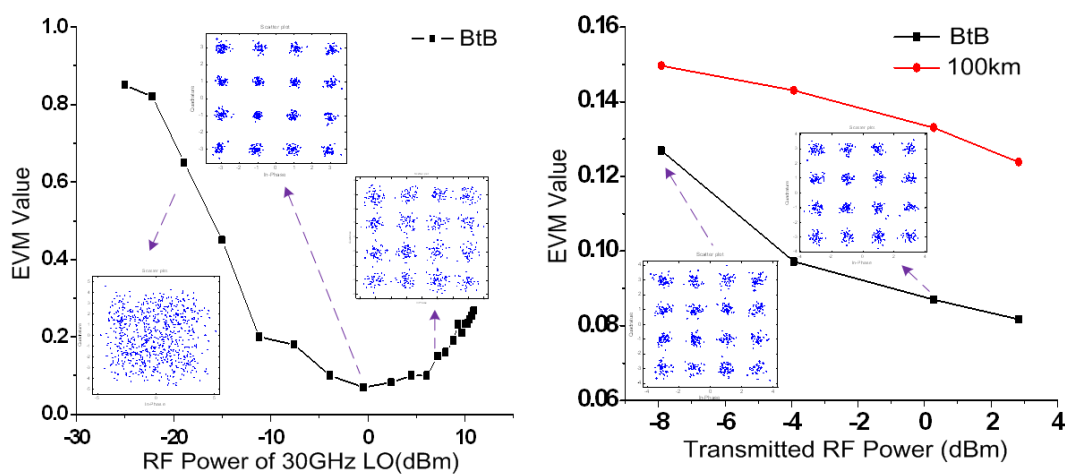
Fig. 3.16. Experimental results of the measured EVM after 3-m wireless transmission. The antennas of the wireless transmitter and the wireless receiver are 15-dBi horn antennas.

3.4.2 60-GHz BPSK RoF System

In the previous experiment, HeteroOCS mmWaves are proven to transmit multiple-carrier vector signals with little beating interference. However, the frequency doubler of the OCS generation is useless when transporting uplink 60-GHz signals from mobile devices back to the RoF gateway router. To overcome the bandwidth limitation of o/e interfaces, an RF superheterodyne-receiver structure can be utilized in a WAP to down-convert the uplink 60-GHz

signals to a low-frequency IF band, which is below the o/e-interface bandwidth. As a result, the IF signals can be transmitted back to the RoF gateway router through the simplest optical transmission setup (Fig. 3.17). If the LO of the WAP has ideal stability and low phase noise, the down-converting process can preserve the amplitude, phase, and frequency information of the original 60-GHz uplink signals.
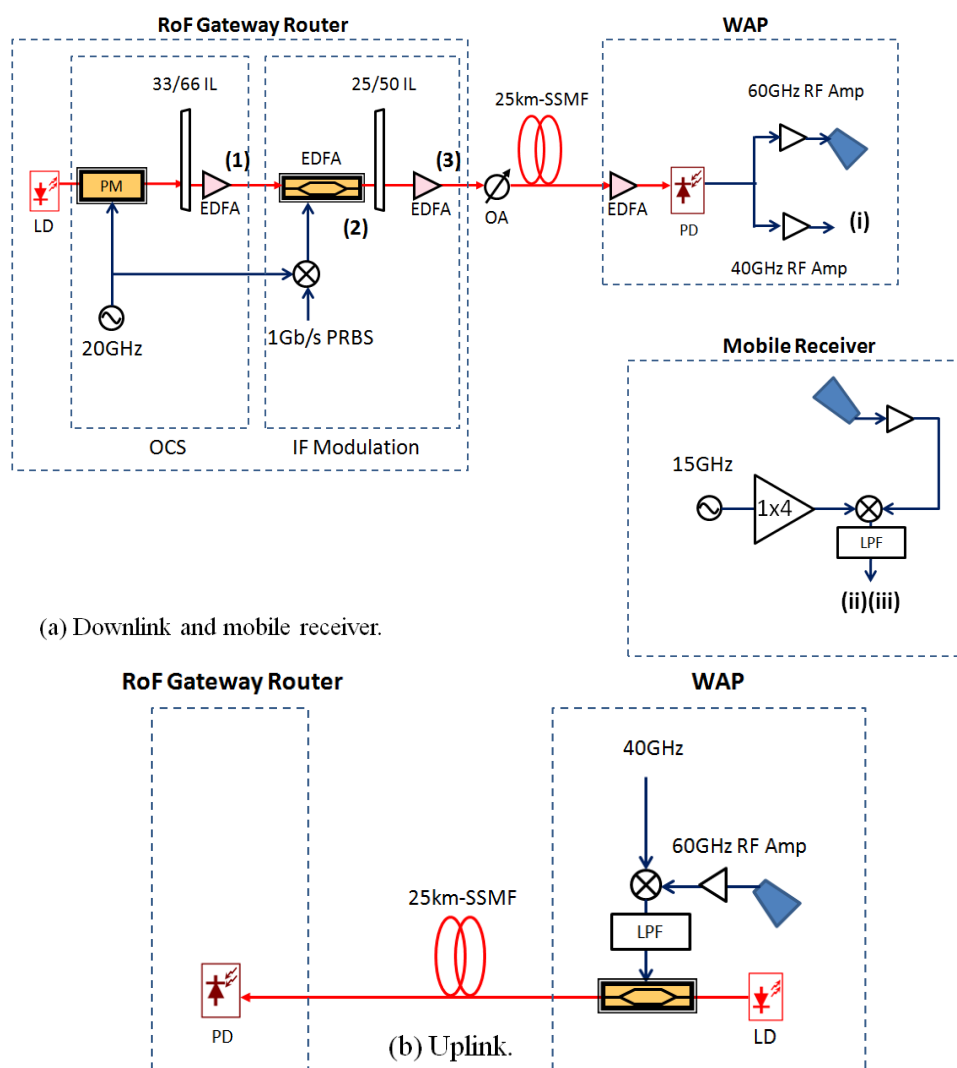
(a) Downlink and mobile receiver.

(b) Uplink.

Fig. 3.17. Experimental setup of the 60-GHz HeteroOCS BPSK System.

The detection of HeteroOCS mmWaves, as derived in Eq. 3.10, generates RF signals at $2\omega_0 + \omega_{IF}$ along with a LO frequency at $2\omega_0$. This LO frequency is spontaneously phase-locked with the LO in the RoF gateway router as long as the linewidth of the LO output is narrow enough. Therefore, this LO frequency can be used as an ideal reference between the uplink 60-GHz signals and the LO in the RoF gateway router to ensure that all the information of the uplink 60-GHz signals is lossless.

To demonstrate the principle of LO-packed HeteroOCS mmWaves, we set up an experiment of a 60-GHz BPSK RoF system, as shown in Fig. 3.17. In the RoF gateway router, the OCS up-conversion and the 1-Gb/s BPSK IF modulation are carried out in series. In general, IF should be much lower than RF in a superheterodyne structure. However, because of facility limitation in our lab, the same frequency source at 20 GHz is used both for the RF of the OCS up-conversion and the IF of the BPSK modulation.

After propagating through a 25-km SSMF, a PD of 60-GHz bandwidth is used as the o/e interface in the WAP. The RF signals generated by the PD are split into two paths. One of the signals passes through a 60-GHz RF amplifier and is sent to a 60-GHz receiver wirelessly. The other path passes through a narrow-band 40-GHz RF amplifier and is measure for its LO frequency. In Fig. 3.18, the measured optical spectra and the eye diagrams are shown respectively for the corresponding locations (1), (2), (3), (i), (ii), and (iii) in the experiment. The measured BER versus the received power is depicted in Fig. 3.19. The power penalty of 25-km-SSMF transmission is about 0.7 dB.

The inset (i) of Fig. 3.18 shows a clear sinusoidal wave at 40 GHz, whose phase is locked with the LO in the RoF gateway router. Therefore, it can be used a source of the LO frequency for the uplink down-conversion process, which only requires a passive double-balanced mixer and a passive RF mixer. When the incoming 60-GHz signals are down-converted to 20GHz IF band, a simple direct ODSB mmWave generation can be used for the uplink transmission.
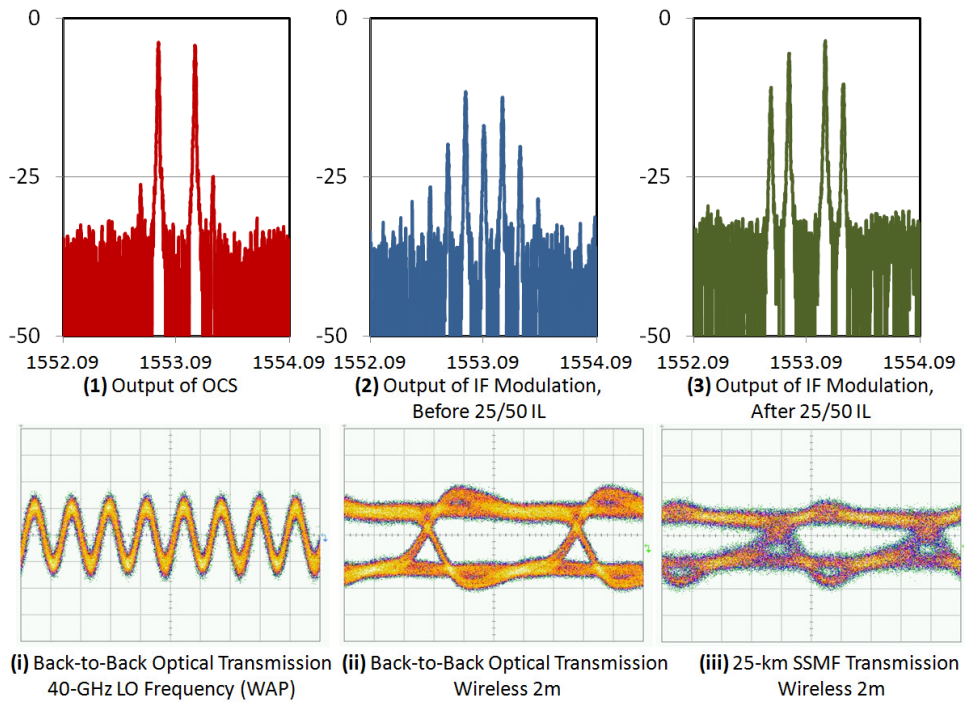
Fig. 3.18. Measured optical spectra (1)(2)(3) and eye diagrams (i)(ii)(iii) of of the 60-GHz HeteroOCS mmWave downlink system.
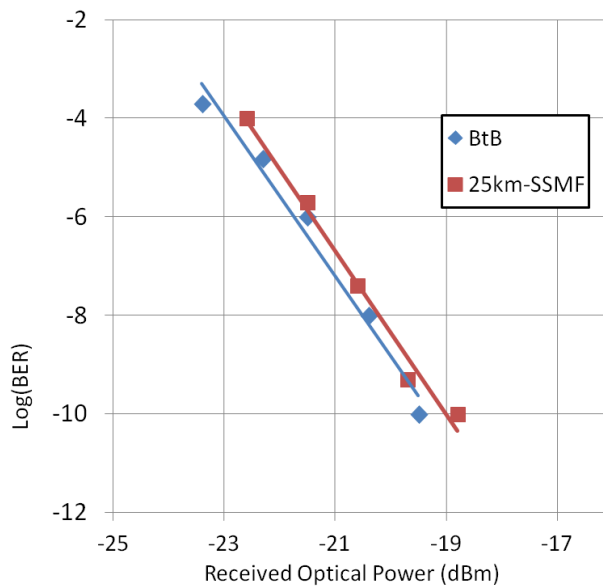
Fig. 3.19. Measured BER versus the WAP received optical power. The wireless transmission distance is fixed at 2 m.

However, like ODSB mmWaves, although the power of the 40-GHz LO frequency is not affected by the chromatic dispersion, the 60-GHz RF power generated by HeteroOCS mmWaves varies periodically along with the fiber length as a result of fiber chromatic dispersion [75]. The power fading can be calculated by the frequency response of a linear dispersion system:

$$H(j\Delta\omega) = \exp\left(-\frac{\alpha}{2}z\right)\exp\left(j\left(\phi_0 - \frac{1}{2}\beta_2\Delta\omega^2 z - \frac{1}{6}\beta_3\Delta\omega^3\right)\right), \qquad \text{(Eq. 3.25)}$$

where ϕ_0 is the initial phase brought by the mmWave modulation process, z is the fiber length. The fiber propagation constant α is the fiber loss coefficient and β_2 is the dispersion parameters:

$$D_{SMF} = -\frac{2\pi c}{\lambda^2}\beta_2 \qquad \text{(Eq. 3.26)}$$

For a SSMF, such as Corning SMF-28 [92], the dispersion coefficient D_{SMF} is 17 ps/nm-km and the loss is 0.22 dB/km. The dispersion parameter β_3 is related to the second-order dispersion coefficient. The typical values of the SSMF parameters are

$$\text{(group index) } n_g = 1.4682 \qquad \text{(Eq. 3.27a)}$$

$$\text{(light speed) } c = 299792456.2\left(\frac{m}{s}\right) \qquad \text{(Eq. 3.27b)}$$

$$\beta_2 = -1.87142892 \times 10^{-26}\left(\frac{s^2}{m}\right) \qquad \text{(Eq. 3.27c)}$$

$$\beta_3 = 0.09 \times 10^{-39}\left(\frac{s^3}{m}\right) \qquad \text{(Eq. 3.27d)}$$

The calculated RF powers of various mmWave generation schemes are shown in Fig. 3.20. The fading period varies with ratio of the OCS frequency (ω_0) to the IF (ω_{IF}). As IF decreases, the length of the HeteroOCS fading period increases. When IF is equal to zero, the length of the HeteroOCS fading period becomes infinite and it is equivalent to HomoOCS. Otherwise, when the OCS frequency reaches zero, the length of the HeteroOCS fading period is minimized and it is equal to an ODSB waveform. However, when the IF sidebands carry data, the data-bandwidth-distance product of HeteroOCS Type-II mmWave signals is worse than conventional HomoOCS mmWave signals because of the two data sidebands of HeteroOCS Type-II mmWaves are further apart than HomoOCS mmWaves. Nevertheless. if HeteroOCS Type-III mmWaves can be generated in the RoF gateway router by designing an adequate IL and

IF/RF values, the negative influence of fiber chromatic dispersion can be minimized since HeteroOCS Type-III mmWaves have a very similar behavior with OSSB+C mmWaves.
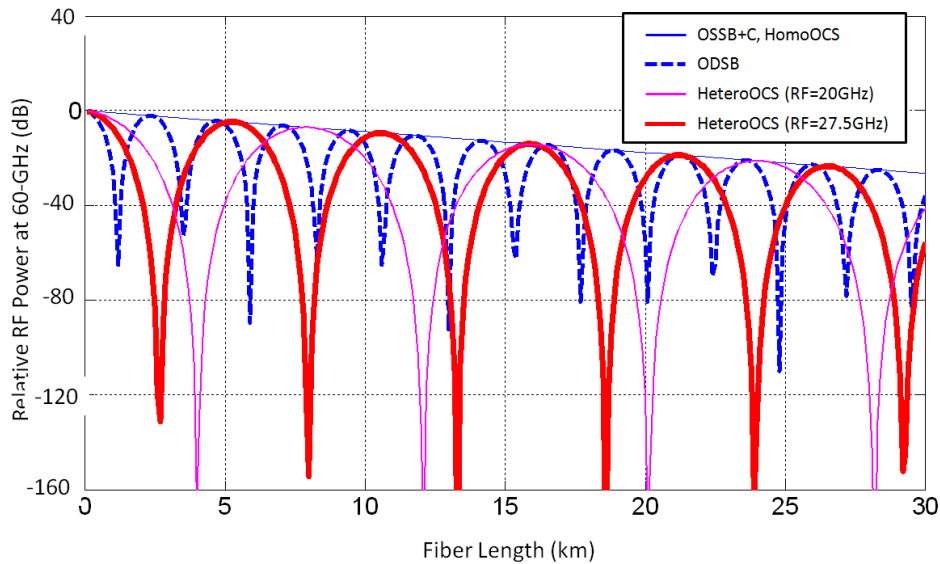
Fig. 3.20. Calculated RF power at 60-GHz of different mmWave wave forms.

3.5 Conclusions

To wrap up the optical mmWaves of RoF systems for the wireless-coverage extension, we propose and investigate the performance and properties of various mmWave generation schemes. A comparison summary of ODSB, OSSB+C, and different OCS modulation schemes is shown in Table 3.1. Each mmWave generation scheme has its fundamental limits, which are needed to be overcome. ODSB and OSSB+C require very high o/e-interface bandwidth. HomoOCS has very high o/e-conversion efficiency but is not suitable for carrying vector signals and multi-band services. HeteroOCS has low o/e-conversion efficiency. However, HeteroOCS can solve the problems of HomoOCS, such as the transportation of undistorted vector signals,

inter-band interference, and insufficient uplink bandwidth. It depends on frequencies, applications and system requirements to decide which modulation scheme is the most suitable scheme. For a 60-GHz RoF system, in general, we believe that HeteroOCS could be the most promising modulation scheme.

Table 3.1. Comparison of various optical mmWave generation schemes.

	ODSB	OSSB+C	OCS			
			Homo	Hetero I	Hetero II	Hetero III
o/e-interface complexity	Low	Medium	Medium	Medium	High	High
o/e-interface bandwidth	High	High	Low	Low	Low	Low
o/e-conversion efficiency	Medium	Medium	High	Lowest	Low	Low
Two-Stage optical up-conversion	N	Y	Y	Y	Y	Y
One-stage electrical up-conversion	Y	N	N	Y	Y	Y
Periodic fading	Y	N	N	Y	Y	N
Uplink ability	Y	Y	N	Y	Y	Y
Speed-distance product	Lowest	Highest	Medium	Medium	Medium	Highest
Inter-band beating interference	N	N	Y	N	N	N
Transporting undistorted vector signal	Y	Y	N	Y	Y	Y

CHAPTER 4

SYNCHRONIZATION-ASSISTED RADIO-OVER-FIBER SYSTEM

4.1 Review of Inter-Chip and Intra-Chip Interconnects

Although the end-to-end transmission distance is quite short, the importance and difficulty of the communication system inside a computer box is not trivial. Computer processing units, evolving from a bipolar junction transistor (BJT) to a complementary metal-oxide semiconductor (CMOS), keep on increasing their computational speed and have overcome several physical limitations to follow the famous Moore's Law for decades. The speed and capability of a processing chip increases as the size of the minimal resolution of the silicon fabrication shrinks. When the resolution of the silicon fabrication approaches the physical limitation and the power budget of processing units approaches the power limitation, processing units evolve from single-core processors to multi-core processors [93]. Multi-core processors can not only increase the computational capability with parallel processing but also lower the power consumption.

However, many benchmark reports of multi-core processors have shown that increasing the core number does not always result into the performance upgrade. This is because in today's general-purpose computer architecture, known as the von Neumann Architecture, instructions and data are stored in the separate chips. No matter how fast a processor clock can be, the memory-fetching latency becomes the unbroken restriction to its overall performance. This restriction is also known as the von Neumann Bottleneck. While today's CMOS technology keeps evolving, logic flops continue to scale faster than the copper-interconnect bandwidth. Integrating more cores inside a processing unit means that more and more memory volume and memory-fetching bandwidth are required for a single chip. Nowadays, the performance of inter-chip interconnects have dominated the overall performance of either high-performance

computing (HPC) clusters or consumer multi-core processing devices, such as personal computers or gaming devices [93, 94].

Therefore, for the von Neumann's architecture, the memory-access throughput of the parallel processing (so-called stream processing) becomes the most desperate criterion to improve the computing capability. For example, a general-purpose graphics processing unit (GPGPU) is a common stream processor module, which handles data on a GPU platform for its powerful double-precision matrix computation, used for HPC parallel computing systems. A 448-core nVidia "Tesla" GPGPU module delivers 525-gigaflop double-precision computations in one processor, and it requires 6-GB dedicated memory and interconnect speed up to 1.15 Tb/s [95]. For high-end applications, processing clusters demand even much higher and faster shared memory. For example, NEC launched the vector supercomputer "SX-9" with a peak processing performance of 839 teraflops in 2007. A single processing unit in "SX-9" contains 64-GB memory and the interconnect speed up to 2048 Gb/s.

The memory-access bandwidth requirement draws interests of the worldwide efforts to improve inter-chip interconnection systems. Unlike long-haul transmission and access networks, the delay tolerance and the power/cost budget of inter-chip transmission systems are extremely tight. The challenges of inter-chip interconnects lie into three major parameters: throughput per pin, power per bit, and cost per bit [96]. Although the core number of a processor keeps increasing, the footprint of a processor chip is not enlarged much. Therefore, even if one waveguide (either a coplanar waveguide or an optical waveguide) can aggregate many high-speed transceivers by various multiplexing mechanisms [97, 98], the throughput per pin does not actually get improved by these multiplexing techniques if the size of each high-speed transceiver is the same. Since the maximal number of pins in a specific area is fixed, the overall off-chip bandwidth is determined by the throughput per pin. On the other hand, the power per bit and the cost per bit normalize the power consumption and cost by the transmission speed in pico-Joule/bit (pJ/b) and $/Gb/s. These two parameters help the industry to determine the

94

practicability of new technology in comparison with conventional copper-interconnection technology.

The conventional technology of interconnects uses copper wires for their high reliability, low cost, and compatibility with current printed-circuit boards. However, the resistance-capacitance charging delay, skin effect, crosstalk and radiation loss all limit its bandwidth-distance product. The distortion from the delay and dispersion can be recovered by the equalization. The path loss of copper wires, which is mostly due to the leakage of the substrate, limits the copper-wire bandwidth-distance product the most. Assuming that there is no surface roughness, a typical differential pair of copper on a conventional FR4 printed circuit board has the loss of 0.7 dB/cm @10 GHz or 1.0 dB/cm @20 GHz, and a differential pair on the low-loss liquid-crystal-polymer substrate has around 0.4 dB/cm @ 10 GHz and 0.7dB/cm @ 20GHz [99, 100]. The high loss of copper wires is tolerable for intra-chip applications, but it limits the throughput of the data access off the chip.

The bandwidth-distance product of copper wires greatly decreases with the wire cross-section area because of the resistance and dispersion. As the processor core number increases, the pin number grows exponentially [94]. Therefore, the requirement of the high pin density in multi-core processors limits the bandwidth-distance of copper interconnects. The large volume of memory requires the distance between memory chips and process chips to be far. Therefore, the bandwidth of copper interconnects is highly limited. The performance of multi-core processors soon grows more slowly than the prediction of the Moore's Law.

While the whole world is looking for the next-generation solution, 3D ICs are believed to be the most promising solution to the bottleneck of copper interconnects. Instead of arranging memory chips on the board nearby the processing chip, silicon interposers can stack the memory chips on top of the processing chip, whose interconnects are achieved by through-silicon vias (TSVs). Such a configuration dramatically reduces the transmission distance between the cores and the memory chips. The distance reduction can greatly lower the transceiver power and increase the bandwidth of interconnects [101]. However, it incurs new problems, such as heat

removing, fabrication compatibility, material-expansion reliability, power distribution, etc., such that the number of stacked chips cannot be too large. Therefore, although the 3D IC can increase the memory-access bandwidth, the small footprint of a processing chip actually limits the amount of available memory on top of it. In the analysis of [102], it shows that adding more cores only exacerbate the electrical "chip-escape" bandwidth even in the 3D-IC configuration.

As a result, many research reports [94, 96, 97, 102, 103] have shown that optical interconnects will eventually replace the copper-wire electrical interconnects because of the extremely high bandwidth-distance product in optical channels. In addition, the size and the pitch of optical waveguides are much smaller than copper wires for the high-density implementation. The power consumption of optical transceivers of vertical-cavity surface-emitting lasers (VCSELs) has been shown to be lower than electrical transceivers for the transmission distance above 10-cm. However, detailed studies show that the power consumption of inter-chip interconnects is dominated by the serialization and clocking circuits [100], which are required both for electrical and optical interconnects, and therefore optical interconnects actually are less efficient in this distance. Moreover, the size of optical drivers and transimpedance amplifiers are still large to achieve very high-density pins. The most difficult part to substitute optical interconnects for electrical interconnects, however, is to overcome the short lifetime of high-speed VCSELs and the high cost of optical coupling/packaging techniques.

In addition to the wired transmission (optical waveguides, TSVs, or copper wires), wireless interconnects start to draw the world's attention because the multi-gigabit capability of wireless transmission can be achieved by mmWave technology. In the past, wireless inter-chip interconnects were not taken seriously because the antenna size is bulky (around a quarter of wavelength) and the wireless channel capacity is low. Recently, the maturity of mmWave technology not only enables gigabit transmission wirelessly over a few meters, but also shrinks the RF module to a smaller footprint to a few millimeters. Using RF to carry signals, more spectrally-efficient modulation formats can be deployed with its phase and polarization diversity, making RF transmission more spectrally efficient than baseband wired links. The wireless

transmission distance is longer than copper-wire transmission at high frequency because it has smaller path loss compared to the copper wire. The RF path loss obeys the Friis transmission equation:

$$\frac{Pr}{Pt}(dB) = G_r + G_t + 2log\frac{\lambda}{4\pi R}. \tag{Eq. 4.1}$$

Here Pr and Pt are the received and transmitted powers respectively; G_r and G_t are the received and transmitted antenna gains in dB respectively; λ is the wavelength of the mmWave; and R is the wireless distance. The mmWave attenuation of the atmosphere is negligible in such a short distance. The path loss of a copper wire is mainly determined by the loss coefficient α:

$$\frac{Pr}{Pt}(dB) = -\alpha R. \tag{Eq. 4.2}$$

It is easily seen that the wireless transmission has much less loss than the wired transmission after a certain distance. Moreover, in a LoS wireless link, the path of the free space has no dispersion at all for any frequency. As a result, minimal equalizations are required for the wireless interconnects. Compared against optical interconnects, the wireless coupling has much higher alignment tolerance in the LoS situation, and the reliability of CMOS electronics is proven to be more accountable than active optical components.

Considering the power consumption, near-field wireless transceivers can achieve power consumption as low a few pJ/b [104, 105], but the transmission distance is limited to very few micrometers. Far-field (over a few centimeters) wireless mmWave transceivers consumes power from 6.4 pJ/b to over 100 pJ/b [106 - 109], depending on the type of CMOS technology and the targeted transmission distance. However, hundreds of RF modules are meant to be installed for the memory-access interconnects, the interference among multiple transmitter-receiver pairs are extremely severe and need to be taken care of in low latency. The BER performance of wireless interconnects is always limited because of the frequency offset and phase noise of the LO. In conventional wireless systems, these impairments are usually recovered in the digital domain, but the DSP latency is not tolerable for wireless interconnects.

Table 4.1 compares the characteristics of the three interconnection types under active development: copper, optical, and wireless interconnects. Although the copper wires have many disadvantages, they are still the most common interconnect method for HPC and multi-core-processor industries, while optical interconnects have started to take over the transmission distance of a few meters between HPC racks in today's fastest HPC systems, such as IBM Blue Water, Tienhe 1A, and Fujitsu K Computer [110]. 3D ICs with TSVs and silicon interposers have been under development for years but are not yet ready for the practical implementation. On the other hand, the research of wireless interconnects has just emerged in various special occasions.

In addition to deploying and modifying mature transmission techniques, including copper, optical, and wireless interconnects, state-of-the-art interconnection technologies such as graphene, carbon nanotubes [117], electromagnetic-bandgap waveguide [118] or silicon photonics [119] are also under development but far from practical implementation yet.

Table 4.1. Comparison List of Various Interconnects.

	Copper Wire [111]	Optical [112]	Wireless [113]
Data Rate	16Gb/s	12Gb/s	11Gb/s
Transmission distance (mm)	76	75	14
Energy (pJ/b)	13	15.6	6.4
BER	10^{-14}@PRBS2^{23}-1	10^{-12}	2^{-11}@PRBS2^7-1
Process	65nm CMOS	130nm CMOS	40nm CMOS
Size(mm^2)	5.4 for 32 Tx/Rx	17.0 for 16 Tx/Rx	0.13
Minimal Pitch	180	62.5	X
P.S.	Inc. clocking circuits		

	Copper Wire [114]	RF [115]	Inductive [116]
Data Rate	10Gb/s	10Gb/s	1Gb/s
Transmission distance (mm)	1 - 175	120	0.015
Energy (pJ/b)	3.8 - 4.6	5.7	3
BER	10^{-12}	10^{-12}@PRBS2^7-1	2^{-12}@PRBS2^{23}-1
Process	45nm CMOS	40nm CMOS	180nm CMOS
Size(mm^2)	0.133	0.40 for 2 Tx/Rx	2.00 for 1024 Tx/Rx
Minimal Pitch	66um (1-mm length)	X	30
P.S.	Using SMA connectors	Plastic RF waveguide	

4.2 Radio-over-Fiber for Wireless Synchronization

There are a variety of techniques to improve the bandwidth of interconnects to resolve the von Neumann bottleneck. Among all the interconnection techniques, wireless transmission has the greatest potential for the purpose of memory-access inter-chip communications in the near future. In the distance of a few centimeters, wireless interconnects have better power efficiency, reliability, and coupling tolerance than optical interconnects. On the other hand, high-frequency RF signals in the air have lower path loss than signals in copper wires and therefore provide more flexible and longer transmission than copper-wire interconnects. This allows much larger area to implant higher-volume memory chips than using copper wires.

However, the BER of wireless transmission is usually too high for the applications of memory-access transmission. In the non-line-of-sight wireless transmission, the BER is limited by the multi-path interference and signal fading. In the LoS wireless transmission for the inter-chip interconnects, the BER is limited by the RF LO and the multi-channel interference. A typical RF front-end of a wireless receiver is composed of the automatic gain control, the I/Q down-conversion, the match filter, the clock recovery, the carrier recovery, the adaptive equalizer, and the demapper. The function of each component is listed in Table 4.2. In common wireless consumer electronics, the first four components are mostly achieved by analog RF circuits. The other components are achieved in the digital domain after ADCs because these functions are too complicated and are limited if done by analog circuits.

Using wireless interconnects, the location of each transceiver is tightly fixed, and the wireless link is LoS. As a result, the transmission condition is fairly simple and the wireless link is robust. However, the BER is still limited by two major factors: the negative effects of the RF LO and the inter-channel interference. The fractional frequency deviation and phase noise of the RF LO can degrade the received RF signals of any crystal-based LO [120]. Even with phase-locked loops (PLLs), the BER is still limited by the imperfection of the RF LO [121] without the help of DSP to compensate the fractional frequency deviation and phase noise of the LO

mismatching. However, DSP requires several clock cycles even just fulfilling simple digital functions. The DSP latency is obviously intolerable in the application of inter-chip interconnects.

Table 4.2. Functions of the RF Front-End.

Component	Function
Automatic Gain Control	Optimal position of constellation diagram in reception window
I/Q Down-Conversion	Retrieval of I and Q baseband signals.
Match Filter	Pulse shaping.
Clock Recovery	Sampling reference for ADCs.
Carrier Recovery	Carrier frequency reference.
Adaptive Equalizer	Compensation for channel distortions.
Demapper	Representation of received data symbols to bits.

Moreover, the interference between adjacent transmitter-receiver pairs is severe for wireless interconnects. Multiple wireless transmitter-receiver pairs are required to communicate with each other simultaneously to aggregate the data rate over 1 Tb/s. With the limited space of HPC blades and circuit boards, the perfect isolation between the closely-spaced transmitter-receiver pairs is difficult to achieve. These wireless transmitter-receiver pairs basically form a MIMO subsystem, but in this situation, DSP of the MIMO demultiplexing is also not an option to cancel the inter-channel interference because of the DSP latency.

4.2.1 Optical Local-Oscillation Distribution

The two major BER limiting factors (the LO frequency mismatching and the inter-channel interference) can be feasibly resolved by the RoF technology. The RoF technology can

synchronize the LO of each transmitter-receiver pair by distributing a centralized LO frequency with optical fibers. In the meantime, the MIMO multiplexing/demultiplexing can be fulfilled without DSP because all the dynamic variations in wireless systems, including LO frequency, locations, power, and timing, are all eliminated in RoF wireless interconnects. An optical local-oscillation distribution (OLOD) RoF system for wireless interconnects is shown in Fig. 4.1. The LO is distributed optically by optical-fiber transmission. Multiple wireless transceivers can share one photodetector to save the power and the cost. The detailed function blocks of the wireless transceivers are shown in Fig. 4.2. Frequency-division multiplexing can be used by deploying various frequency multipliers to up-convert the data to various RF bands. For the wideband wireless systems, multiple RF transceivers still need to use the same RF band. These RF transceivers in the same RF band form a wireless MIMO subsystem, which can be multiplexed and demultiplexed by simple analog circuits.
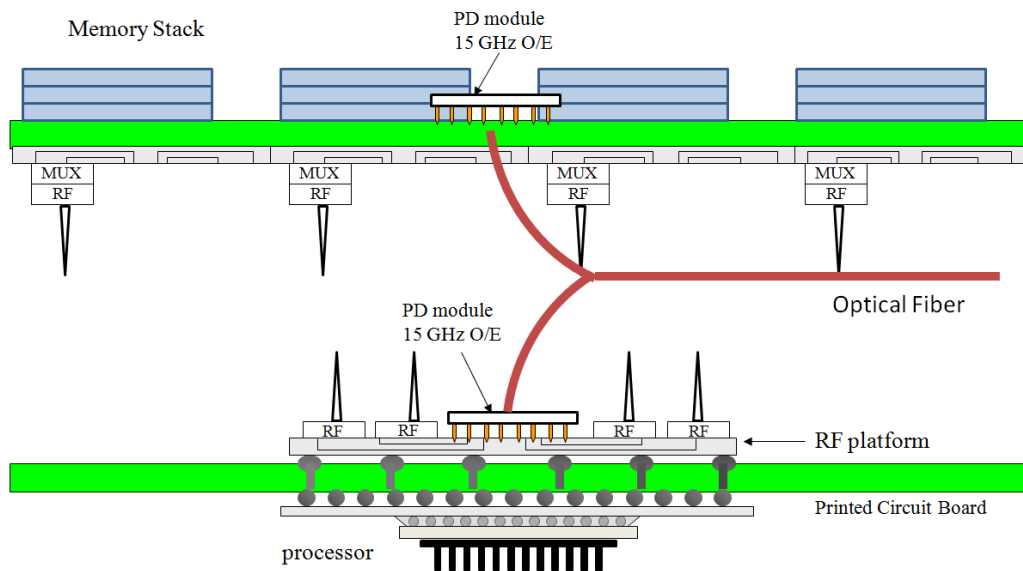
Fig. 4.1. Schematic of OLOD MIMO memory-access system.
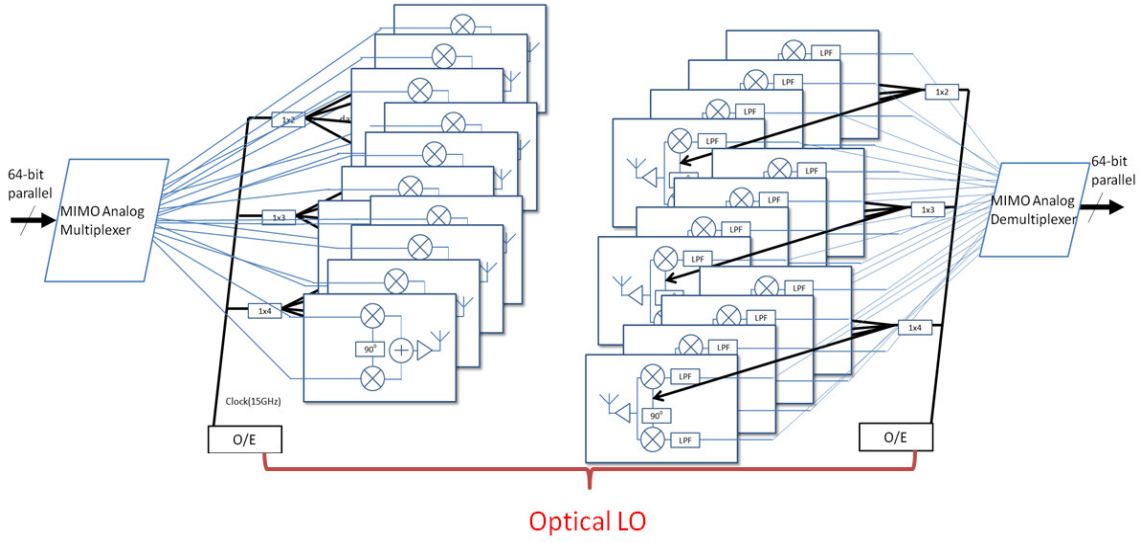
Fig. 4.2. Schematic of the OLOD MIMO transmitter and receiver.

When all the wireless transceivers share the LO frequency from a single frequency source, they are "synchronized" as long as the difference of their LO distribution distances are much smaller than the LO coherent length. "Synchronization" means that their LO frequency does not have fractional frequency deviation and phase noise. For example, if the LO frequency from a crystal-based PLL is

$$f_{LO}(t) = \cos{(\omega_{LO}t + \phi(t))}, \qquad (Eq.\ 4.3)$$

where ω_{LO} is the angular frequency of the PPL frequency and $\phi(t)$ is the random phase noise. Each crystal-based PLL has fractional frequency deviation around 200 ppm. The LO phase noise can be modeled as a Wiener process with no PLL and or be modeled as an Ornstein-Uhlenbeck process with a PLL [121]. When a wireless transmitter and a wireless receiver use the LO frequency of different crystals, the fractional frequency deviation and phase noise will generate fast and slow phase variations respectively to generate errors to the received signals. Without DSP to compensate these phase variations dynamically, it is very difficult to track the phase variations perfectly in the wireless receiver. However, when using RoF systems to distribute the

LO reference from the same frequency source, even if the stability of this frequency source is poor, the phase variations of all the transmitter-receiver pairs will be the same spontaneously. That is, the LO of the transmitter and the LO of the receiver are perfectly synchronized if their frequency comes from the same frequency source.

4.2.2 MIMO Wireless Interconnects

Multiple wireless transmitter-receiver pairs in the same RF band form a MIMO subsystem. In conventional mobile MIMO systems, the multiplexing and the demultiplexing have to be done in the digital domain because there are so many dynamic variations, such as the locations, timing, phase, and frequency. In fixed wireless interconnects, once the LOs are synchronized by OLOD, it is possible to use analog circuits to demultiplexing the MIMO signals without dynamic tracking systems.

To represent the MIMO operation explicitly, the linear algebra is used here to represent the MIMO channel. Assuming H is an NxN complex matrix, the linear-algebra operator is defined by the following: H^{-1} represents the inverse matrix of H; H^H represents the Hermitian transpose (or conjugate transpose) of H; H^* is a matrix, each entry of which is a complex conjugate of H. Assuming all the data symbols are synchronized in each wireless receiver, an NxN MIMO system (with N transmitter antennas and N receiver antennas) in a narrow-band additive-white-Gaussian-noise (AWGN) channel can be modeled as

$$\vec{y} = H\vec{x} + \vec{w}, \tag{Eq. 4.4}$$

where H represents the NxN channel matrix to express the amplitudes and the phases between transmitter antennas and receiver antennas; $\vec{y}, \vec{x}, \vec{w}$ represent the Nx1 signal vectors of the received signals, transmitted signals, and additive noise respectively. When all the signals are in the same RF band, the channel matrix and signal vectors are represented by complex phasors to express the phases and amplitudes of the RF signals. If the channel matrix is known by the

transmitters and the receivers, the transmitted signals $\vec{x}$ can be recovered by simple linear algebra. That is, a series of additions and scalar amplifications, which can be easily fulfilled by analog circuits, can be applied to demultiplex the MIMO signals.

Although theoretically the MIMO channel capacity (bit/s/Hz) can be increased as high as possible when the antenna number is increased, the maximal channel capacity is bounded by the Shannon's limit because the transmitted power is finite. In addition to the SNR and bandwidth of the MIMO system, the MIMO channel capacity is determined by the channel matrix. For the flat-fading assumption, the channel capacity of the NxN MIMO channel H with the equal-power transmission is

$$C_{FLAT} = \log_2 \ \det \left(I_N + \frac{E_s}{NN_0} HH^H \right),$$ (Eq. 4.5)

where E_s is the average signal energy, and $N_0/2$ is the noise spectral density of the AWGN channel; I_N represents the NxN identity matrix [122]. As a result, using the MIMO spatial multiplexing, it is possible to utilize a LoS mmWave MIMO subsystem to build a terabit transmission system with a very simple demultiplexing scheme. If the antennas are carefully arranged and designed, the polarization of electromagnetic waves can also be used to further increase the signal diversity in the mmWave MIMO subsystem [123].

4.3 MIMO Analog Multiplexing and Demultiplexing

4.3.1 Receiver Demultiplexing

A MIMO transmission system is composed of multiple transmitters and receivers. A MIMO demultiplexer can be installed to recover the transmitted signals from all the receivers. When the signals of all the MIMO receivers and the channel matrix are known in one MIMO demultiplexer, there are three common MIMO demultiplexing methods: the zero-forcing (ZF) method, the Match Filter (MF) method, and the Minimal Mean Square Error (MMSE) method.

These methods use a linear matrix to multiply the received vector to recover the original transmitted vector instantaneously. Because of OLOD and fixed antenna positions, the matrix multiplication can be achieved by a series of analog circuits of amplifications and additions.

The most straightforward to demultiplex the MIMO signals is the zero-forcing (ZF) method. If the channel matrix is invertible, all the original signals can be recovered simultaneously by the inverse channel matrix:

$$\vec{\hat{x}} = H^{-1}\vec{y} = \hat{x} + H^{-1}\vec{w}. \tag{Eq. 4.6}$$

The original signals are estimated by $\vec{\hat{x}}$. However, the performance of the MIMO ZF demultiplexer depends on the channel matrix H. If H is ill-conditioned, the noise vector will be amplified by H^{-1} dramatically to degrade the accuracy of the estimation. The condition number of H depends on the angle (θ) and the distance-pitch ratio (R/d), as depicted in Fig. 4.3.
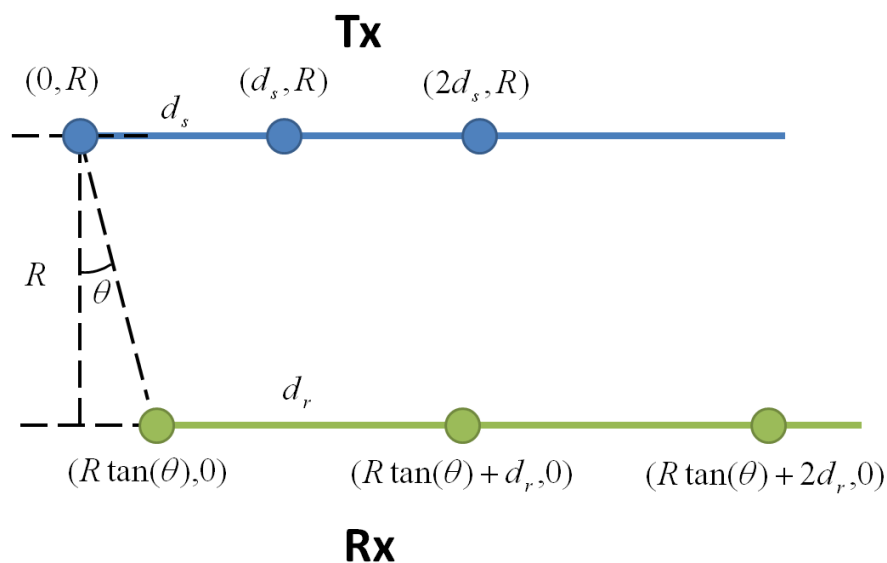
Fig. 4.3. 1D Array of a MIMO transmitter and a MIMO receiver.

A 2x2 MIMO OOK transmission system is simulated with R equal to 15 cm and θ equal to 75$^{\text{o}}$ in the line-of-sight condition. The SNR is defined by

$$SNR = E\left[\frac{\overrightarrow{x^{\text{H}}}H^{\text{H}}H\vec{x}}{\overrightarrow{w^{\text{H}}\vec{w}}}\right].$$ (Eq. 4.7)

As shown in Fig. 4.4, when the antenna pitch d is wide, the condition number of the channel matrix is small with the best BER performance. In addition, the condition number increases with the number of the transmitter-receiver pairs. Figure 4.5 shows the simulation results of the 2x2, 4x4, 6x6, and 8x8 MIMO transmissions when d is equal to 1.0 cm. In conclusion, the BER performance of the MIMO ZF demultiplexing is mainly determined by the condition number of the channel matrix in the AWGN channel.
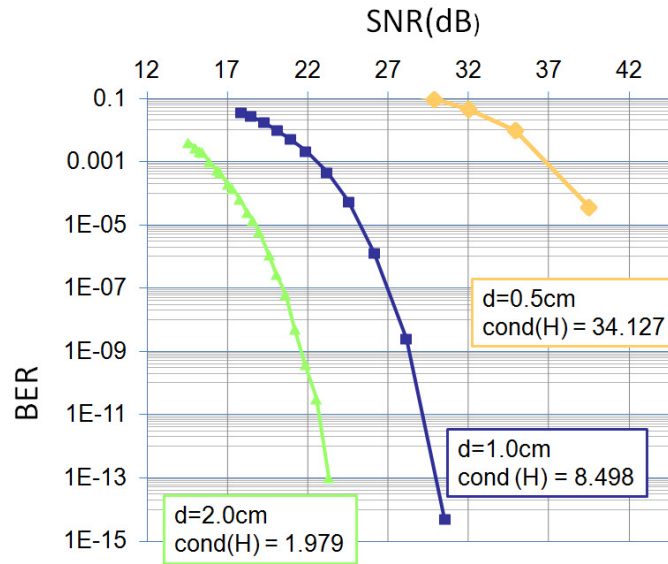
Fig. 4.4. BER versus SNR for different antenna pitch distances. Cond(H): condition number of the channel matrix H..
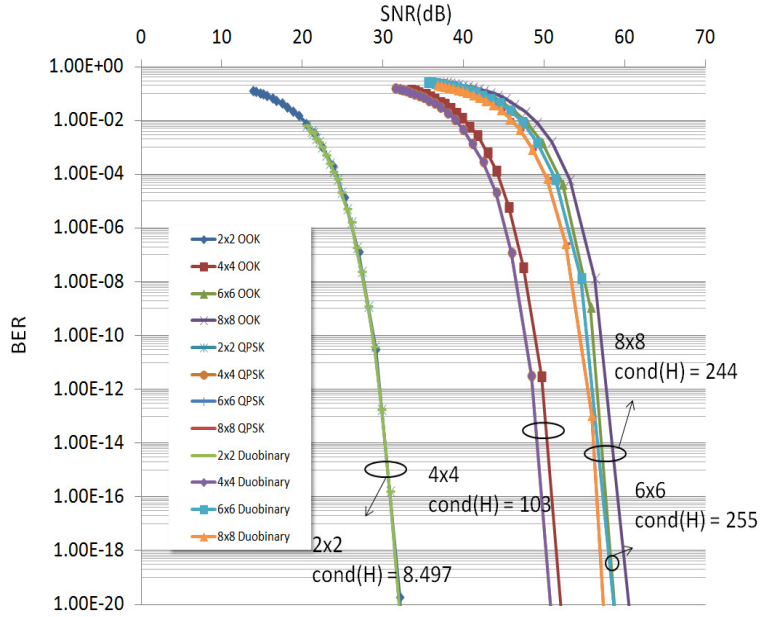
Fig. 4.5. BER versus SNR for modulation formats and antenna number. The pitch distance is fixed at 1 cm. Cond(H): condition number of the channel matrix H.

The ZF method cancels out the interference of the MIMO channel but ignores the existence of noise. On the other hand, the MF method ignores the inter-channel interference of the MIMO channel but maximizes the signal power. The MF method uses the complex conjugate of the channel matrix to maximize the power of the transmitted vectors. However, for wireless interconnects, the inter-channel interference dominates the impairment factors of the MIMO transmission. As a result, the performance of the MF method is usually inferior to the ZF method when the distance of each transmitter-receiver pair is very close.

However, the inter-channel interference does not have to be cancelled out completely. It only has to be lower than the noise level. Instead of cancelling out the inter-channel interference and amplifying the noise, the MMSE method estimates the original signal by minimizing the mean square error. The mean square error is

$$MSE = [(M(H\vec{x} + \vec{w}) - \vec{x})^H (M(H\vec{x} + \vec{w}) - \vec{x})], \qquad (Eq. 4.8)$$

107

where M is the demultiplexing matrix. Using the MMSE method [124], the optimal M to minimize the mean square error can be found as

$$M = H^H(HH^H + \frac{N_0}{E_s}I_N)^{-1}. \qquad \text{(Eq. 4.9)}$$

Notice that when the spectral density of noise is zero, the MMSE demultiplexer is equivalent to the ZF demultiplexer. Without the ZF constraint that forces $MH = I_N$, the MMSE demultiplexer can find an optimal point between the inter-channel interference and the noise of the MIMO channel.

   To illustrate the BER performance of the three MIMO demultiplexing methods, we have set up the simulations of a linear transmitter (Tx) array and a linear receiver (Rx) array, which is parallel to each other. The antenna pitch of MIMO transmitter is ds; the antenna pitch of MIMO receiver is dr; the perpendicular distance between the transmitter and the receiver is R; the center of the Tx array and the Rx array are aligned. The MIMO channel is assumed to be a perfectly synchronized AWGM channel.

   Neglecting the multi-path interference, the simulation results of the 2x2 MIMO wireless transmission with various SNRs and R are shown in Fig. 4.6. "Pre D" is the pre-distortion method, which is explained in the next section. In the high SNR regime, the BER performance of MMSE and ZF is very similar because the system performance is dominated by the inter-channel interference. At a certain distance, when the inter-channel interference is minimized by the spatial arrangement of the transmitters and the receivers, the MF method can be dramatically improved. However, MMSE is still the best method in terms of BER performance however the spatial arrangement of all the antennas is. In Fig. 4.7, the BERs versus different distances are shown at the SNR of 18 dB. The BER gets worse when the antenna number is increased because the inter-channel interference is increased with the number of antennas. The fluctuation of the BER curves along the distance is due to the variation of the channel-matrix condition number. A high condition number means the variance of each wireless channel is little, and therefore the transmitted signals from adjacent transmitters become more indistinguishable in the MIMO

demultiplexer. Similar results happen when varying the antenna pitch. As shown in Fig. 4.8, the BER curve fluctuates with the receiver antenna pitch for a 2x2 MIMO subsystem and a 4x4 MIMO subsystem. When the inter-channel interference is much higher than the noise in the MIMO channel, the MSEE performance is similar to the ZF performance. That is, their performance is both highly dependent on the condition number of the channel matrix.
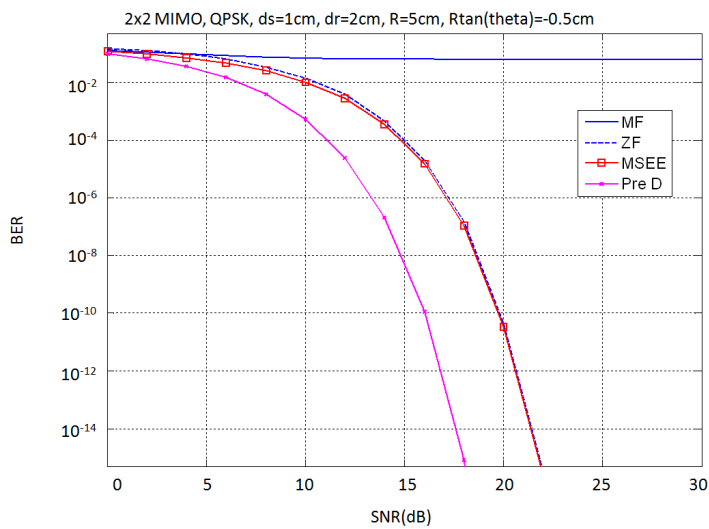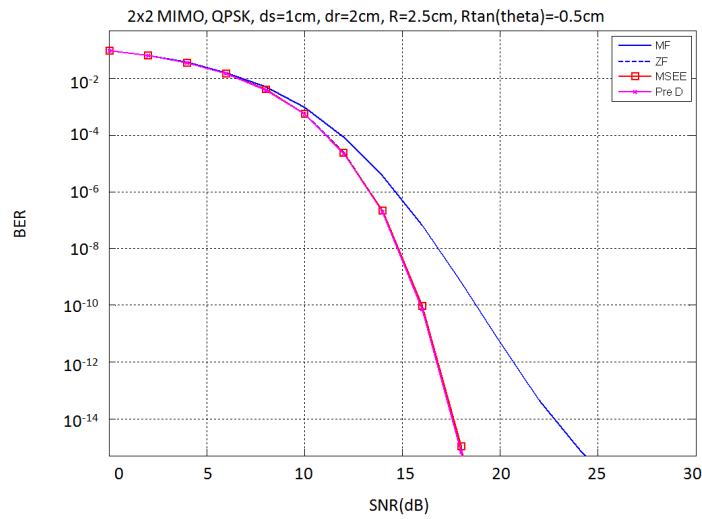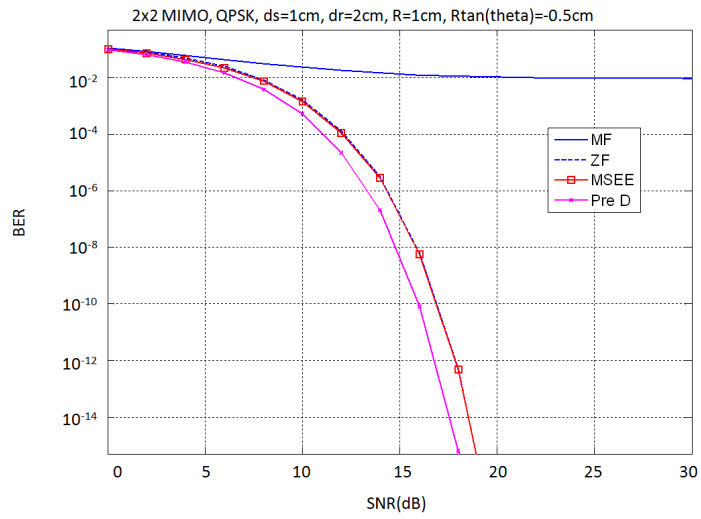
Fig. 4.6. Simulation results of the BER versus SNR of 2x2 MIMO transmission.
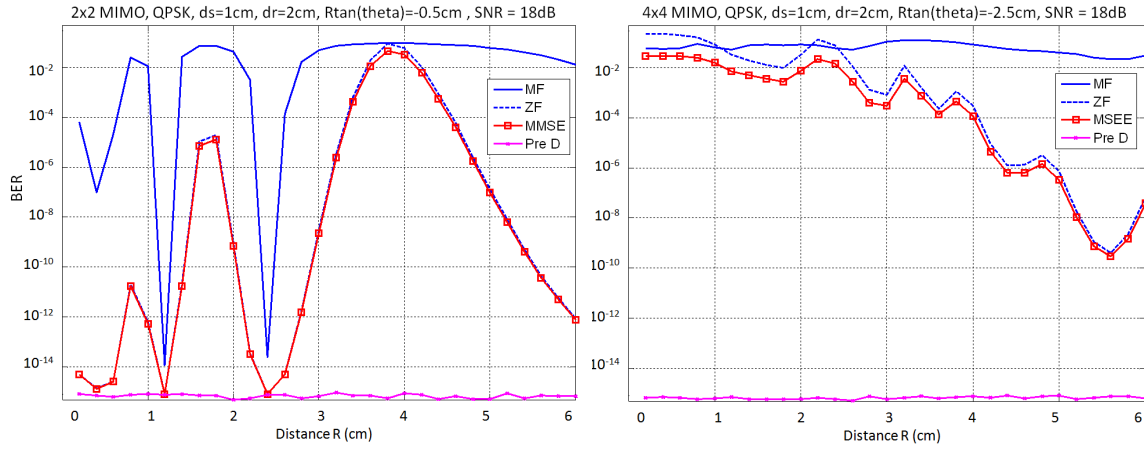
Fig. 4.7. Simulation results of the BER versus R of MIMO transmission.
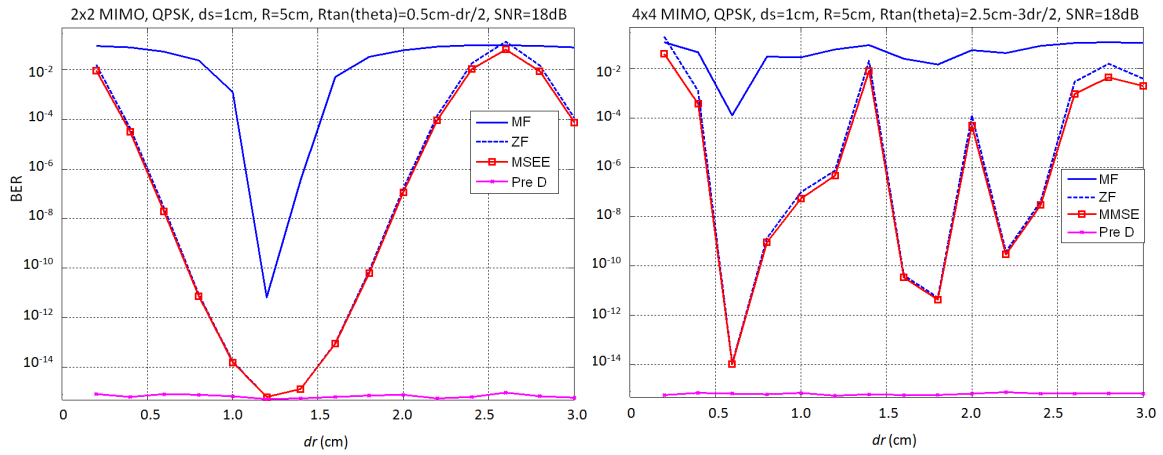
Fig. 4.8. Simulation results of the BER versus *dr* of MIMO transmission.

4.3.2 Transmitter Multiplexing

Rather than demultiplexing the received signals in the MIMO receivers, the transmitted signals can be pre-distorted before sending them out to the air in the MIMO transmitters. When all the transmitted signals are known in the MIMO multiplexer of a wireless transmitter, the signals can be multiplexed by the pre-distortion matrix D. Assuming the noise only comes from the wireless channel, the received MIMO signals are

$$\vec{y} = HD\vec{x} + \vec{w}. \tag{Eq. 4.10}$$

If the channel matrix is known in the multiplexer and the pre-distortion matrix D is equal to H^{-1}, the MIMO receiver can directly receive the original transmitted signal $\vec{x}$ without any MIMO demultiplexing method. Using the pre-distortion matrix, the receiver antenna can be placed far apart since each receiver does not have to know the received signal of the other receivers. However, all the transmitters have to be connected to the MIMO multiplexer closely to prevent the loss of wired links.

Because the pre-distortion method neutralizes the effect of the channel matrix before the wireless signals propagating in the wireless channel, the performance of the pre-distortion method is independent from the condition number of the channel matrix if the wireless transmitters and receivers are ideal. As shown in Fig. 4.6, Fig. 4.7, and Fig. 4.8, the BER performance of the pre-distortion method is mainly determined by the SNR. When the condition number of the channel matrix is low, the BER performance of the MMSE and ZF method is close to the pre-distortion method. Otherwise, the pre-distortion has the best performance.

A 2x2 60-GHz MIMO test bed is set up to demonstrate the MIMO analog multiplexing. Owing to the limited availability of our lab equipment, we generate the two transmitted OOK signals optically. As shown in Fig. 4.9, two two-Gb/s mmWave signals at the 60-GHz band are generated by the OCS generation and then separated to two SSMFs with difference lengths to uncorrelated the data sequence. Two o/e-conversion modules convert the optical signals to the RF signals. The OCS mmWave generation requires the 30-GHz LO, which is obtained by the

112

frequency quadrupler with a 7.5-GHz LO. For the RF receiver, the 60-GHz LO is obtained by the 15-GHz LO and the other frequency quadrupler.
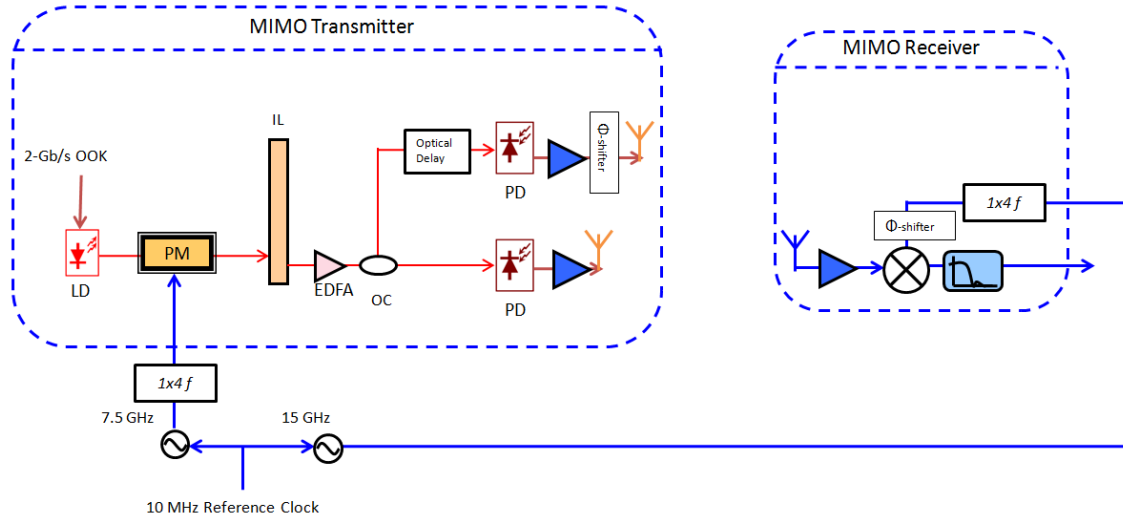
Fig. 4.9. Experimental setup of the OLOD 2x2-Gb/s-OOK wireless transmission with MIMO analog multiplexer.

The two LOs are synchronized by a 10-MHz external reference clock. The wireless transmitters are located at the fixed position and one wireless receiver is used to down-convert the signals directly. Without the MIMO demultiplexing, the phase difference of the wireless transmission is set by the wireless transmitter to have the channel matrix normalized as

$$HD = \frac{1}{\sqrt{2}}[1 \quad j].$$ (Eq. 4.11)

As a result, the OOK signals of the in-phase transmitter are directly down-converted while the OOK signals of the out-of-phase transmitter are eliminated in the wireless receiver. In the experiment, the transmitted symbol rate is two Gb/s. The pitch between the two transmitter antennas is 10 cm, and the wireless distance is 50 cm. The OSNR is estimated by the optical spectrum analyzer at the resolution of 0.1nm. The BER measurements versus OSNRs are shown

113

in Fig. 4.10. Because the RF mixer cannot eliminate the out-of-phase signals perfectly as a result of the connector impedance mismatching, the MIMO transmission requires one-dB higher OSNR than the single-input-single-output transmission. To the limitation of the BERT, the error-free MIMO transmission of the overall four-Gb/s throughput can be achieved at the OSNR of 29.6 dB for both the SISO and the MIMO subsystems.
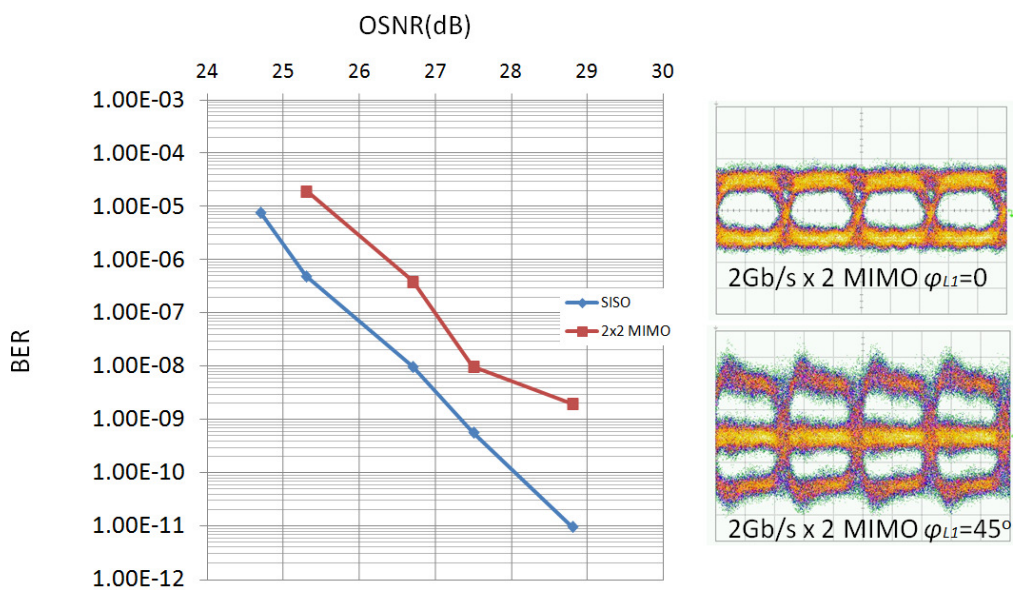
Fig. 4.10. BER measurements versus OSNR of the 2Gb/s x 2 OOK MIMO transmission. The insets on the right side shows the measured 2x2 MIMO error-free eye diagram at OSNR=29.6dB; φ_{L1} is the phase difference between the received mmWaves and the receiver LO.

4.4 Conclusions

Conventionally, copper wires and VCSEL-and-fibers are already deployed in the HPC interconnect system. Copper wires are the main medium for the ultra-short-reach interconnects, such as intra-chip and inter-chip transmission systems. Because of the high loss and the low bandwidth-distance product of copper wires, the copper-wire transmission distance is tightly

114

limited. As the demands of higher inter-chip transmission keep rising, the copper-wire interconnects gradually face more and more rigorous challenge. The optical interconnects of VCSELs and optical fibers are the proven technology for data communications over hundreds of meters. On the contrary of copper wires, the extremely high bandwidth-product and the low loss of optical fibers can easily support terabit data transmission. Therefore, optical interconnects have been deployed in modern top 500 HPC systems for the inter-rack and inter-board communications. However, the size, power consumption, optical coupling difficulty, and cost of optical transceivers are the main reasons to restrict the application of optical transmission in the high-density and short-distance inter-chip interconnects.

In the meanwhile, wireless interconnects have great potential to efficiently support the inter-chip interconnects with the moderate power consumption and flexible access arrangement. Capacitive-coupling and inductive-coupling of wireless interconnects have been considered as potential candidates to establish the connections between stacked chips in a 3D IC to replace TSVs because of the fabrication complexity and mechanical difficulty of TSVs [125]. With OLOD and MIMO analog multiplexing-demultiplexing, the effective transmission distance of wireless interconnects can be greatly improved. As a result, rather than 3D ICs, more flexible inter-chip architectures and memory-access systems can be designed to fulfill future HPC interconnect requirement.

CHAPTER 5

CONCLUSIONS

5.1 Summary of Radio-over-Fiber Properties and Applications

5.1.1 High-Capacity Optical Transmission

In conventional high-capacity optical transmission, multiple wavelength-precise lasers are required to establish a DWDM system to multiplex terabit signals into multiple optical channels. However, the management of a large number of lasers is very costly and has great difficulty in scalability. The RoF system uses an RF carrier to generate multiple orthogonal carriers from one laser. These orthogonal channels provide great advantages in flexibility, manageability, spectral efficiency, and FDE feasibility. Either digital or optical multiplexing/demultiplexing can be applied for the multiple-orthogonal-carrier system to facilitate the optical transceiver design.

As a result, multiple-orthogonal-carrier optical systems, including OFDM and OWDM systems, are under the rapid development to fulfill the bandwidth-demanding backbone networks. In corporation with digital CO receivers, extremely high-capacity transmission can be achieved to transmit hundreds terabits per second per fiber within 10 THz. The spectral efficiency higher than 10 bit/s/Hz is almost unachievable in conventional single-carrier optical systems, but it can be realized by multiple-orthogonal-carrier optical systems.

In this research, we investigated the performance limitation of optical OFDM and OWDN signals, including peak-to-average-power ratio, phase noise, and optical or digital multiplexing. As shown in Table 5.1, there is no universal solution for the high-spectral-efficiency systems. The best choice of transmission technique will be the leverage among spectral efficiency, performance, complexity. With better understanding of these multiple-

orthogonal-carrier signals, the long-haul system architect can choose the optimal transmission technique based on the system requirement.

In addition to point-to-point high-capacity backbone transmission systems, the flexibility and manageability of multiple-orthogonal-carrier systems can be a promising candidate for PON access networks. Using the orthogonal-frequency-division multiple-access controlling, the multiple-orthogonal-carrier systems can integrate the link-layer protocol, such as the quality of service and the dynamic bandwidth allocation, easily into the physical layer. On the other hand, although OWDM does not have as high flexibility as OFDM access systems, it can rapidly scale up the transmission speed of PON access network easily by using low-cost optical-demultiplexing system architectures.

Table 5.1. Comparison of multiple-orthogonal-carrier systems

	Digital Multiplexing (OFDM)				Optical Multiplexing (OWDM)		
	CO-baseband-OFDM	CO-RF-OFDM	DDO-RF-OFDM	PM-OFDM	CO Digital Demux	CO Optical Demux	DDO Optical Demux
Spectral Efficiency	Medium	Medium	Medium	Low	High	High	Medium
Digital Complexity	High	High	High	High	Low	Low	Low
Optical Complexity	High	Medium	Low	Medium	Medium	Medium	Low
Interface Bandwidth	Low	Medium	Medium	Medium	High	High	High
Digital Equalization Complexity	Low	Low	Low	Low	High	High	High
PAPR and Nonlinearity	High	Medium	Medium	Low	Medium	Medium	Medium
BER vs OSNR	Medium	Medium	Medium	Low	Low	Medium	High

5.1.2 Wireless-over-Fiber mmWave Generation

The earliest definition of RoF systems refers to the application of extending the wireless coverage. The wireless coverage is limited by the propagation loss, obstacle absorption and reflection. Using optical-fiber communications to carry the wireless signals can dramatically reduce the propagation loss and make a detour of the transmission path to avoid obstacles. For low-frequency microwaves, RoF systems can replace leaky coaxial cables to help the signal penetrate concrete walls and grounds to extend the wireless coverage of microwaves under the ground or inside a building more efficiently. For high-frequency mmWaves, RoF systems can dramatically reduce the complexity of high-speed picocell or femtocell wireless networks. Unlike radio-and-fiber systems such as FiWi and WOBAN packet-switching backhaul networks, RoF systems extend the simple physical-layer extent and reduce the amount of higher-layer network deployment to save the total system cost.

In this research, various OCS techniques are proposed to improve the transmission of multi-gigabit radio-over-fiber transmission at 60-GHz. Simple, high conversion-efficiency homodyne OCS system has been employed for low-cost wireless devices, and heterodyne OCS is verified to adopt almost any kind of full-duplex wireless signal transmission. With the rapid development of radio-frequency optical components, radio-over-fiber systems are believed to be the most promising solution to establish a cost-effective and power-efficient multi-gigabit backhaul network for WLAN. If the deployment of radio-over-fiber technology is coming to a reality, not only in-building HD-video and mobile computing users benefit from the high-speed and convenient presence of wireless networks, but a wide variety of dream applications can be realized to help telemedicine, centralized medical monitoring, cloud computing, high-speed sensor networks. With the capabilities of transparency in formats and protocols and high capacity of radio-over-fiber system, a universal distributed-antenna system beyond the current 60-GHz standards for in-door applications can make a huge impact on more possibilities beyond our imagination.

118

In addition to extending the wireless reach, RoF systems can also be used for the link protection and restoration. The frequency beating of optical mmWave signals result into the generation of the equivalent baseband and RF signals simultaneously. As a result, the optical mmWave signals can be used to transport baseband signals along the fibers and RF signals through a wireless channel simultaneously without any modification. The wireless channel can be used as a backup link for the fiber link in a rough terrain. Or the optical fibers can be used as an alternative link when the wireless coverage is diminished by severe weather conditions.

Other applications include dynamic corporate access or connectivity. In many areas, optical fibers have been already installed and fixed inside walls and floors. When new buildings or units are constructed, mmWave RoF technology can expand the high speed links to the new access points via wireless links using existing fiber installations. Similar concepts can also be applied to wireless sensors or surveillance systems. When the fiber installation has already been fixed but the sensors or surveillance systems sometimes require relocations from time to time, using RoF technology can provide the optical-speed flexible access wirelessly based on the original fiber infrastructure.

5.1.3 Ultra-Short Reach Optical Interconnects

For HPC interconnects, optical interconnects have been gradually taking over the transmission length above 1 meter in top 500 HPC computers and kept improving its efficiency in shorter distances. The size, reliability, and power consumption are the many limiting factors for optical interconnects to conquer the area of centimeter-scale transmission. Although it is almost consent that optical interconnects are the long-term solution for HPC interconnects, on-chip interconnects are still ruled by the copper wires in the short-term interconnection roadmap [126, 127]. Beyond the 22-nm CMOS technology, air-gap copper wires and TSVs are expected to meet the requirement of on-chip interconnects. However, the clock rate of off-chip

interconnects within a few centimeters is expected to stride across the multi-gigabit transmission soon in the roadmap. In this distance, wireless interconnects have the opportunity to take over the lead.

Because of the performance issues related to phase noise, transceiver size, and power consumption, wireless interconnects technology has not been explored widely. In this research, we have proposed a novel RoF OLOD system for wireless LO synchronization. It is proven to increase the transmission distance and reduce the power consumption of fixed-position wireless transmission systems. From Table 4.1, the doubts regarding the size and power consumption are eliminated with recent development of millimeter-wave technology. For HPC interconnects, we still believe optical interconnects, such as active optical cables, are the suitable solution for a transmission distance longer than 1 m, whereas copper is no doubt a better candidate for intra-chip interconnects. However, for the distance around a few centimeters, such as processor-to-processor or processor-to-memory signal transmission, the wireless interconnects proposed and demonstrated in this thesis will make a major impact on next-generation HPC architectures.

The drawback of RoF OLOD systems is that the wireless link and the optical link have to be active simultaneously, limiting its applications in various environments. On the other hand, pre-distortion MIMO subsystems have great potential in fixed-position VHT wireless transmission. The applications of MIMO subsystems are versatile. From HPC interconnects to long-distance base-station interconnects in a rugged terrain, the MIMO transmission can play an important role either with digital de/multiplexing or analog de/multiplexing.

5.2 Future Works

The development of RoF systems have only been in an early stage for a few years. Unlike conventional single-carrier optical fiber systems, RoF signals suffer from severe chromatic dispersion and therefore require better understanding and need more careful dispersion

management schemes. For example, dispersion-induced phase noise, which is only seen in long-haul CO systems, is now observed in a short-distance RoF system because the coherency of multiple optical carriers in RoF systems can be degraded by the dispersive wall-off. As a result, the physical properties of RoF systems, including dispersion, nonlinearity, optical/digital demultiplexing, frequency-dependent attenuation, etc., are of great interests in the RoF research groups, especially for the fiber distance above 50 km.

For the RoF systems used for the wireless-coverage extension, the point-to-point fiber-wireless transmission has been thoroughly studied and experimentally demonstrated for years. Using HeteroOCS mmWave systems, the difficulty and uncertainty of the duplex fiber-wireless transmission can be resolved. However, RoF systems are designed for multi-user applications, such as pico-cells or femto-cells. Multiple-access controlling schemes are rarely designed for RoF systems, and multi-user scenarios are rarely studied and experimentally tested for mmWave transmission systems. To promote the RoF wireless-coverage extension systems to more practical systems, link-layer issues, such as multi-services and multi-users, require further studies and experimental tests.

In the end, RoF MIMO wireless interconnects are still at preliminary stage. So far, only theoretical studies of channel properties and simple proof-of-concept experiments have been done. Future works should include the mmWave antenna design, the mmWave RF-IC design, the MIMO multiplexing/demultiplexing analog IC Design, the packaging of the RF-module arrays, the integration of the o/e interface for the OLOD technique, and the MIMO channel modeling and the capacity analysis. Also, the compatibility of optical devices and CMOS devices is always the issue that determines the practicability of the heterogeneous systems.

5.3 Concluding Remarks

For the first time, we have generalized the meaning of RoF systems from wireless-signal access extension to spectrally efficient long-haul systems and all the way down to short-distance (a few centimeters) interconnect systems. In our generalized RoF systems, versatile properties can be applied to various levels of high- throughput and low-latency computing and communications applications. In long-haul systems, RoF systems can generate multiple orthogonal carriers to remove the guard band between adjacent channels and therefore dramatically improve the spectral efficiency. In the WLAN or PON access networks, existing fiber installations can be employed to extend the wireless coverage of a complicated wireless router and can greatly reduce the cost of numerous wireless access points. In HPC interconnects, our new RoF technique can help to synchronize the LO of the wireless transceivers and realize the MIMO analog multiplexing/demultiplexing functions at a low power budget. Moreover, there can be more inspiring, interesting and more diverse usages of RoF technology based on the studies of the generalized RoF systems developed in this dissertation. However, in order to compete with the conventional digital baseband transmission, there is still room for the RoF technology to be improved. With the rapid advance of mmWave technology and optical technology, we expect to see the RoF technology to become more prevalent in the near future.

References

[1] National Telecommunications and Information Administration, "United States Frequency Allocations," 1996. Available: http://www.sss-mag.com/pdf/freqchrt.pdf

[2] S. Bhandare, A. Joshi, D. Becker, "Optical Coherent Receiver With a Switchable Electrical Dispersion Compensator for 10 Gb/s DPSK Transmission up to 300 km of SSMF in Metro Optical Networks," *IEEE Journal of Lightwave Technology*, vol. 28, no. 1, pp. 47-58, 2010.

[3] S. J. Savory, G. Gabiolo, V. Mikhailv, R. I. Killey, and P. Bayvel, "Ultra-Long Haul QPSK Transmission Using a Digital Coherent Receiver," in *2007 Digest of the IEEE/LEOS Summer Topical Meetings*, pp. 13 - 14, 2007.

[4] X. Zhou and J. Yu, "Digital Signal Processing for Coherent Optical Communication," in *18th Annual Wireless and Optical Communications Conference*, WOCC'09, pp. 1-5, 2009.

[5] M. G. Taylor, "Coherent Detection for Optical Communications Using Digital Signal Processing," in *IEEE Conference on Optical Fiber Communication and the National Fiber Optic Engineers Conference*, OFC/NFOEC'07, pp. 1-3, 2007.

[6] A. Leven, N. Kaneda, S. Corteselli, "Real-Time Implementation of Digital signal Processing for Coherent Optical Digital Communication Systems," *IEEE Journal of Selected Topics in Quantum Electronics*, vol. 16, no. 5, pp. 1227-1234, 2010.

[7] N. Pleros, K. Vyrsokinos, K. Tsagkaris, and N. D. Tselikas, "A 60 GHz Radio-over-Fiber Network Architecture for Seamless Communication with High Mobility," *IEEE/OSA Journal of Lightwave Technology*, vol. 27, no. 12, pp. 1957-1967, 2009.

[8] A. F. Benner, "Cost-Effective Optics: Enabling the Exascale Roadmap," in *IEEE Symposium on High Performance Interconnects*, HOTI'09,pp. 133-137, 2009.

[9] G. Shainer, E. Gutkind, B. Lee, M. Kagan, and Y. Kliteynik, "Optics for Enabling Future HPC Systems," in *IEEE Symposium on High Performance Interconnects*, HOTI'09,pp. 138-142, 2009.

[10] T.-C. Chen, "Device Technology Innovation for Exascale Computing," in *IEEE Symposium on VLSI Technology*, pp. 8-11, 2009.

[11] D. Qian, M.-F. Huang, E. Ip, Y-K- Huang, Y. Shao, J. Hu, and T. Wang, "101.7-Tb/s (370×294-Gb/s) PDM-128QAM-OFDM transmission over 3×55-km SSMF using pilot-based phase noise mitigation," in *IEEE Conference on Optical Fiber Communication and the National Fiber Optic Engineers Conference*, OFC/NFOEC'11, PDPB5, pp. 6-10, 2011.

[12] F. M. Mousavi and K. Kikuchi, "Performance limit of long-distance WDM dispersion-managed transmission system using higher order dispersion compensation fibers," *IEEE Photonics Technology Letters*, vol. 11, no. 5, pp. 608-610, 1999.

[13] R. I. Killey, V. Mikhailov, S. Appathurai, and P. Bayvel, "Investigation of nonlinear distortion in 40-Gb/s transmission with higher order mode fiber dispersion compensators," *IEEE/OSA Journal of Lightwave Technology*, vol. 20, no. 12, pp. 2282-2289, 2002.

[14] X. Zhou and J. Yu, "Digital Signal Processing for Coherent Optical Communication," in *18th Annual Wireless and Optical Communications Conference*, WOCC'09, pp. 1-5, 2009.

[15] G. Goldfarb and G. Li, "Chromatic dispersion compensation using digital IIR filtering with coherent detection," *IEEE Photonics Technology Letters*, vol. 19, no. 13, pp. 969-971, 2007.

[16] K. Kikuchi, "Coherent Transmission Systems," in *34th European Conference on Optical Communication*, ECOC'08, pp. 1-39, 2008.

[17] R. Noe, "PLL-Free Synchronous QPSK Polarization Multiplex/Diversity Receiver Concept with Digital I&Q Baseband Processing," *IEEE Photonics Technology Letters*, vol. 17, no. 4, pp. 887-889, 2005.

[18]   D.E. Crivelli, H.S. Carter, M.R. Hueda, "Adaptive digital equalization in the presence of chromatic dispersion, PMD, and phase noise in coherent fiber optic systems," in *IEEE Global Telecommunications Conference*, GLOBECOM'04, pp. 2545-2551, 2004.

[19]   R. W. Chang, "Synthesis of band-limited orthogonal signals for multi-channel data transmission," *Bell System Technical Journal*, vol. 46, pp. 1775-1796, 1966.

[20]   P. H. Moose, "A Technique for orthogonal frequency division multiplexing frequency offset correction," *IEEE Transactions on Communications*, vol. 52, no. 10, pp. 2908-2914, 1994.

[21]   S. Attallah, "Blind Estimation of Residual Carrier Offset in OFDM Systems," *IEEE Signal Processing Letters*, vol. 11, no. 2, pp. 216-219, 2004.

[22]   U. Tureli, H. Liu, M. D. Zoltowski, "OFDM Blind Carrier Offset Estimator: ESPRIT," *IEEE Transactions on Communications*, vol. 48, no. 9, pp. 1459-1461, 2000.

[23]   Y.-H. You, K.-T. Lee, and S.-J. Kang, "Pilot-Aided Frequency Offset Tracking Scheme for OFDM-Based DVB-T," *IEEE Transactions on Consumer Electronics*, vol. 54, Nol. 3, pp. 1053-1058, 2008.

[24]   J. H. Yu and Y. Y. Su, "Pilot-Assisted Maximum-Likelihood Frequency-Offset Estimation for OFDM Systems," *IEEE Transactions on Communications*, vol. 52, no. 11, pp. 1997-2008, 2004.

[25]   C. Yan, S. Li, Y. Tang, X. Luo, J. Fang, "A Novel Frequency Offset Estimation Method for OFDM Systems with Large Estimation Range," *IEEE Transactions on Broadcasting*, vol. 52, no. 1, pp. 58-61, 2006.

[26]   G. Ren, Y. Chang, H. Zhang, and H. Zhang "An Efficient Frequency Offset Estimation Method with Large Range for Wireless OFDM Systems," *IEEE Transactions on Vehicular Technology*, vol. 56, no. 4, pp. 1892-1895, 2007.

[27]   M. Morelli and U. Mengali, "An Improved Frequency Offset Estimator for OFDM Applications," *IEEE Communication Letters*, vol. 3, no. 3, pp. 75-77, 1999.

[28] J.-J. van de Beek, M. Sandell, and P. O. Borjesson, "ML Estimation of Time and Frequency Offset in OFDM Systems," *IEEE Transactions on Signal Processing*, vol. 45, no. 7, pp. 1800-1805, 1997.

[29] T. M. Schmidl and D. C. Cox, "Robust Frequency and Timing Synchronization for OFDM," *IEEE Transactions on Communications*, vol. 45, no. 12, pp. 1613-1621, 1997.

[30] S.-H. Fan, J. Yu, D. Qian, G.-K. Chang, "A Fast and Efficient Frequency Offset Correction Technique for Coherent Optical Orthogonal Frequency Division Multiplexing," *IEEE/OSA Journal of Lightwave Technology*, vol. 29, no. 13, pp. 1997-2004, 2011.

[31] S. L. Jansen, I. Morita, T. C. W. Schenk, and H. Tanaka, "121.9-Gb/s PDM-OFDM Transmission with 2-b/s/Hz Spectral Efficiency over 1000 km of SSMF," *IEEE/OSA Journal of Lightwave Technology*, vol. 27, no. 3, pp, 177-188, 2009.

[32] W. Shoeh, H. Bao, Y. Tang, "Coherent Optical OFDM: Theory and Design," *OSA Optics Express*, vol. 16, no. 2, pp. 841-859, 2008.

[33] Q. Zou, A. Tarighat, A. H. Sayed, "Joint Compensation of IQ Imbalance and Phase Noise in OFDM Systems," in *Fortieth Asilomar Conference on Signals, Systems and Computers*, ACSSC'06, pp, 1435-1437, 2006.

[34] X. Zhou, J. Yu, M.-F. Huang, Y. Shao, T. Wang, L. Nelson, P. Magill, M. Birk, P. I. Borel, D. W. Packham, and R. Lingle, "64-Tb/s (640x170-Gb/s) PDM-36QAM Transmission over 320km Using Both Pre- and Post-Transmission Digital Equalization," in *IEEE Conference on Optical Fiber Communication and the National Fiber Optic Engineers Conference*, OFC/NFOEC'10, pp. 1-3, 2010.

[35] A. Sano, H. Masuda, T. Kobayashi, M. Fujiwara, K. Horikoshi, E. Yoshida, Y. Miyamoto, M. Matsui, M. Mizoguchi, H. Yamazaki, Y. Sakamaki, and H. Ishii, "69.1-Tb/s (432x171-Gb/s) C- and Extended L-Band Transmission over 240 km Using PDM-16-QAM Modulation and Digital Coherent Detection," in *IEEE Conference on Optical Fiber*

Communication and the National Fiber Optic Engineers Conference, OFC/NFOEC'10, pp. 1-3, 2010

[36] I. Roudas, A. Vgenis, C. S. Petrou, D. Toumpakaris, J. Hurley, M. Sauer, J. Downie, Y. Mauro, and S. Raghavan, "Optical polarization demultiplexing for coherent optical communications systems," *IEEE/OSA Journal of Lightwave Technology*, vol. 28, no. 7, pp. 1121-1134, 2010.

[37] R. C. J. Hsu, A. Tarighat, A. Shah, A. H. Sayed, B. Jalali, "Capacity enhancement in coherent optical MIMO (COMIMO) multimode fiber links," *IEEE Communications letters*, vol. 10, no. 3, pp. 195-197, 2005.

[38] R. Ryf, S. Randel, A. H. Gnauck, C. Bolle, R. Essiambre, P. J. Winzer, D. W. Peckham, A. McCurdy, and R. Lingle, "Space-division multiplexing over 10 km of three-mode fiber using coherent 6 x 6 MIMO processing, " in *IEEE Conference on Optical Fiber Communication and the National Fiber Optic Engineers Conference*, OFC/NFOEC'11, PDPB10, pp. 1-3, 2011.

[39] T. Pollet, M. van Bladel, and M. Moeneclaey, "BER Sensitivity of OFDM Systems to Carrier Frequency Offset and Wiener Phase Noise," *IEEE Transactions on Communications*, Vo. 43, no.234, pp. 191-193, 1995.

[40] Bo Liu, Xiangjun Xin, Lijia Zhang, Jianjun Yu, Qi Zhang, and Chongxiu Yu, "A WDM-OFDM-PON architecture with centralized lightwave and PolSK-modulated multicast overlay," *OSA Optics Express*, vol. 18, no. 3, pp. 2137-2143, 2010.

[41] D. Qian, S. Fan, N. Cvijetic, J. Hu, and T. Wang, "64/32/16QAM-OFDM using Direct-Detection for 40G-OFDMA-PON Downstream," in *IEEE Conference on Optical Fiber Communication and the National Fiber Optic Engineers Conference*, OFC/NFOEC'11, OMG4, 2011.

[42] Arthur Lowery and Jean Armstrong, "Orthogonal-frequency-division multiplexing for dispersion compensation of long-haul optical systems," *OSA Optics Express*, vol. 14, no. 6, pp. 2079-2084, 2006.

[43] P. C. Becker, N. A. Olsson, and J. R. Simpson, *Erbium-Doped Fiber Amplifiers Fundamentals and Technology*, San Diego Academic Press, Ch. 6, pp. 153-195, 1999.

[44] W. Shieh, X. Yi, Y. Ma, and Q. Yang "Coherent Optical OFDM: Has Its Time Come?" *IEEE/OSA Journal of Optical Networking*, vol. 7, no. 3, pp. 234-255, 2008.

[45] S. L. Jansen, I. Morita, T. C. W. Schenk, N. Takeda, and Tanaka, "Coherent Optical 25.8-Gb/s OFDM Transmission over 4160-km SSMF," *IEEE/OSA Journal of Lightwave Technology*, vol. 26, no. 1, pp. 6-15, 2008.

[46] B. J. Schmidt, A. J. Lowery, and J. Armstrong, "Experimental Demonstrations of Electronic Dispersion Comensation for Long-Haul Transmission Using Direct-Detection Optical OFDM," *IEEE/OSA Journal of Lightwave Technology*, vol. 26, no. 1, pp. 196-203, 2008.

[47] L. Xu, J. Hu, D. Qian, and T. Wang, "Coherent Optical OFDM Systems Using Self Optical Carrier Extraction," in *IEEE Conference on Optical Fiber Communication and the National Fiber Optic Engineers Conference*, OFC/NFOEC'08, pp. 1-3, 2008.

[48] B. Gobel, S. Hellerbrand, N. Haufe, and Norbert Hanik, "PAPR Reduction Techniques for Coherent Optical OFDM Transmission," in *11th International Conference on Transparent Optical Networks*, ICTON'09, Mo.B2.4, 2009.

[49] X. Liang, W. Li, W. Ma, and K. Wang, "A Simple Peak-to-Average Power Ratio Reduction Scheme for All Optical Orthogonal Frequency Division Multiplexing Systems with Intensity Modulation and Direct Detection," *OSA Optics Express*, vol. 17, no. 18, pp. 15614-15622, 2009.

[50] J. Yu, X. Zhou, and M.-F. Huang, "8x114 Gb/s, 25GHz-Spaced, PolMux-RZ-8QAM Straight-Line Transmission over 800km of SSMF," in *IEEE 35th European Conference on Optical Communication*, ECOC'09, O4.02, 2009.

[51] Z. Dong, Z. Cao, J. Lu, Y. Li, L. Chen, and S. Wen, "Transmission Performance of Optical OFDM Signals with Lowe Peak-to-Average Power Ratio by a Phase Modulator," *Optics Communications*, vol. 282, no. 21, pp. 4194-4197, 2009.

[52] N. Kaneda, Q. Yang, X. Liu, S. Chandrasekhar, W. Shieh, Y.-K. Chen, "Real-Time 2.5 GS/s Coherent Optical Receiver for 53.3-Gb/s Sub-Banded OFDM," *IEEE/OSA Journal of Lightwave Technology*, vol. 28, no. 4, pp. 494-501, 2010.

[53] K.-P. Ho, J. M. Kahn, "Optical frequency comb generator using phase modulation in amplified circulating loop," *IEEE Photonics Technology Letters*, vol. 5, no. 6, pp. 721-725, 1993.

[54] J. Yu, Z. Dong, X. Xiao, Y. Xia, S. Shi, C. Ge, W. Zhou, N. Chi, Y. Shao, "Generation, transmission and coherent detection of 11.2 Tb/s (112×100Gb/s) single source optical OFDM superchannel," in *IEEE/OSA Optical Fiber Communication Conference and Exposition and the National Fiber Optic Engineers Conference*, OFC/NFOEC'11, PDPA6, pp. 6-10, 2011.

[55] G. Goldfarb, G. Li, and M. G. Taylor, "Orthogonal Wavelength-Division Multiplexing Using Coherent Detection," *IEEE Photonics Technology Letters*, vol. 19, no. 24, pp. 2015-2017.

[56] Z. Zheng, Z. Qian, G. Shou, and Y. Hu, "Orthogonal Wavelength-Division-Multiplexing Using SSFBGs in Passive Optical Networks," in *IEEE/OSA Asia Communications and Photonics Conference and Exhibition*, ACP'10, WL73, pp. 1-2, 2010.

[57] F.C. Garcia Gunning. T. Healy, X. Yang, and A.D. Ellis, "0.6Tbit/s Capacity and 2bit/s/Hz Spectral Efficiency at 42.6Gsymbol/s Using a Single DFB Laser with NRZ Coherent WDM and Polarisation Multiplexing," in *IEEE European Conference on Lasers and Electro-Optics and the International Quantum Electronics Conference*, CLEOE-IQEC'07, pp. 1-1, 2007.

[58] S.K. Ibrahim, F.C.G. Gunning, and A.D. Ellis, "Performance Evaluation and Comparison of DPSK CoWDM Systems based on Odd/Even and Array Configurations," in *IEEE/OSA Conference on Lasers and Electro-Optics and Quantum Electronics and Laser Science Conference* CLEO-QELS'10, CThC3, pp. 1-2, 2010.

[59]   D. Hillerkuss, M. Winter, M. Teschke, A. Marculescu, J. Li, G. Sigurdsson, K. Worms, S. Ben Ezra, N. Narkiss, W. Freude, and J. Leuthold, "Simple all-optical FFT scheme enabling Tbit/s real-time signal processing," *OSA Optics Express*, vol. 18, no. 9, pp.9324-9340, 2010.

[60]   K. Yonenaga, A. Sano, E. Yamazaki, F. Inuzuka, Y. Miyamoto, A. Takada, and Takashi Yamada, "100 Gbit/s All-Optical OFDM Transmission Using 4 x 25 Gbit/s Optical Duobinary Signals with Phase-Controlled Optical Sub-Carriers," in *IEEE/OSA Optical Fiber Communication Conference and Exposition and the National Fiber Optic Engineers Conference*, OFC/NFOEC'08, JThA48, pp. 1-3, 2008.

[61]   Z. Dong, J. Yu, X. Tang, and W. Jian, "432Gbit/s O-OFDM QPSK signal transmission over 400km SMF-28 with EDFA-only amplification," in *IEEE/OSA Optical Fiber Communication Conference and Exposition and the National Fiber Optic Engineers Conference*, OFC/NFOEC'11, JThA36, pp. 1-3, 2011.

[62]   K. Takiguchi, M. Oguma, H. Takahashi and A. Mori, "Integrated-optic eight-channel OFDM demultiplexer and its demonstration with 160 Gbit/s signal reception," *IET Electronics Letters*, vol.46, no.8, pp.575-576, 2010.

[63]   Hung-Chang Chien, Ming-Fang Huang, Jie Liu, Arshad Chowdhury, Jianjun Yu and, Gee-Kung Chang, "Novel architectures for orthogonal wavelength division multiplexed passive optical networks (OWDM-PONs) in a 25-GHz Grid," in *IEEE/OSA Optical Fiber Communication Conference and Exposition and the National Fiber Optic Engineers Conference*, OFC/NFOEC'11, OThB6, pp. 1-3, 2011.

[64]   WirelessHD Specification ver. 1.1, May 2010. Available: http://www.wirelesshd.org

[65]   IEEE P802.11ad Task Group. Available: http://www.ieee802.org/11/

[66]   WiGig Alliance. Available: http://wirelessgigabitalliance.org

[67]   IEEE 802.15 WPAN Millimeter Wave Alternative PHY Task Group 3c (TG3c). Available: http://www.ieee802.org/15/pub/TG3c.html

[68] B. Xu, S. Hischke, and B. Walke, "The Role of Ad Hoc Networking in Future Wireless Communications," in *IEEE International Conference on Communication Technology Proceedings*, vol. 2, pp. 1353-1358, 2003.

[69] P. Chowdhury, M. Tornatore, S. Sarkar, B. Mukherjee, "Building a Green Wireless-Optical Broadband Access Network," *IEEE/OSA Journal of Lightwave Technology*, vol. 28, no. 16, pp. 2219-2229, 2010.

[70] Z. Zheng, J. Wang, and J. Wang, "A Study of Network Throughput Gain in Optical-Wireless (FiWi) Networks Subject to Peer-to-Peer Communications," in *IEEE International Conference on Communications*, 2009. ICC'09, pp.1-6, 2009.

[71] H.-G. Bach, A. Beling, G. G. Mekonnen, R. Kunkel, D. Schmidt, W. Ebert, A. Seeger, M. Stollberg, and W. Schlaak, "InP-Based Waveguide-Integrated Photodetector with 100-GHz Bandwidth" *IEEE Journal of Selected Topics in Quantum Electronics*, vol. 10, no. 4, pp. 668-678, 2004.

[72] S. Mayyshev, A. Chizh, Y. Vasileuski, "High-Speed Photodiodes for Microwave and Millimeter-Wave Systems," in *IEEE Microwave, Radar and Remote Sensing Symposium*, MRRS'08, pp. 116-121, 2008.

[73] Z. Zhu, X. Zheng, G. Xu, Y. Guo, and H. Zhang, "A Super-Tripling Technology Used in Radio-over-Fiber Systems for Multiservice Wireless Signals Within a Millimeter-Wave Band," *IEEE Photonics Technology Letters*, vol. 21, no. 20, pp. 1520-1522, 2009.

[74] H. Chi and J. Yao, "Frequency Quadrupling and Upconversion in a Radio over Fiber Link," *IEEE/OSA Journal of Lightwave Technology*, vol. 26, no. 15, pp. 2706-2711, 2008.

[75] X. Qi, J. Liu, X. Zhang, and L. Xie, "Fiber Dispersion and Nonlinearity Influences on Transmissions of AM and FM Data Modulation Signals in Radio-over-Fiber System," *IEEE Journal of Quantum Electronics*, vol. 40, no. 8, pp. 1170-1177, 2010.

[76] J. Ma, C. Yu, X. Xin, J. Zeng, and L. Chen, "Fiber Dispersion Influence on Transmission of the Optical Millimeter-Waves Generated Using LN-MZM Intensity Modulation," *IEEE/OSA Journal of Lightwave Technology*, Vo. 25, no. 11, pp. 3244-3256, 2007.

131

[77] Z. Jia, J. Yu, Y.-T. Hsueh, A. Chowdhury, H.-C. Chien, J. A. Buck, and G.-K. Chang, "Multiband Signal Generation and Dispersion-Tolerant Transmission Based on Photonic Frequency Tripling Technology for 60-GHz Radio-over Fiber Systems," *IEEE Photonics Technology Letters*, vol. 20, no. 17, pp. 1470-1472, 2008.

[78] Yu-Ting Hsueh, Hung-Chang Chien, Zhensheng Jia, Arshad Chowdhury, Jianjun Yu. , Gee-Kung Chang, " 8×2.5-Gb/s, 60-GHz radio-over-fiber access network with 125-km extended reach using remote optical carrier suppression," in *21st Annual Meeting of the IEEE Lasers and Electro-Optics Society*, LEOS'08, Nov. 2008.

[79] J. J. V. Olmos, T. Kuri, T. Sono, K. Tamura, H. Toda, and K. Kitayama, "Reconfigurable 2.5-Gb/s Baseband and 60-GHz (155-Mb/s) Millimeter-Waveband Radio-over-Fiber (Interleaving) Access Network," *IEEE/OSA Journal of Lightwave Technology*, vol. 26, no. 15, pp. 2506-2512, 2008.

[80] W. Ayub, M. Ramzan, S. A. Haider, and S. M. H. Zaidi, "Radio-over-Fiber Architecture Integrating Broadband Wireline and Wireless Services," in *IEEE International Symposium on High Capacity Networks and Enabling Technologies*, HCNET'08, pp. 102-106, 2008.

[81] A. Chowdhury, J. Yu, H.-C. Chien, M.-F. huang, T. Wang, and G.-K. Chang, "Spectrally Efficient Simultaneous Delivery of 112Gbps Baseband Wireline and 60 GHz MM-wave Carrying 10Gbps Optical Wireless Signal in Radio-over-Fiber WDM-PON Access Systems," in *IEEE 35th European Conference on Optical Communication*, ECOC'09, pp, 1-2, 2009.

[82] W.-J. Jian, C.-T. Lin, P.-T. Shih, L.-Y. W. He, J. Chen, and S. Chi, "Simultaneous Generation and Transmission of 60-GHz Wireless and Baseband Wireline Signals with Uplink Transmission Using an RSOA," *IEEE Photonics Technology Letters*, vol. 22, no. 15, pp. 1099-1101, 2010.

[83] C. G. Schäffer, R.-P. Braun, G. Grosslopf, and F. Schmidt, "Compensation of Fiber Dispersion in an Optical mm-wave System in the 60GHz-Band," in *IEEE International Microwave Symposium Digest*, pp. 1529-1532, 1998.

[84] A. Wiberg, P. Pérez-Millán, M. V. Andrés, P. A. Andrekson, and P. O. Hedekvis, "Fiber-optic 40-GHz mm-wave link with 2.5-Gb/s data transmission," *IEEE Photonics Technology Letters*, vol. 17, no. 9, pp. 1938-1940, 2005.

[85] G. D. Golden, C. J. Foschini, R. A. Valenzuela, and P. W. Wolniansky, "Detection Algorithm and Initial Laboratory Results Using V-BLAST Space-Time Communication Architecture," *IET Electronics Letters*, Vi, 35, no. 1, pp. 14-16, 1999.

[86] R. W. Heath Jr. and A. J. Paulraj, "Switching Between Diversity and Multiplexing in MIMO Systems," *IEEE Transactions on Communications*, vol. 53, no. 6, pp. 962-968, 2005.

[87] E. Akay, E. Sengul, and Ayanoglu, "Achieving Full Spatial Multiplexing and Full Diversity in Wireless Communications," in *Wireless Communications and Networking Conference*, WCNC'06, pp. 2046-2050, 2006.

[88] A. Pollok, W. G. Cowley, I. D. Holland, "Multiple-Input Multiple-Output Options for 60-GHz Line-of-Sight Channels," in *Australian Communications Theory Workshop*, pp. 101-106, 2008.

[89] A. Chowdhury, H.-C. Chien, and G.-K. Chang, "Demonstrations of Simultaneous All-Optical Up-Conversion of Gigabit Wireless Services at 60-GHz and 64-GHz in Converged Optical Wireless System Carried by Single Wavelength Lightwave," in *IEEE Conference on Optical Fiber Communication and the National Fiber Optic Engineers Conference*, OFC/NFOEC'10, OWQ5, 2010.

[90] Z. Xu, X. Zhang, and J. Yu, "Frequency Upconversion of Multiple RF Signals Using Optical Carrier Suppression for Radio over Fiber Downlinks," *OSA Optics Express*, vol. 15, no. 25, pp. 16737-16747, 2007.

[91] Cheng Liu, Hung-Chang Chien, Zhen Gao, Wei Jian, Arshad Chowdhury, Jianjun Yu, Gee-Kung Chang, " Multi-band 16QAM-OFDM vector signal delivery over 60-GHz DSB-SC optical millimeter-wave through LO enhancement," in *IEEE Conference on Optical Fiber*

Communication and the National Fiber Optic Engineers Conference, OFC/NFOEC'10, OThJ2, 2010.

[92] Available: http://www.corning.com/opticalfiber/products/index.aspx

[93] M. A. Taubenblatt, "Optical interconnects for high performance computing," in *IEEE Conference on Optical Fiber Communication and the National Fiber Optic Engineers Conference*, OFC/NFOEC'11, OThH3, 2011.

[94] M. S. Parekh, P. A. Thadesar, M. S. Bakir, "Electrical, optical and fluidic through-silicon vias for silicon interposer applications," in *IEEE 61st Electronic Components and Technology Conference*, ECTC'11, pp. 1992-1998, 2011.

[95] Available: http://www.nvidia.com/object/product_tesla_C2050_C2070_us.html

[96] S. Scott, "Optical interconnects in future HPC systems," in *IEEE Conference on Optical Fiber Communication and the National Fiber Optic Engineers Conference*, OFC/NFOEC'11, OWH5, 2011.

[97] A. Liu, L. Laio, Y. Chetrit, J. Basak, H. Nguygen, D. Rubin, and M. Paniccia, "Wavelength division multiplexing based photonic integrated circuits on silicon-on-insulator platform," *IEEE Journal of Selected Topics in Quantum Electronics*, vol. 16, no. 1, pp. 23-32, 2010.

[98] M.-C. F. Chang, H. Shin, and L. Zhang, "RF-interconnect for future inter- and intra-ULSI communications," in *IEEE Technical Digest on International Electron Devices Meeting*, IEDM'01, pp. 23.4.1-23.4.4, 2001.

[99] D. A. B. Miller and H. M. Ozaktas, "Limit to the Bit-Rate Capacity of Electrical Interconnects from the Aspect Ratio of the System Architecture," *Journal of Parallel and Distributed Computing*, vol. 41, no. 1, pp. 42-52, 1997.

[100] R. Kollipara, M. Li, D. Mullen, W. Beyene, C. Madden, C. Yuan, H. Kusamitsu and T. Ito, "Evaluation of a module based memory system with an LCP flex interconnect," in *IEEE 59th Electronic Components and Technology Conference*, ECTC'09, pp. 1200-1206, 2009.

[101] Available: http://techresearch.intel.com/ProjectDetails.aspx?Id=151

[102] M. Ritter, "Optical technologies for data communication in large parallel systems," in *Topical Workshop on Electronics for Particle Physics*, TWEPP'10, pp. 1-12, Sept 2010.

[103] I. A. Young, E. Mohammed, ; J. T. S. Liao, A. M. Kern, S. Palermo, B. A. Block, M. R. Reshotko, P. L. D. Chang, "Optical I/O Technology for Tera-Scale Computing," *IEEE Journal of Solid-State Circuits*, vol.45, no.1, pp.235-248, 2010.

[104] Y. Wang, A. M. Niknejad, V. Gaudet, and K. Iniewski, "A CMOS IR-UWB Transceiver Design for Contact-Less Chip Testing Applications, " *IEEE Transactions on Circuits and Systems - II Express Briefs*, vol. 55, no. 4, pp. 334-338, 2008.

[105] R. Canegallo, L. Ciccarelli, F. Natali, A. Fazzi, R. Guerrieri, and P. Rolandi, "3D Contactless Communication for IC Design," in *IEEE International Conference on Integrated Circuit Design and Technology and Tutorial*, ICICDT'08, pp. 241-244, 2008.

[106] K. Kawasaki, Y. Akiyama, K. Komori, M. Uno, H. Takeuchi, T. Itagaki, Y. Hino, Y. Kawasaki, K. Ito, A. Hajimiri, "A Millimeter-Wave Intra-Connect Solution," *IEEE Journal of Solid-State Circuits*, vol. 45, no. 12, pp. 2655-2666, 2010.

[107] J. Lee, Y. Huang, Y. Chen, H. Lu, and C. Chang, "A low-power fully integrated 60 GHz transceiver system with OOK modulation and on-board antenna assembly," in *IEEE International Solid-State Circuits Conference*, ISSCC'09, pp. 316-317a, 2009.

[108] V. V. Kulkarni, M. Muqsith, K. Niitsu, H. Ishikuro, T. Kuroda, "A 750 Mb/s, 12 pJ/b, 6-10 GHz CMOS IR-UWB Transmitter with Embedded On-Chip Antenna," *IEEE Journal of Solid-States Circuits*, vol. 44, no. 2, pp. 394 - 403, 2009.

[109] W.-H. Chen, S. Joo, S. Sayilir, R. Willmot, T.-Y. Choi, D. Kim, J. Lu, D. Peroulis, B. Jung, "A 6-Gb/s Wireless Inter-Chip Data Link Using 43-GHz Transceivers and Bond-Wire Antennas," *IEEE Journal of Solid-State Circuits*, vol. 44, no. 10, pp. 2711-2721, 2009.

[110] Available: http://www.top500.org

[111] K, Chang, H. Lee, J.-H. Chun, T. Wu, TJ Chin, K. Javiani, J. Shen, X. Shi, W. Beyene, Y. Frans, B. Leibowitz, N. Nguyen, F. Quan, J. Zerbe, R. Perego, F. Assaderaghi, "A

160Gb/s/link, 64GB/s Bidirectional Asymmetric Memory Interface Cell," in *IEEE Symposium on VLSI Circuits Digest of Technical Papers*, pp. 126-127, 2008.

[112] F. E. Doany, C. L. Schow, L. Schares, C. Baks, D. M. Kuchta, R. A. John, Y-J. Chang, J. A. Kash, "A 160-Gb/s Bidirectional Parallel Optical Transceiver Module for Board-Level Interconnects using a Single-Chip CMOS IC," in *57th Electronic Technology and Components Conference*, ECTC'07, 2007.

[113] K. Kawasaki, Y. Akiyama, K. Komori, M. Uno, H. Takeuchi, T. Itagaki, Y. Hino, Y. Kawasaki, K. Ito, A. Hajimiri, "A millimeter-wave intra-connect solution," *IEEE Journal of Solid-State Circuits*, vol. 45, no. 12, pp. 2655-2666, 2010.

[114] G. Balamurugan, F. O'Mahony, M. Mansuri, J. E. Jaussi, J. T. Kennedy, B. Casper, "A 5-to-25Gb/s 1.6-to-3.8mW/Gb/s reconfigurable transceiver in 45nm CMOS," in *IEEE International Solid-State Circuits Conference*, ISSCC'10, pp. 372-374, 2010.

[115] S. Fukuda, Y. Hino, S. Ohashi, T. Takeda, S. Shinke, M. Uno, K. Komori, Y. Akiyama, K. Kawasaki, A. Hajimiri, "A 12.5+12.5Gb/s full-duplex plastic waveguide interconnect," in *IEEE International Solid-State Circuits Conference*, ISSCC'10, pp. 150-152, 2011.

[116] N. Miura, D. Mizoguchi, M. Inoue, K. Niitsu, Y. Nakagawa, M. Tago, M. Fukaishi, T. Sakurai, T. Kuroda, "A 1Tb/s 3W inductive coupling transceiver for inter-chip clock and data link," *IEEE International Solid-State Circuits Conference*, ISSCC'10, pp. 1676 - 1685, 2006.

[117] X. Chen, D. Akinwande, K.-J. Lee, G. Close, S. Yasuda, B. C. Paul, S. Fujita, J. Kong and H.-S. P. Wong, " Fully Integrated Graphene and Carbon Nanotube Interconnects for Gigahertz High-Speed CMOS Electronics," *IEEE Transactions on Electron Devices*, vol. 57, no. 11, pp. 3137-3143, 2010.

[118] A. Suntives and R. Abhari, "Design and characterization of the EBG waveguide-based interconnects," *IEEE Transactions on Advanced Packaging*, Vo. 30, no. 2, pp. 163 – 170, 2007.

[119] M. J. R. Heck, H.-W. Chen, A. W. Fang, B. R. Koch, D. Liang, H. Park, M. N. Sysak, J. E. Bowers, "Hybrid Silicon Photonics for Optical Interconnects," *IEEE Journal of Selected Topics in Quantum Electronics*, vol. 17, no. 2, pp. 333-346, 2011.

[120] J. A. Key-Bolotin and C.-S. Tsang, "Measureing phase noise at K-band," in *IEEE Aerospace Conference*, vol. 5, pp. 193-209, 1999.

[121] D. Petrovic, W. Rave, and G. Fettweis, "Effects of Phase Noise on OFDM Systems With and Without PLL: Characterization and Compensation," *IEEE Transactions on Communications*, vol. 55, no. 8, pp. 1607-1616, 2007.

[122] Sergio Verdú, "Spectral Efficiency in the Wideband Regime," *IEEE Transactions on Information Theory*, vol. 48, no. 6, pp. 1319-1343, 2002.

[123] A. Pollok, W.G. Cowley, and I.D. Holland, "Multiple-input multiple-output options for 60 GHz line-of-sight channels," Australia Communications Theory Workshop, 2008. AusCTW 2008.

[124] J. R. Barry, E. A. Lee, D. G. Messerchmitt, *Digital Communication: Third Edition*, Springer Publisher, pp. 495, 2003.

[125] N. Miura, D. Mizoguchi, T. Sakurai, T. Kuroda, "Analysis and design of inductive coupling and transceiver circuit for inductive inter-chip wireless superconnect," *IEEE Journal of Solid-State Circuits*, vol. 40, no. 4, pp. 829-837, 2005.

[126] M. Haurylau , H. Chen , J. Zhang , G. Chen , N. A. Nelson , D. H. Albonesi , E. G. Friedman, " On-Chip Optical Interconnect Roadmap: Challenges and Critical Directions," *IEEE Journal of Selected Topics in Quantum Electronics*, vol. 12, no. 6, pp. 1699-1705, 2006.

[127] "Internation technology roadmap for semiconductors." Available: http://public.itrs.net

VITA

Shu-Hao Fan was born in Tainan, Taiwan, 1983. He received his B.S. degree in electrical engineering from National Taiwan University, Taipei, Taiwan, in 2004. After one and half a year army life, he entered Georgia Institute of Technology, Atlanta, GA, U.S.A. for the graduate study. He is an IEEE member and serves as an OSA/IEEE reviewer. His current interests include wireless/optical hybrid systems, coherent and direct detection optical OFDM systems, and optical interconnects.